TECHNISCHE UNIVERSITÄT WIEN
Vienna University of Technology

ATOMINSTITUT

DIPLOMARBEIT

Charakterisierung eines 'Badurek'-Resonators für sehr kalte Neutronen

Ausgeführt am
Atominstitut
der Technischen Universität Wien

unter der Anleitung von
Prof. Dr. Gerald Badurek,
Ass.-Prof. Dr. Erwin Jericha

durch
Joachim Bosina
Engerthstraße 41/2/11
1200 Wien

Wien, Mai 2015 Joachim Bosina

Abstract

In 1962 G.M. Drabkin proposed a method which should allow the selection of monochromatic particles from an incident polychromatic beam of polarized neutrons by means of spatial magnetic spin resonance. The significant advantage of this method compared to conventional monochromators based on crystal Bragg reflection or mechanical speed selectors is the feasibility to vary both the transmitted neutron wavelength and the spectral resolution by purely electronic means. In the following decades such Drabkin-type of resonators were successfully realized and their capabilities thoroughly explored. In 1991 G. Badurek proposed a completely new extremely versatile version of such a resonator which can not only act as monochromator with variable wavelength resolution but also allows chopping of the continuous incident beam into short pulses in the sub-millisecond regime. Of particular importance is the possibility to decouple the wavelength resolution from the achievable minimal pulse duration.

The realization of such an advanced 'Badurek' resonator type is goal of the so-called MONOPOL project at the Atominstitut of the Vienna University of Technology. Embedded in this comprehensive project the main task of the present master thesis was the development of a so called *Monopol Control Modul* as an indispensable tool to fully exploit the inherent potential of the 'Badurek-Resonator'. Furthermore the actual status of this resonator as characterized from a series of test experiments performed with very cold neutrons at the ILL in Grenoble in summer 2014 is presented in detail and possible further improvements are discussed.

Kurzfassung

1962 schlug G.M. Drabkin erstmals eine Methode vor, mit der es mit Hilfe von räumlicher magnetischer Spinresonanz möglich sein sollte, monochromatische Teilchen aus einem polychromatischen Strahl polarisierter Neutronen zu selektieren. Der signifikante Vorteil dieser Methode verglichen mit konventionellen, auf Bragg-Reflexion an Kristallen oder mechanischen Geschwindigkeitselektoren beruhenden Monochromatoren ist die Möglichkeit, sowohl die transmittierte Wellenlänge als auch die Wellenlängenauflösung auf rein elektronische Weise zu variieren. In den darauffolgenden Jahrzehnten wurden solche Drabkin-Resonatoren erfolgreich realisiert und ihr Potential eingehend ausgelotet. 1991 schlug G. Badurek eine völlig neue, extrem vielseitige Version eines solchen Resonators vor, die nicht nur als Monochromator mit flexibler Wellenlängenauflösung fungieren kann, sondern auch das Choppen des kontinuierlichen einfallenden Strahls in kurze Pulse von Sub-Millisekunden Dauer erlaubt. Von besonderer Bedeutung ist dabei die Möglichkeit, die Wellenlängenauflösung von der minimal erzielbaren Pulsdauer zu entkoppeln.
Die Realisierung eines derartigen ‚Badurek-Resonators' ist das Ziel des so genannten MONOPOL Projekts am Atominstitut der technischen Universität Wien. Eingebettet in dieses umfangreiche Projekt war es die wesentliche Aufgabe der vorliegenden Diplomarbeit, ein so genanntes *Monopol-Control-Modul* zu entwickeln, das eine unverzichtbare Komponente für die volle Nutzung des inhärenten Potentials des ‚Badurek-Resonator' darstellt. Außerdem werden der aktuelle Status dieses Resonators im Detail präsentiert, wie er sich anhand einer Reihe von Testexperimenten charakterisieren lässt, die im Sommer 2014 am ILL Grenoble mit sehr kalten Neutronen durchgeführt wurden, sowie weitere mögliche Verbesserungen diskutiert.

Contents

1 Theory **6**
- 1.1 The neutron . . . 6
  - 1.1.1 Spin and polarization . . . 10
- 1.2 Neutron sources . . . 10
  - 1.2.1 Nuclear reactions . . . 11
  - 1.2.2 Nuclear fission . . . 11
  - 1.2.3 Spallation . . . 12
- 1.3 Polarizing mirrors . . . 12
- 1.4 Spin flippers . . . 13
  - 1.4.1 Current sheets . . . 14
- 1.5 Choppers . . . 15
- 1.6 Wavelength selection with crystals . . . 15
- 1.7 Drabkin resonator . . . 16
  - 1.7.1 Badurek resonator . . . 18

2 History of previous works **20**
- 2.1 History of the Drabkin resonator . . . 20
- 2.2 History of the Badurek resonator . . . 21
  - 2.2.1 Gösselsberger PhD thesis - the MONOPOL-project . . . 21
  - 2.2.2 Prototype 1.0 . . . 21
  - 2.2.3 Prototype 2.0 . . . 22
  - 2.2.4 Prototype 3.0 . . . 23
  - 2.2.5 Prototype 3.1 . . . 23
  - 2.2.6 Future . . . 25

3 Technical description of the Monopol-Setup **26**
- 3.1 Resonator 3.1 . . . 27
  - 3.1.1 Problems with the prototype 3.1 . . . 28
- 3.2 Magnetic environment . . . 30
  - 3.2.1 Fluxgate SENSYS FGM3D . . . 30
  - 3.2.2 Guiding field . . . 31
  - 3.2.3 Protection against the magnetic field of the earth and other sources . . . 33
  - 3.2.4 The compensation-field coils in x-direction . . . 34
  - 3.2.5 The compensation-field coils in y-direction . . . 35
  - 3.2.6 Passive magnetic field shield . . . 36
- 3.3 Spin flippers . . . 37
- 3.4 Super mirrors . . . 39
- 3.5 Chopper . . . 40
- 3.6 The box . . . 41
  - 3.6.1 Steps to achieve airtightness . . . 42
- 3.7 Periphery . . . 44
  - 3.7.1 Needed power supplies . . . 44
- 3.8 Electronic control of the resonator . . . 44
  - 3.8.1 Central Master Controller . . . 46
  - 3.8.2 Coil controllers . . . 47

4 Software **51**
4.1 GUI-CSV writer . . . 51
4.1.1 Possible improvements: . . . 52
4.2 Monopol-Arm . . . 54
4.3 Firmware of coil controller: NR-Komplett . . . 55
4.4 Monopol Control System - MCS . . . 55

5 List of possible improvements of the MONOPOL-setup **56**

6 Measurment and results **57**
6.1 Preparations . . . 57
6.1.1 Adjustment of the neutron beam . . . 57
6.2 Measurements . . . 58
6.2.1 Measurement of the optimal settings of the current sheet 2013 . . . 58
6.2.2 Measurement of the polarization and the spin flip efficiencies 61
6.2.3 Measurement of the spectral spin-flip efficiency of the resonator and the current sheet . . . 61
6.2.4 Testing different pulse settings of the resonator . . . 65
6.2.5 Different shaping of the stage magnetic field distribution . 67
6.2.6 Variation of the resonator lengths . . . 69
6.2.7 Resonator sweeps at fixed guiding field . . . 72
6.2.8 Synchronization of the chopper and the resonator . . . 73
6.2.9 Overlaping of two TWM-pulses in helium . . . 76
6.3 Spectra of the VCN-beam . . . 77
6.3.1 Spectrum measured with the chopper and the resonator in helium . . . 81
6.3.2 Spectrum in TWM and helium . . . 83
6.4 Darwin plots . . . 84
6.4.1 Timing-Darwin . . . 84
6.4.2 Shaping-Darwin . . . 86

7 Conclusion **87**

A Measurements of guiding field coils paramters **88**
A.1 Relation between current and produced B field . . . 88
A.2 Number of windings W . . . 88

B Used components of the box **89**
B.1 List of all plug-in connectors of the three feed-trough-panels . . . 89
B.2 List of all used components . . . 91

C Used power supplies **92**

D Components of the VCN-coil-controllers **93**

Introduction

Within the MONOPOL project, this master thesis covers the characterization of a state-of-the-art Badurek resonator and the measurements done during a beam time at the ILL in Grenoble in 2014. The goal of the MONOPOL project is to develop a Badurek resonator which is capable of being a very flexible neutron beam preparator for other experiments.
A Badurek resonator is an advanced Drabkin resonator. The basic principle used by these resonators is spatial spin resonance of the neutron spin. Applied spatially oscillating magnetic fields induce spin flips in a polarized neutron beam. This effect strongly depends on the velocity of the neutrons. Therefore, this device creates monochromatic polarized neutron pulses.
The first section "Theory" contains all the theory needed for the understanding of the principle of spatial spin resonance and its application in a Badurek-resonator.
The second section "History of previous works" consists of a summary of articles and theses in the field of Drabkin resonators. Specially, I give a review about the research which was done at the Atominstitut of the Vienna University of Technology (ATI) within the last five years.
In the following sections "Technical description" and "Software" I present a very detailed characterization of the current prototype and all its components. I tried to present all necessary information for all following students who will work on this project in order to make their research easier. I also describes possible opportunities to improve the current setup. A short summary of these is in the section five. Some technical details are also in the appendix.
In the sixth section, I present all the measurements that E. Jericha, W. Mach and I did during the beam time at the VCN-cabin of the ILL in Grenoble in 2014.
In the last section I conclude my thesis and present possible future developments.

1 Theory

1.1 The neutron

Protons p^+, neutrons n^0 and electrons e^- are the only three massive particles that are considered as stable particles. Even though the neutron is only stable in the atomic nucleus. All three particles are fermions with a spin of $\frac{1}{2}$. As fermions, these particles never have the same quantum state (energy, spin, angular momentum,...) at the same location. Together they are the building blocks of every atom. The positively charged protons and the neutral neutrons are in the center of the atom and form the atomic nucleus. The negatively charged electrons surround the nucleus. The atom is neutral if it consists of the same number of protons and electrons. Atoms with the same proton number are from the same element. Different isotopes of one element have the same proton number but a different neutron number. We call the atomic nucleus alone also nuclide. We distinguish between different nuclides only by their proton number and their neutron number.
Electrons are elementary particles. They are leptons like the neutrinos and interact mainly by the electromagnetic force with the environment. An electron

has approximately 2000 times less mass than a proton or a neutron. The anti particle of the electron is the positively charged positron.
Protons and neutrons are baryons. Baryons are composite particles made of three quarks. Quarks are also elementary particles. The lightest quarks are the $\frac{2}{3}$e positively charged "up" quark and the $\frac{1}{3}$e negatively charged "down" quark. They are also the only stable quarks. Protons are composed of two up and one down quark. Neutrons are made of one up and two down quarks. This different composition results in a different charge and a little bit different mass. A neutron is a little bit heavier than a proton and an electron together.
As baryons, protons and neutrons attract each other and themselves due to the STRONG FORCE. This force has only a very short range of influence. It is approximately 1 pm $= 1 \cdot 10^{-15}$ m. This is nearly the size of one proton or one neutron. Therefore, neutrons and protons attract only their nearest neighbors due to the strong force. The binding energy between a proton or a neutron with the rest of the nuclide can be more than 8 MeV $= 12.8 \cdot 10^{-12}$ J. This is the energy equivalent to the creation of 8 electron-positron pairs. In contrast, the COULOMB FORCE has an infinite range of influence. Its strength only decreases by the square of the distance between the charges. The Coulomb force which acts on one proton is the sum of the repulsion of all other protons in the nucleus. Neutrons bind the protons together even though the positively charged protons recoil each other. In the atomic nucleus of light elements an equal amount of neutrons and protons is required. In heavy elements more neutrons than protons are needed to prevent the disintegration of the atomic nucleus due to the repulsion of the protons. Very heavy nuclides have a chance to decay into lighter nuclides by α-decay, cluster decay or spontaneous fission due to the fact that the electromagnetic repulsion becomes comparable to the binding energy due to the strong force.
The WEAK FORCE is always weaker than the strong force or the electromagnetic force. It has no influence on the binding between two particles. The weak force only induces decays. The most important decay is the beta decay:

$$n^0 \Rightarrow p^+ + e^- + \nu_{\bar{e}} \tag{1}$$

During this decay one down quark transforms into an up quark by producing a virtual W^--boson. The W^--boson decays into the electron and the neutrino. The electron preserves the charge conservation (Q: 0=1-1+0). The quasi-massless anti-electron-neutrino $\nu_{\bar{e}}$ preserves the lepton number (L: 0=0+1-1), the angular moment due to the spins ($\frac{1}{2} = \frac{1}{2} + \frac{1}{2} - \frac{1}{2}$) and they also explain the broad energy spectrum of the electron. Only the fact that a neutron has more mass than all the other three particles allows this decay. In the atomic nucleus the masses of the neutrons and the protons change due to the binding energy between the baryons. Therefore, a bonded neutron will only decay if becoming a proton increases enough the binding energy to produce an electron and a neutrino. This is only the case if there are much more neutrons than protons. If there are more protons than neutrons the beta decay is reversed into the beta-plus decay:

$$p^+ \Rightarrow n^0 + e^+ + \nu_e \tag{2}$$

For heavy elements a K-capture is also possible. There an electron from the K-shell collapses into a proton:

$$p^+ + e^- \Rightarrow n^0 + \nu_e \tag{3}$$

These decays do not change the total sum of protons and neutrons (mass number). For every mass number, only nuclides with the highest binding energy between its compounds are stable. They have the optimal ratio between proton number and neutron number. The strong force and the Coulomb force fix this ratio. In general, if the nuclide is far away from the stable nuclide, it will decay faster. The half life of beta decays varies between billions of years and nanoseconds. The lifetime of the unbound neutron is 880.3±1.1 s [1]. This is a very important parameter for the standard model of particle physics specially for the understanding of the weak force. Nevertheless the value of this parameter is not know very precisely. In comparison to the life time of the free neutron, the other parameters are very well known, such as the magnetic moment of the neutron $\mu_n = -1.9130427 \pm 0.0000005\ \mu_N$. Therefore, the measurement of the neutron life time is one of the major goals in neutron physics.
Free neutrons are used for life time experiments and also for many other experiments. Due to the short life time of neutrons, a neutron source is always close to these experiments. All neutron sources have in common that they use a nuclear reaction. The neutrons from these sources normally have a kinetic energy of approximately 1-10 MeV. They scatter with the atomic nuclei of the surrounding matter due to the strong force and transfer their kinetic energy to the surrounding. We call this process moderation. The fastest moderation takes place in elements with a low atomic number because the energy transfer is the highest if both particles have the same weight. This process ends when neutrons have the same kinetic energy as the atoms of the moderator. A Maxwell-Boltzmann distribution describes the kinetic energy distribution of the moderator and we associate the mean energy with at a certain temperature.

$$\overline{E_{kin}} = \frac{m\bar{v}^2}{2} = k_B T \tag{4}$$

Therefore, we can describe neutrons as a gas with a certain temperature according to their kinetic energy. Neutrons at room temperature (300 K) have a mean kinetic energy of 25 meV. A change in the moderator temperature or the residence time in the moderator influence the neutron spectrum. With this in mind we divide the energy spectrum of neutrons into different sections (see in table 1). There exists many possibilities to categorize the spectrum. Most of the other definitions have similar splittings and use similar names. The range of one section can vary strongly between the definitions.
In table 1 not only the temperature is a synonym for the neutron kinetic energy but also the velocity of the neutron and even with the De Broglie wavelength.

$$p = mv = \frac{h}{\lambda} \tag{5}$$

In addition, other effects are important in the experiments with neutrons: During the moderation and also if the neutrons have reached thermal equilibrium with the surroundings, neutrons can be absorbed by the atomic nucleus or induce other nuclear reaction like fission. The probability of such reactions

Table 1: Neutron energies [3](p.3)

Name	Energy	Wavelength	Velocity	Temperature
relativistc neutrons	> 10 GeV	<0.28 fm	>0.996 c	
high energy neutrons	0.05-10 GeV	4-0.28 fm	0.314-0.996 c	
very fast neutrons	10-50 MeV	6.4-4 fm	0.145-0.314 c	
fast neutrons	0.5-10 MeV	40-6.4 fm	0.015-0.145 c	
intermediate neutrons	1-500 keV	900-40 fm	0.001-0.015 c	
resonant neutrons	1-100 eV	28-2.8 pm	13.8-138 $\frac{km}{s}$	
epithermal neutrons	0.1-1 eV	90-28 pm	4373-13800 $\frac{m}{s}$	>1160 K
thermal neutrons	5-100 meV	4-0.9 Å	978-4373 $\frac{m}{s}$	58-1160 K
cold neutrons	0.5-5 meV	12.8-4 Å	309-978 $\frac{m}{s}$	5.8-58 K
very cold neutrons (VCN)	0.1-0.5 meV	28.6-12.8 Å	138-309 $\frac{m}{s}$	1.2-5.8 K
ultra cold neutrons (UCN)	<100 µeV	>28.6 Å	<138 $\frac{m}{s}$	<1.2 K

depends strongly on the nuclide. Strong absorbers like boron often surround the neutron source to protect the surroundings from the neutron radiation. Small holes in the shielding and special pipes guide neutrons to the test sides in the form of neutron beams. The velocity distribution of these beams depends on the moderator temperature and on the average time the neutrons have to moderate. In order to control the beam parameters, we insert devices which monochromatize the beam or chop the beam into pulses.
We use neutron beams to study materials and their structures similar as with X-rays. Both are very penetrating because they consists of neutral particles. However, we see different aspects of the material due to the different interactions. X-rays interact only electromagnetically. The interaction is much stronger for elements with high atomic number due to their strong electromagnetic field around the nucleus. Neutrons interfere with the atomic nuclei by the strong force and with the magnetic moment of the atom by the electromagnetic force. The strength of the interactions depends on the nuclide. Neutrons interact strongly with hydrogen or uranium but very weakly with carbon, oxygen or silicon. This makes them perfect to study organic compounds or the water contended in stones, which is very hard to analyze with X-rays. We can even distinguish with neutron scattering between different isotopes like hydrogen and deuterium.
Due to the fact that X-rays and thermal neutrons have similar wavelengths but a very different energy and velocity, we can study with neutrons different phenomenons in solid mater: like the slow traveling phonons (1000-9000 $\mathrm{m{\cdot}s^{-1}}$).

Table 2: Important neutron properties

Property	Value
mass m_n	939.565379(21) $\frac{MeV}{c^2}$ [1] $= 1.674927351(74) \cdot 10^{-27}$ kg [2]
charge	$(-2 \pm 8) \cdot 10^{-22}$ e [1]
lifetime τ_n	880.3±1.1 s [1]
magnetic moment μ_n	$-1.9130427(5)\ \mu_N$ [1] $= -0.96623647(23) \cdot 10^{-26}\ \frac{J}{T}$ [2]
gyromagnetic ratio γ_n	$1.83247179(43) \cdot 10^8\ \frac{1}{sT}$ [2]
g-factor g_n	-3.82608545(90) [2]

1.1.1 Spin and polarization

The neutron has a spin of $\frac{1}{2}$. This means that the spin can be in only two quantum states. We call these states: "up" $|\uparrow\rangle$ and "down" $|\downarrow\rangle$. The spin and the fact that the neutron is a composite particle are responsible for the magnetic dipole moment of the neutron even though a neutron has no charge. Therefore, neutrons are sensible to the electromagnetic force. In an external magnetic field the magnetic moment of the neutron aligns parallel or anti parallel to the magnetic field lines. This also represents both spin quantum states in the direction of the external magnetic field. If we measure again the spin-state of the same neutron in the same direction with a similar aligned magnetic field, we will gain the same results. If we measure the spin state with a magnetic field perpendicular to the first one, the result will be completely random with a 50% probability of having an up or down spin state. This is due to the quantum nature of the spin. If we know the spin state in one direction, we lose every information about the spin states in the other directions. If I compare spin states of a neutron, I will always refer to only one spatial direction.
In a large ensemble of neutrons, both states are occupied equally due to energy degeneration. Locally we can separate both states by using super mirrors for example (see more in Section 1.3). The polarization P describes the occupation of both states:

$$P = \frac{N_\uparrow - N_\downarrow}{N_\uparrow + N_\downarrow} \tag{6}$$

$N_\uparrow$ and $N_\downarrow$ are the number of neutrons in the quantum state $|\uparrow\rangle$ or $|\downarrow\rangle$ [4].
We can describe the polarization as a vector $\mathbf{P}$ with the absolute value P pointing in the same direction as the spin states.
A neutron beam is polarized if the polarization P deviates significantly from zero. A polarized beam depolarizes slowly due to scattering with matter and other effects, which represents a measurement of the neutron spin in arbitrary direction. To prevent the depolarization, we build a guiding field around the polarized neutron beam. This homogeneous magnetic field fixes the parallel component of the polarization vector.
The total polarizing vector $\mathbf{P}$ rotates around the fixed component. We call the frequency of the rotation the Larmor frequency ω_L:

$$\omega_L = \gamma_n \mid \mathbf{B} \mid \tag{7}$$

The direction of $\mathbf{P}$ can follow a slow rotation of the guiding field. We call this adiabatic. If the guiding field turns up side down much faster than ω_L, $\mathbf{P}$ will stay with the same orientation, but is differently aligned to the external magnetic field. We call this process non adiabatic. We can use both processes to build spin flippers.

1.2 Neutron sources

Unbounded neutrons are not stable. Every experiment with neutrons needs a source of free neutrons close by. All neutron sources have in common that we put enough energy into a nucleus to compensate the binding energy of one or many neutrons. There are three possible ways to create a free neutron: nuclear reactions, fission and spallation.

1.2.1 Nuclear reactions

Some nuclides have loosely bound neutrons compared to the other baryons in the nucleus like ^{9}Be. Alpha particles, accelerated protons, fast neutrons or high energy photons can provide this binding energy and induce a nuclear reaction. Sources of alpha particles are radioactive substances like Pu or ^{241}Am. In a mixture of ^{9}Be and ^{241}Am, the decay of americium can induce a nuclear reaction in the beryllium and this mixture will produce free neutrons. The total neutron-flux can be up to 10^7 neutrons per second.

1.2.2 Nuclear fission

If an atom absorbs a neutron, the neutron transfers all its kinetic energy to the nucleus. Additionally, the binding energy between the neutron and the nucleus excites the nucleus. For heavy elements this excitation energy can be beyond a certain point of stability. The nucleus deforms so much that the proton-proton repulsion becomes stronger than the binding energy due to the strong force. The nucleus splits into two parts. After this nuclear fission some neutrons are also set free. The reason for this is that heavy elements have much more neutrons than protons in order to be stable, lighter elements have almost the same number of protons and neutrons. All the spare neutrons decay or are set free. These free neutrons can induce new fissions. We call this *chain reaction*. In order to keep the chain reaction at a constant rate, we need to reduce the neutrons available for the induced fission to a constant level. The exceeding neutrons have to be absorbed or leave the reactor core. We can use these neutrons for experimentation. A nuclear reactor is a good source for neutrons. The neutron flux can be up to $10^{15}\mathrm{cm}^{-2}\cdot\mathrm{s}^{-1}$. Regular nuclear power plants are optimized for electric power production. The reactor core with the fuel elements is in a huge pressure vessel in order to have a higher boiling temperature of the coolant. This pressure vessel should have as few openings for connections as possible because of safety reasons. Therefore, additional neutron beam guides are not desired. In order to use a nuclear reactor as a neutron source, we use small research reactors. They are not used to produce electricity. The coolant has a temperature below 100°C. Hence, we don't need a pressure vessel. Many neutron beam pipes can be close by the core. They guide neutrons through holes in the neutron-absorber shielding of the reactor core to the experimentation sites. Besides, research reactors are smaller than nuclear power plants. They produce only a fraction of the energy. Therefore, the safety requirements are much lower. For this thesis two research reactors are important. The TRIGA MARK II of the Atominstitut in Vienna [5] and the HFR at the Institut-Laue-Langvin (ILL) in Grenoble [6].
The TRIGA-reactor is a 250 kW open pool reactor. It contains approximately 80 20%-enriched fuel elements. These elements are made of a special uranium-zirconium-alloy which has hydrogen implanted as a moderator. This special mixture causes the reactor to be very safe and easy to handle. The first two generations of the MONOPOL resonators were tested at a dichromatic beam line of this TRIGA-reactor. In the future a new thermal-white-neutron-beam test site will be built at this reactor. There the future testing of the upgraded MONOPOL setup will take place.
HFR (high flux reactor) in Grenoble is the heart of the ILL, an international research facility. It is the most powerful neutron source in the world. The reactor

core consists only of one fuel element. This lasts only 50 days but produces 50-60 MW providing the highest neutron flux that is possible with a nuclear reactor ($1.5 \cdot 10^{15}\mathrm{cm}^{-2}\cdot\mathrm{s}^{-1}$). In order to achieve that, the fuel element consists of weapon-graded uranium and the surrounding moderator is D_2O, which has a much smaller absorption cross section than normal water. Many experiments are connected to this neutron source. To provide not only thermal neutrons two cold sources are installed. At these sources, the beam guides start at liquid deuterium tanks. These two tanks are situated near the fuel element in the D_2O moderator. It needs a lot of effort to keep the deuterium liquid but then we can produce neutron beams consisting of cold neutrons. One beam guide leaves the core horizontally and the other vertically. In the vertical beam guide the neutrons lose energy due to the gravitational force. The neutron spectrum shifts from cold to VCN. In a special turbine some of these neutrons are further decelerated and become UCN. The neutrons which are too fast for this process fly straight through this turbine without deceleration to a test site. This test site (PF2B) was used twice to test the MONOPOL 3.1 in 2013 and 2014. The preparations for the beam time in 2014 and the results are the main purpose of this master thesis.

1.2.3 Spallation

High energy particles with an energy around 1 GeV or above can induce spallation. If this particle hits the nucleus, the nucleus will disintegrate in many small parts like neutrons, protons and light elements. If the target material is an element with a high atomic number more neutrons will be set free. For example tungsten set free more than 20 neutrons. Particle accelerators produce the high energy particles. There the charged particles like protons are always accelerated in bunches. That is why this kind of neutron source produces only neutron pulses. The biggest neutron sources of this kind are the nTOF at CERN, ISIS at Harwell in Great Britain, SNS in Oak Ridge in the United States and SINQ at the PSI in Switzerland. Also cosmic radiation contains many particles with enough energy. The earth's atmosphere is the target material. There, the highest neutron flux is in the region of airplane travel. Subsequently ^{14}N-neutron scattering produces ^{14}C. In 1937 Marietta Blau and Hertha Wambacher discovered the processes of spallation in photo emulsions which were exposed to cosmic radiation.

1.3 Polarizing mirrors

Neutrons scatter in materials due to the strong force and the magnetism. The probability of the scattering depends strongly on the nuclide for both mechanisms. The sign of the magnetic scattering depends on the alignment between the spins of the target and the neutron. Consequently, the normal elastic scattering and magnetic scattering add up or subtract each other. In some materials the magnetic scattering and the nucleon scattering have nearly the same strength [7]. If we build mirrors out of these materials and place them in a strong magnetic field, all atoms will align their spin. For one spin state, the scattering probability adds up and the beam is reflected. For the other spin state, the scattering probability is close to zero and the beam is transmitted only. The reflected beam is polarized. Usually, we place an absorber behind the

mirror to prevent the transmitted beam to be accidentally reflected somewhere. Neutron reflection is similar to the reflection of photons. There exists also total reflection for small incident angles. Mirrors made out of many layers with different thickness increases the incident angle for total reflection. We call them super mirrors. Slower neutrons have larger angles of total reflection. There exists super mirrors which reflects VCN for angles higher than 10°. If iron or cobalt is in every second layer, the reflected beam is also polarized.
More mirrors used increase the efficiency P but decreases the beam intensity.

$$P_{P_{eff}} = 2P_P/(1+P_P)^2 \text{ [16]} \tag{8}$$

A very good but expensive method is to use nuclear reactions. For some nuclear reactions the probability is strongly depending on the alignment of the spins (for example the neutron capture of ^{3}He). If we guide the neutron beam through a gas of ^{3}He which is polarized due to a strong homogeneous magnetic field around the gas tank, the beam will be polarized because one spin state is absorbed and the other is transmitted. With this method P can be up to 0.9999 [8].

1.4 Spin flippers

Spin flippers change the spin state of the neutrons. In polarized beams, they invert the polarization vector of the total beam. There are many possibilities for this task [53](p.11-15). Mostly, we use magnetic fields (static or time depending). We measure the efficiency of spin flippers with two spin flippers and two polarizing mirrors. The first mirror polarizes the beam. The second one analyzes it. In between there are the two spin flippers. We measure four times in four different configurations: both spin flippers turned on (N_{11}), both turned off (N_{00}), one turned off and the other turned on (N_{10}) and vice versa (N_{01}). With these four values we calculate the spin-flip-efficiency values e_1 and e_2 and the polarization P ([39](p.28), [34](p.19), [41](p.25) and [30]):

$$\frac{N_{10}}{N_{00}} = \frac{1-e_1P_PP_A}{1+P_PP_A} \quad \rightarrow \quad e_1 = \frac{N_{01}-N_{11}}{N_{10}-N_{00}} \tag{9}$$

$$\frac{N_{01}}{N_{00}} = \frac{1-e_2P_PP_A}{1+P_PP_A} \quad \rightarrow \quad e_2 = \frac{N_{10}-N_{11}}{N_{01}-N_{00}} \tag{10}$$

$$\frac{N_{11}}{N_{00}} = \frac{1+e_1e_2P_PP_A}{1+P_PP_A} \quad \rightarrow \quad P_PP_A = \frac{(N_{01}-N_{00})(N_{00}-N_{10})}{N_{10}N_{01}-N_{00}N_{11}} \tag{11}$$

It is also possible to measure the four different configurations with a pulsed neutron beam and a time-resolving detector. In this time-of-flight setting (see more in Section 1.5) we measure the spectral function of the neutron spin-flip probabilities $p_1(\lambda)$ and $p_2(\lambda)$ [13, 17]:

$$p_1(\lambda) = \frac{1}{2}\left(1+\frac{N_{11}(\lambda)-N_{01}(\lambda)}{N_{00}(\lambda)-N_{10}(\lambda)}\right) \tag{12}$$

$$p_2(\lambda) = \frac{1}{2}\left(1+\frac{N_{11}(\lambda)-N_{10}(\lambda)}{N_{00}(\lambda)-N_{01}(\lambda)}\right) \tag{13}$$

$$\tag{14}$$

The equations (12) and (13) have only precise efficiency values for wavelengths inside the spectrum of the neutron beam. In addition, the precision of the spin-

flip efficiency of one spin flipper depends strongly on the bandwidth of the other spin flipper.

1.4.1 Current sheets

The current-sheet spin flipper consists of three components: a guiding field, a compensation field and a current sheet. The guiding field stabilizes the polarization (Figure 1 on page 14). The compensation field, which is anti-parallel to the guiding field, creates a field free region. We realize this with a pair of Helmholtz coils. In this field free region we place the current sheet. This is a single sheet or foil made of aluminum because aluminum has a very low neutron absorption. We place this sheet perpendicularly to the neutron beam. Current up to 100 A running through the sheet parallel to the guiding field produces a strong magnetic field around the sheet always perpendicular to the guiding field.
The polarization vector **P** of the neutron beam is aligned first with the guiding field. If the neutrons approach the current sheet, the guiding field strength decreases slowly to zero due to the compensation field and the magnetic field of the current sheet increases. The direction of the total magnetic field rotates slowly around the direction of flight of the neutron beam. **P** follows adiabatically the total magnetic field. In front of the current sheet **P** is perpendicular to the guiding field and the neutron beam. Directly behind the current sheet the guiding field strength is still compensated to zero. The magnetic field of the current sheet changes the direction. The total magnetic field changes the direction too. The neutrons feel this instantaneously when they pass through the current sheet. The neutron spin has no time to follow the total magnetic field and remains in the same direction. Now **P** is aligned in the opposite way to the magnetic field. Behind the current sheet, the magnetic field of the current sheet decreases and the guiding field strength increases again. The total magnetic field direction rotates back parallel to the guiding field. Again **P** follows adiabatically the rotation of the total magnetic field. In the end the neutrons flipped their spin state in comparison to the guiding field.
The right adjustment of the compensation field current is important. Otherwise, there is not a field free region close to the current sheet. Therefore, the total magnetic field in front and behind the current sheet are not completely anti-parallel. This leads to a depolarization during the spin flip and an increase of the noise in the measurement results.

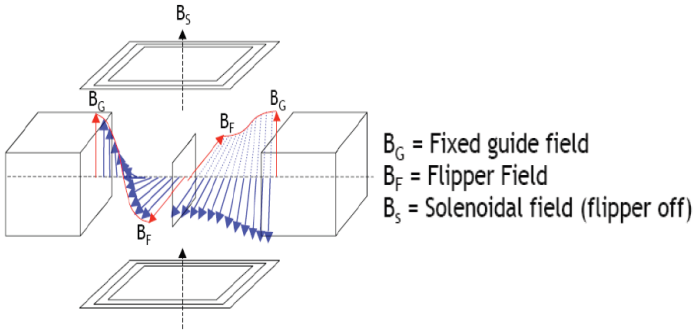

Figure 1: Principle of the current sheet [40]

1.5 Choppers

Many neutron sources continuously emit neutrons. Some experiments need neutron pulses. The length of these neutron pulses increases over time due to the velocity difference between the neutrons. Faster neutrons are in the lead and slower neutrons fall behind. We can use this effect to analyze the neutron spectrum of the beam. This is the principle of Time-of-flight measurements (TOF). The short neutron pulses fly over some meters. Afterwards a time sensitive detector detects them. The arrival time in the detector depends on the speed of the neutrons. The time depending intensity is proportional to the spectrum of the neutron beam.
Choppers can produce the needed short pulses [54](p.4). They are fast rotating neutron absorbers. Common are rotating disks with small windows close to the edge (disk-choppers). If the beam hits the disk, it will be absorbed and if the beam hits the window, it will be transmitted. For thermal neutrons these disks have to rotate quite fast. As a result, other forms are common like stacks of metal and absorber plates (Fermi-choppers). Only if the beam hits the stack edgewise, it can pass. A combination of many choppers is acting as a wavelength selector because only with certain velocities neutrons can pass all choppers. An extreme version of this idea is a turbine. Only a nearly monochromatic fraction of the beam can pass these turbines. The rest hits the turbine and becomes absorbed. All choppers have in common that they have a good signal to noise ratio but they are not very flexible. Due to the fast rotation, we can vary the time between two pulses only very slowly. Furthermore, the opening time of the chopper is linked to the pulse frequency. Therefore, the minimum pulse length is limited by the frequency when the neutron pulses start to overlap in the detector due to the velocity distribution in the neutron beam. In addition, we have to take into account that every TOF-spectrum is a convolution of the real spectrum and the chopper opening function [53](p.70) [54](p.56) [58](p.26-32). At last, choppers reduce the beam intensity proportional to the ratio between opening and total time.

1.6 Wavelength selection with crystals

Due to the particle-wave dualism, we can describe the propagation of neutrons as waves. The wavelength λ of thermal neutrons is similar to the distance between the lattice planes in a single crystal (like X-rays). One neutron-wave scatters with many atoms of the crystal under same condition because of the constant distances of the atoms in a lattice plane (Fig. 2). These planes have also constant distances d. The partial waves of the neutron, which are scattering on the lattice planes, start to interfere with themselves. In some angles θ the interference is constructive and in the rest it is destructive. Bragg's law describes this reflection condition:

$$n\lambda = 2dsin(\theta) \tag{15}$$

We use this phenomenon to monochromatize the neutron beam. We place a crystal or a multilayer structure into the beam. Only certain wavelengths are scattered under certain angles. This forms a new beam, which consists of only some different wavelengths. The reason why there are more wavelengths possible is that more orders n are available in the spectrum to fulfill the Bragg's condition

(15). An example is the dichromatic beam at the TRIGA of the Atominstitut. This beam consists of two wavelengths: 1.3 Å and 2.6 Å (other orders are suppressed by the polarizing mirror).
Crystal monochromators can produce very monochromatic beams. The big drawback is that we lose a lot of beam intensity. Similar to X-rays, we can analyze the spectrum by the variation of the angles between the incidence beam, the crystal and the detector. We can also analyze crystal structures by using two crystals. One crystal monocromatizes the beam and the other analyzes the beam. If we know the structure of one crystal, we measure the structure of the other. The accuracy of all these analyses depends strongly on the precise motion of the moving parts.

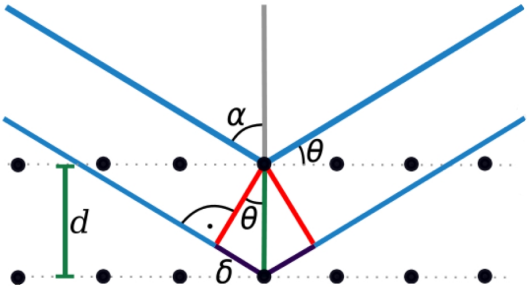

Figure 2: Diffraction of neutrons or X-rays in a crystal [40]

1.7 Drabkin resonator

In the early 60ies G. M. Drabkin invented [9] a new instrument to monochromatize polarized neutron beams. We call it "Drabkin resonator". This is an accordion-pleated aluminum-foil [10] with the length L. The spatial period of the resonator is $2a$. A current running through the foil produces an alternating magnetic field $\mathbf{B}_1$ in the U-shapes of the foil perpendicular to the beam. In the rest frame of the neutrons, this spatial alternating field looks like a time depending field. The resonator works on the neutrons like a radio-frequency spin flipper [26, 42] but every neutron has its own resonance frequency ω_R due to the different velocity v [10, 29].

$$\omega_R(v) = \frac{\pi v}{a} \quad \rightarrow \quad \omega_R(\lambda) = \frac{\pi h}{ma\lambda} \tag{16}$$

Due to an additional guiding field $\mathbf{B}_0$ around the resonator, the polarization of the neutrons $\mathbf{P}$ precesses with the Larmor-frequency ω_L. For some neutron velocities the alternating field of the resonator always interacts with the polarization synchronous to the Larmor precession and induces a spin flip ($\omega_L = \omega_R$). The probability $\mathrm{P}(\lambda)$ describes the chance of a spin flip depending on the wavelength [10, 13, 27][47](p.30-34). All neutrons with the velocity of the resonance

are spin flipped (P(λ_0)=1).

$$\omega_L = \omega_R \rightarrow \gamma_n \mid B_0 \mid = \frac{\pi h}{m_n a \lambda} \tag{17}$$

$$\lambda_0 = \frac{h\pi}{m_n \gamma_n} \cdot \frac{1}{aB_0} \approx 6.78 \cdot 10^{-15} Wb \cdot \frac{1}{aB_0} \text{ [28]} \tag{18}$$

$$P(\omega) = \frac{(\gamma_n B_1')^2}{(\omega - \omega_0)^2 + (\gamma_n B_1')^2} \cdot sin^2 \left(\frac{\sqrt{\omega - \omega_0)^2 + (\gamma_n B_1')^2}}{2} \right) \text{ [10]} \tag{19}$$

$$P(\lambda) = \frac{\xi^2}{\left(\frac{\lambda - \lambda_0}{\lambda}\right)^2 + \xi^2} \cdot sin^2 \left(\frac{\pi L \lambda}{2a\lambda_0} \sqrt{\left(\frac{\lambda - \lambda_0}{\lambda}\right)^2 + \xi^2} \right) \text{ [27, 47]} \tag{20}$$

$$\text{ratio of the magnetic fields: } \xi = \frac{2}{\pi} \frac{B_1}{B_0} \tag{21}$$

$$\text{amplitude condition: } \frac{L}{a}\xi = 2k + 1 (k = 0, 1, 2, 3, ...) \text{ [27]} \tag{22}$$

$$\text{wavelength resolution: } \frac{\triangle \lambda_{\frac{1}{2}}}{\lambda} \cong 1.6 \frac{a}{L} \text{ [10, 27]} \tag{23}$$

The shape of the spin flip probability around the resonance wavelength is proportional to the square of Fourier-transformation of the spatial distribution of $\mathbf{B}_1$. The first Drabkin resonator was a rectangular shaped foil which is folded in a meander shape. Each section has an equal length of $2a$. Consequently, the magnetic field $\mathbf{B}_1$ has the same value in every stage. We describe the distribution of $\mathbf{B}_1$ as a rectangular function. Its Fourier transformation is a sinx/x function. As a result, the probability function P has the form of $\sin^2 x/x^2$. It has a main maximum and many side maxima around it. We can only extinguish the side maxima by using two different Drabkin resonators where the side maxima of one resonator match with the side minima of the other resonator [12]. A more elegant method is to use a different field strength distribution [13]. A perfect distribution is a Gaussian distribution, because the Fourier transformation of the Gaussian function is again a Gaussian function with only one maximum. The technical realization is to vary the broadness of the meander shaped resonator foil. At the thinner parts, the current density increases and produces a stronger magnetic field.

A big drawback is that the shape of the resonator is fixed. To have a different magnetic field distribution, we have to change the resonator. Furthermore, this is similar for the wavelength resolution. These drawbacks are solved only by the improvements which lead to the Badurek resonator.

In order to use the Drabkin resonator as a beam monochromator, we additionally need two super mirrors to polarize and analyze the beam, a homogeneous guiding field and a normal broadband spin flipper [11](Fig 3). The resonator flips only the resonant wavelengths and the broadband spin flipper flips the total spectrum. Only neutrons which are flipped twice can pass the analyzer. These are the neutrons with a wavelength close to the resonance. The big advantage of this setup is that the resonance wavelength depends only on the settings of the magnetic fields $\mathbf{B}_0$ and $\mathbf{B}_1$. We can change them much faster than the parameters of monochromator crystals or neutron turbines. We can even change it in one neutron pulse [15]. The disadvantage is that the efficiency of the polarizer and the analyzer are the main contribution to the background. In order

to suppress all parts of the neutron spectrum except the wanted wavelength, we need a degree of polarization higher than 0.99, which is possible [8].

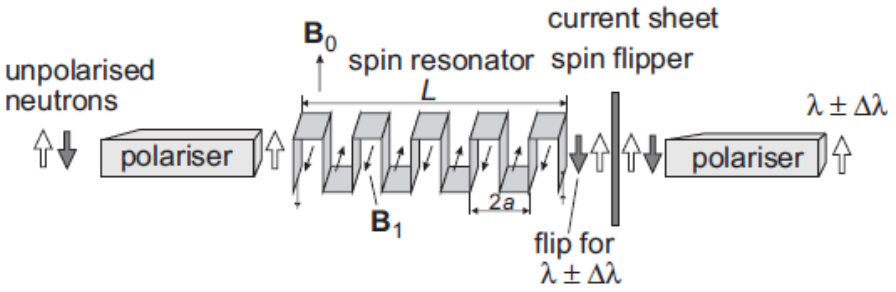

Figure 3: Using a Drabkin resonator as beam monochromator [28][33]

We can use the resonator in a static mode, which means the resonator is permanently turned on, or we can turn it on and off. A turned off resonator blocks the beam. If we turn the resonator on and off periodically, we call this conventional mode. In this mode the resonator behaves like a chopper. In comparison to normal choppers, we are very flexible because we can vary the pulse length and the time between two pulses after every pulse independently. The resonator electronic is the only restriction. The shortest possible pulse length depends only on the length L of the resonator. Only if one punch of resonant neutrons is able to fly through the entire resonator, the pulses will have the full intensity. Rise time and fall time of the pulse depends also on L because all neutrons in the resonator which fly only partially through the active resonator can flip their spins. Here also the background contribution due to the inefficiency of the polarizer and the analyzer is a major drawback of the Drabkin resonator.
With very high efficiency of the polarizer and the analyzer the Drabkin resonator setup is a very flexible instrument for beam preparation. We can create monochromatic polarized pulses, which we can use at continuous sources but also at pulsed sources like spallation sources [16, 19, 20]. We can use the Drabkin resonator also to produce space-time focusing points [15]. In these points many monochromatic neutron pulses are at the same time at the same place. This is an ideal starting point for TOF-measurements or we just create a point with increased beam intensity. We have the advantage that we can create a spectrum as we like with a pulse length as we want.

1.7.1 Badurek resonator

Gerald Badurek published the idea of an advanced Drabkin resonator in 1991 [16]. The basic idea is to separate the meander-shaped resonator foil into many single coils. Every coil has its own power supply and can be turned on and off independently with an own MOSFET (Figure 4 on page 19). One coil together with its supporting structure and its electronic controller is called “stage”. If one electronic device controls many stages at the same time we call it “coil controller”. We call this advanced Drabkin resonator with separated stages “Badurek resonator”.

The advantages of this resonator type are shorter pulse length and flexible shaping of the magnetic field $\mathbf{B}_1$. We can vary the magnetic field strength in every stage by varying the current through the coils. We do not need a special geometry in order to have a shaping to suppress efficiently the side maxima. Therefore, we can use equally shaped stages.
We realize the shorter pulse length with the so called traveling wave mode (TWM)[27]. In contrast to the conventional mode only some stages are active at the same time. The pulse starts when the first neutrons of the pulse enter the resonator and the first stage is turned on. Shortly before these neutrons enter the next stage, we turn this stage on. Every stage is active only for the time of the wanted pulse length. The minimal pulse length depends only on the length a of one stage and not on the length L of the resonator. In addition, the fall time and rise time are much shorter.
We gain also a lot more flexibility. The only restriction is the electronic control. We can easily split the Badurek resonator into many small independent resonators by only changing the programming of the electronics. We can also vary the stage number N of the resonator and thereby the active length L. We can combine stages by changing the polarity of the coils. This changing of the stage length a also effects the needed guide field strength $\mathbf{B}_0$. Varying a, L, and N change the wavelength resolution without changing the real geometry.
At the Atominstitut of the Vienna University of Technology the research group around Badurek, Jericha and Gösselsberger started the MONOPOL-project in order to build prototypes of the BADUREK-resonator and to exploits its limits. This master thesis is part of this project.

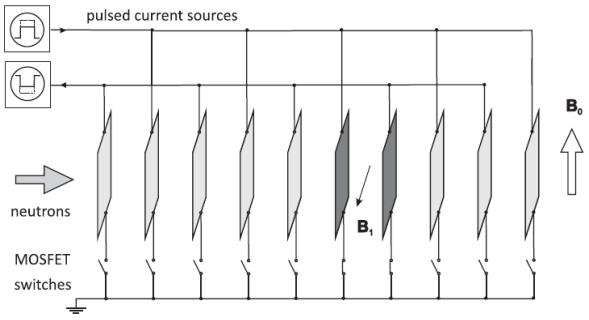

Figure 4: Working principle of the Badurek resonator [27]

2 History of previous works

In this section I want to present what has been done so far in the development of the DRABKIN-resonator and its advanced version the BADUREK-resonator.

2.1 History of the Drabkin resonator

• In 1962 Drabkin from the Leningrad Nuclear Physics Institute (PNPI) first published the principle of a Drabkin resonator [9]. In the following years he and other members of his institute developed this concept of spatial spin resonance much further:
• 1967: Drabkin, Trunov and Runov built the first resonator and first measured its properties [10].
• 1977: Agamalyan, Drabkin and Lebedev published the first spectra of a Drabkin resonator used as a monochromator [11].
• 1979: Agamalyan, Schweizer, Otchik and Kharvronim published the first theoretical description and the corresponding measurements of eliminating the side maxima by using two Drabkin resonators [12].
• 1982: Agamalyan and Deriglazov published the theoretical and practical dependence between the geometry of the resonator and the wavelength distribution [13]. They presented the importance of Gaussian shaping for the first time.
• 1988: Agmalayan, Drabkin and Sbitnev published a short compendium of their previous works in the Leningrad Nuclear Physics Institute [14]. They also gave a very detailed theoretical description of the principal of spatial spin resonance in the Drabkin resonator.
• 1991: Alefeld, Kollmar, Badurek and Drabkin published the first results of the creation of space-time focusing points with a Darbkin resonator [15]. This paper was also a turning point. Since then also many international research groups have investigated the possibilities of the Drabkin resonator.
In the same year Badurek, Kollmar, Seger and Schalt published the first time the usage of a Drabkin resonator in an inverted TOF-measurement [16].
• 1995: Grigoriev, Runov, Okorokov, Tretyakov, Gubin, Kopitsa and Runova further investigated on the possibilities of the Drabkin resonator. They first developed the theoretical background of using the resonator in a guiding field with a gradient in order to reduce the wavelength resolution of the resonator. They also proved this in a real experiment [17].
• 2000: Klimko and nearly the same Russian research group from the PNPI presented the effects of modulation of the spatial periodicity on the wavelength resolution in theory and in experiments [18].
• 2001: Parizzi, Lee and Klose investigated the possible usage of the Drabkin resonator for spallation sources like the SNS in Oak Ridge [19, 20, 21].
• Since 2003 also a Japanese research group around Yamazaki and Furusaka has studied the usage of Drabkin resonators at the JSNS at J-Parc [22, 23, 24, 25].

G. M. Drabkin, the inventor of the Drabkin resonator, died at the age of 92 on July 27, 2014.

2.2 History of the Badurek resonator

In 1991 Gerald Badurek from the Atominstitut (ATI) of the Vienna Technical University, Kollmar, Seeger and Schalt mentioned the idea of splitting the Darbkin resonator into many independent coils in order to reduce the active length of the resonator the first time [16].
In 2003 Badurek and Erwin Jericha published the concepts of the Badurek resonator and the possible traveling wave mode (TWM) in Physics B 335 [27].

2.2.1 Gösselsberger PhD thesis - the Monopol-project

The MONOPOL project started with the beginning of the PhD-thesis of Christoph Gösselsberger [47] in 2009. The Austrian FWF (Projekt Nr. I 528-N20, MONOPOL) and the European Union (Grant Agreement No. 226507-NMI3) financed this project. The goal was to construct a Badurek resonator which can fulfill the requirement of PERC:
This Proton Electron Radiation Channel (PERC) is a future large scale experiment at FRM II in Garching for neutron beta-decay. It consists (like the preceding experiment PERKEO III) of a large evacuated decay volume for neutrons. Large magnetic field coils around this volume guide the charged decay products out of the neutron beam into detectors. To gain information about the weak force out of these decay products, we need a well preprepared neutron beam. The device for the preparation could be a Badurek-resonator. The requirements are: a beam cross section of 6 x 6 cm^2, a wavelength resolution smaller than 0.1 at 5 Å, high degree of polarization, a precisely defined time structure and a maximal transmitting intensity.
Together with Badurek and Jericha, Gösselsberger supervised many students, who did their master thesis, project works or bachelor thesis for the MONOPOL-project.
In 2010 G. Badurek, Ch. Gösselsberger, E. Jericha published the first results in PhysicaB [28]. They discussed the advantage of the novel resonator type due to its time and wavelength structure.
In 2011 Gösselberger et al. published the progress in Physics-Procedia [29]. They described the design of a Badurek resonator, the calculation and simulation of the time structure of the neutron beam, the efficiency of the resonator and wavelength spectrum, the possible operation modes and the possible technical realization to suit the PERC-requirements.
For the simulation in these two papers Anton Buder programmed a software as his bachelor's thesis [50]. This software is loosely based on SPARTAN, a neutron simulation software written by Andreas Welzl during his bachelor's thesis [31] and project work [32].

2.2.2 Prototype 1.0

In 2010 they and many students built the first prototype of a Badurek resonator. It consists only of 10 coils and was used in a thermal dichromate neutron-beam (2.6 Å and 1.3 Å) at the TRIGA-reactor of the ATI.
Gregor Wautischer described the effects of the coil shape on side maxima during his project work [33]. He simulated possible coil shapes and proposed the stage design of the prototype 1.0.
During his bachelor's thesis [34] David Birschitzky set the prototype 1.0 into

operation. He used a power supply which was capable of producing pulses and a normal DC spin flipper.
In order to develop a coil controller which is capable of the TWM, Bernhard Rauer searched for possible hardware components during his project work [35]. He described very detailed the usage of the LPC2378 micro controller and the I^2C-bus. Both components have been used for all developed coil controllers.
For his master thesis [36] Sebastian Nowak developed the first controller and tested it on the prototype 1.0. He also investigated new designs of the stages and the coil controllers [37]. His idea of using side stages to homogenize the magnetic field in the neutron beam influenced the design of the next generation prototype 2.0.
Michael Klopf tried to develop Nowak's controller further in his project thesis [38]. He implemented a resonator electronic consisting of two levels.
During the project work of Wilfried Mach and Tobias Rechenberger [39] the Prototype 1.0 was completed. They gained the first results with the use of Nowak's newly built controller. They also first demonstrated the advantage of the traveling-wave mode in comparison to the conventional mode. They also characterized the prototype 1.0 very detailed.
Robert Raab developed the current-sheet spin-flipper used for the prototype 1.0 during his first project work [40]. He also characterized the small guiding field of this first resonator by simulating the experiment in CST. Later the guiding field and the current sheet were replaced because they were too small for the next-generation prototypes 2.0 and 3.1. Raab reused the supporting structure and compensation field coils of the spin flipper for the current sheet "2013".
During his second project work [41] Robert Raab optimized the set-up of the current sheet and its compensation field. He also measured the magnetic field in the resonator and compared it with the simulations. He did many different measurements which are possible with the prototype 1.0 (e.g.: TOF, transmission, polarization, search for the perfect current settings or the spin-flip efficiency measurements. All experiments in different settings with or without a chopper, the spin flipper, resonator or the super mirror).
In 2012 Gösselsberger, Abele, Badurek, Jericha, Mach, Nowak, Rechenberger published the first experimental results of the MONOPOL project in the Journal of Physics [30]. They described the design of the prototype 1.0, the first measurements at the TRIGA, measurements of the effect of an anti- or normal Gaussian shape in comparison to equally shaped magnetic fields, spin flip efficiencies and time structures measurement of the normal pulse-mode.

2.2.3 Prototype 2.0

In 2012 Tina Gerstmayr, Sarah Gumpenberger, Michael Bacak, Andreas Hawlik and Bernhard Hinterleitner formed the next generation of students. Under the supervision of Badurek, Jericha and Gösselsberger, they built the second and more advanced resonator-prototype called MONOPOL 2.0. This prototype 2.0 consists of 48 stages with two side stages each. It can handle a 6 x 6 cm^2 thermal neutron beam. Therefore, they built larger guiding field coils which have been used since then (Section 3.2.2). They tested the prototype 2.0 manually at the same dichromat beam of the TRIGA reactor in Vienna like the prototype 1.0. Maximilian Zach developed a coil controller for the resonator 2.0 but was not able to finish his work before the long shut down period of the Viennese TRIGA

reactor due to the replacement of the fuel elements. After the restart of the reactor, the prototype 3.1 was already the focus of the MONOPOL project. This prototype 3.1 is designed for VCN and therefore it needs a different controller.
The bachelor's theses [42] of Michael Bacak, Andreas Hawlik and Bernhard Hinterleitner describe: the simulation and testing of the stages with CST, SPARTAN and COMSOL, detailed informations and measurements of the new guiding field and the new gradient spin flipper. This spin flipper can handle the large cross section of PERC but had a poor flip efficiency of only 80%. Therefore, it was not used for later experiments.
The master thesis of Sarah Gumpenberger [43] contains a more detailed description of the stages and the measurements done.
In contrary, Tina Gerstmayr stresses in her master thesis [44] more about the current distribution in one stage, the construction of MONOPOL 2.0, the electric controller of the static power supplies and also about the measurements with different resonator settings (used coil number, combined stages,...).
Maximilian Zach [45] tried to design a controller for thermal neutrons. There he presented: the possible layouts, the realization of the stage controllers, the inductance of it, the heat-production and the best power supply. The coil controllers have already shunt resistors to increase the needed voltage and to be able to use normal power supplies. He measured the inductance and resistance of one stage of the prototype 2.0.
In the end of 2012 Gösselsberger and all involved students and scientists published the results of development of the prototype 2.0 and the demonstration of the traveling-wave mode with the prototype 1.0 in Physics Procedia [46].

2.2.4 Prototype 3.0

The most important task of the MONOPOL project at the time of 2012-2013 was to develop a coil controller for 48 or more stages. The principle design was already developed in the master theses of Sebastian Nowak [36] and Maximilian Zach [45]. Stefan Seifried further developed the ideas during his bachelor's thesis [48]. He created an interface between the user and the coil controllers on the basis of the work of Rauer [35]. He programmed the MONOPOL-ARM development environment Eclipse (M.A.D.E.). He used it to program a web server on the new central master controller (CMC), which consists of a LPC2378 micro controller. An ETHERNET cable connects the CMC with a computer. An I^2C Bus and a PWM connects the CMC with the coil controllers. Seifried further developed the program so that we can send a .csv-file with the resonator settings to the central master control and this controller programs all the coil controllers according to the file. We operate the resonator via the web-interface on the CMC programmed by Seifried (see more Section 4.2).
To generate csv-files Anton Buder programmed a practical software called CSV-GUI as a project work [51] (Section 4.1). In addition, Stefan Kugler developed a program called SpinflipControl which is similar to CSV-GUI but was never used [52].

2.2.5 Prototype 3.1

The next generation of master students was Bernhard Berger, Robert Raab and Stefan Baumgartner. Michael Bacak, Andreas Hawlik and Bernhard Hinterleit-

ner still worked for their project theses on the MONOPOL-project.
The next step for the MONOPOL-collaboration was to test the Badurek resonator in a white neutron beam. At the TRIGA reactor of the ATI there existed no beam line to test the resonator in a white neutron spectrum. Therefore, they applied for a beam time at the ILL in Grenoble. They received the permission to use the PF2B VCN-cabin in summer 2013. The white VCN-spectrum of PF2B simplifies the construction and the testing of coil controllers because the currents are smaller and the flight times of the neutrons are longer. On the other hand, they had to design a new prototype and adapt the experiment due to the strong absorption of VCN in matter.
The reason why the new prototype was called 3.1 is because they changed the stage design in the end of the development of the prototype 3.0 [53](p.50).
Robert Raab wrote in his master thesis [53] about the problems of absorption in the stages and the development of a new stage design. He also designed and constructed a new current-sheet spin-flipper for the large cross-section of PERC. Bernhard Berger described in his master thesis [54]: the other problems with VCN like the need for a passive magnetic field protection and the VCN-coil controller which Baumgartner and he developed. Stefan Baumgartner was mainly developing the resonator electronics together with Bernhard Berger. He also improved the complete software of the resonator electronics after the beam time in Grenoble 2013. This was very important for the next testing period in Grenoble in 2014. During the beam time 2013, all three master students tested the prototype 3.1 under supervision of Erwin Jericha and Gerald Badurek.
Michael Bacak, Andreas Hawlik and Bernhard Hinterleitner wrote in their project thesis [57] mainly about the construction of the magnetic shielding (active and passive), the prototype 3.1, and the box and the absorption of neutrons in aluminum and air.
Matthias Schmidtmayr and Domic Blöch did their bachelor's theses [58] about the adaption of the resonator 3.1 for VCN. They described the construction of the stages very well. This manual is very useful to build new stages in order to replace damaged ones. They also helped to interpret the data which were measured during the beam time 2013.
Floran Pribahsnik simulated during his project thesis [59] the prototype 3.1 to compare it with the results of the beam time at the ILL in 2013. He concluded that the principles are well understood, because the simulation and the real measurements fit very well.
Maja Sajatovic and Matthias Scheiner studied during their bachelor's theses [60] in more details the possibilities of simulations and compared them to the real measurements done in 2013. They also investigated in possible malfunctions like wrongly timing of the traveling wave, not working coils or bad adjusted magnetic fields.
For the beam time in September 2014 in Grenoble I was preparing the MONOPOL-setup with the help of Wilfried Mach and Erwin Jericha. The three of us were in Grenoble at the ILL and explored the limits of the prototype 3.1. I present the measurements and results in this master thesis.

2.2.6 Future

During the last testing period in Grenoble we discovered many opportunities to improve the setup. Already before the beam time in Grenoble, the head of the electronic workshop at the ATI started to design a new coil controller for thermal neutrons. In addition, Wilfried Mach, Erwin Jericha, Michael Bacak [61], Andreas Hawlik [62] and many more are constructing a new thermal-white beam line at the TRIGA reactor in Vienna. There they want to test the MONOPOL with the new electronics. After the construction of PERC and extensive testing in Vienna, the MONOPOL-project can reach the final goal and can be used as a beam preparator in the PERC-experiment.

3 Technical description of the Monopol-Setup

In the following sections I will describe in detail all components of the MONOPOL-setup. I will also depict possible improvements of each component.

I use the following coordinate system:
x-direction: in direction of travel of the neutron beam. This means from right to left if you stand in front of the MONOPOL-setup.
y-direction: horizontal and perpendicular to x and z-direction, pointing from the middle of the box towards the side panels.
z-direction: vertical upwards.

A short overview of all components:
An aluminum box contains (Fig. 5): the resonator and its electronics (coil controllers), one or two current-sheet spin flippers, two super mirrors for polarizing and analyzing the neutron beam, two fluxgates to monitor the magnetic field in the beam line, a pair of Helmholtz coils to produce a guiding field for the spin in z-direction, a second pair of Helmholtz coils and a solenoid to compensate parasitic homogeneous magnetic field in y-direction and in x-direction respectively.
Outside the box (Figure 6 on page 27), there is an OLIMEX-board as the CMC, which is the interface between a computer and the coil controllers, all needed power supplies, a water cooling system, a He-3 detector, a chopper and some computers to control all components.

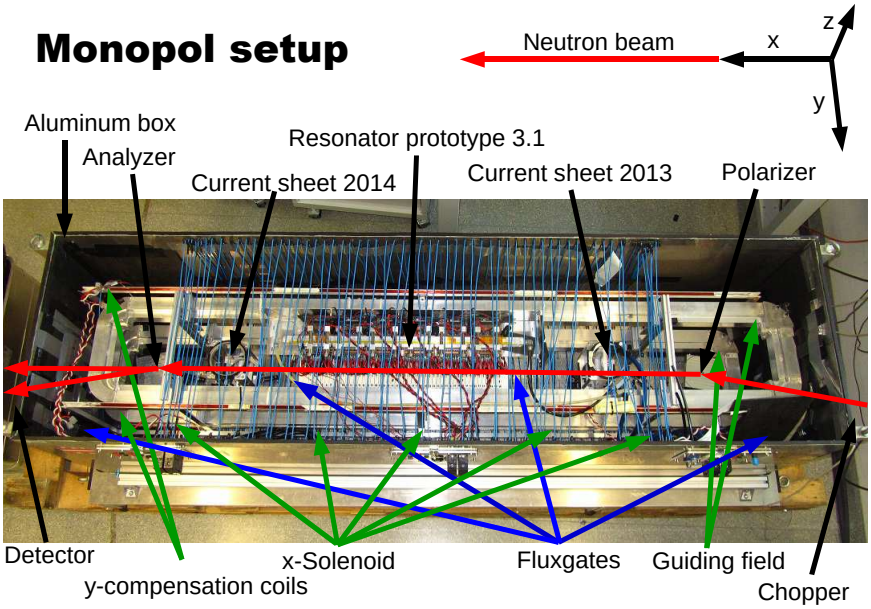

Figure 5: The MONOPOL-setup during storage after the beam time 2014. Some parts are missing because they were borrowed or stored separately.

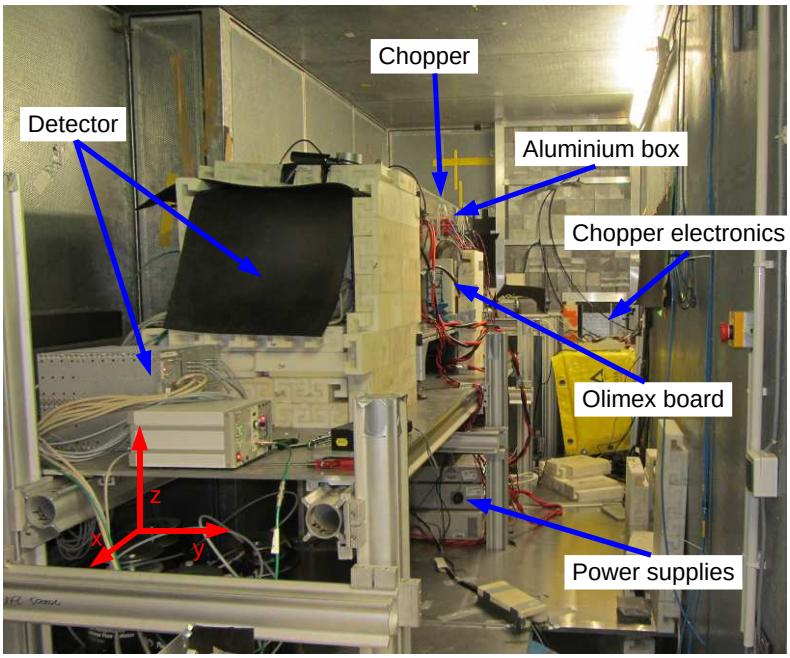

Figure 6: The MONOPOL-setup during operation in 2014. ©Mach

3.1 Resonator 3.1

Robert Raab designed the Resonator 3.1 during his master thesis [53](p.24-54). Due to the fact that aluminum strongly absorbs VCN, he reduced the thickness of the stage-coils from stable 0.3 mm aluminum sheets to deformable 0.1 mm aluminum foils (Figure 7 on page 28). Therefore, he developed a more stable stage design without side stage. He folded the edges of the aluminum foil once to increase the stability. The double layers act also as side stages. The prototype 3.1 only needs 48 electronic channels for operation instead of the 144 channels of the prototype 2.0. The produced magnetic field is as homogeneous in the area of the neutron beam as in the resonator 2.0 but needs a 62% higher current [53](p.50).

Raab, the project students Michael Bacak, Andreas Hawlik and Bernhard Hinterleitner [57](p.14-21,24-25,27) assembled with the bachelor students Dominic Blöch and Matthias Schmidtmayr the prototype 3.1 together. You can find a good construction manual in their bachelor's theses [58](p.18-25).

The prototype consists of a plastic-box, which has two entrance windows for the neutron-beam on both end planes. This small box stands on two metal legs. The top is open to insert 48 stages. Above the plastic box a metal plate carries six coil controllers.

I measured the thickness of one stage as $a = 1.21(3)$ cm. In the previous works I found the value 1.2 cm [57](p.7). In Table 9 on page 47 in Section 3.8.2 you can find more information about the flight times of the neutrons and the needed currents in the stages.

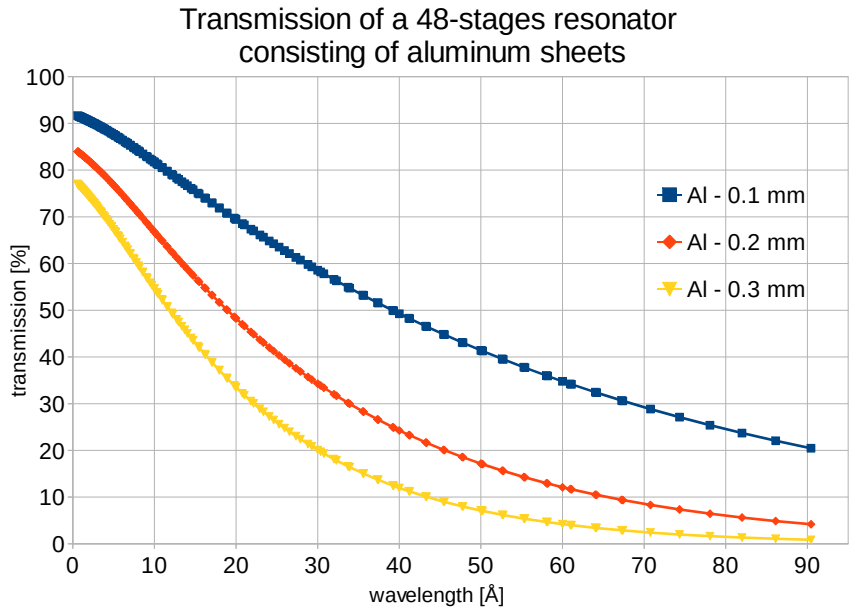

Figure 7: The calculated transmission through a resonator due the Beer-Lambert law. The values of the total neutron cross-section are taken from ENDF [64].

3.1.1 Problems with the prototype 3.1

The prototype 3.1 has some disadvantages in comparison to the prototype 2.0. First, the quality of processing of the plastic parts is a lot worse. The workshop of the Atominstitut built prototype 2.0 very precisely. In contrast, an external company produced the resonator 3.1. Although they used CNC-milling machines, similar parts are not equally shaped. The construction team had many problems to insert all 48 stage coils because of the different thickness. They needed a lot of time to find an order where every stage fit in the prototype 3.1. To lose this order never again, I wrote a number on every coil to be able to insert all stages without difficulties.
Another problem is the needed thickness of aluminum in order to transmit the VCN-beam. The thin foils, which are bended to the coils of the stage, are very ductile and we have to flatten the coils from time to time. In addition, the coils are a little bit too long and are only loosely fixed by two plastic bars in the plastic frame of the stage. Therefore, the foils deform easily. It will be better if the supporting structure inside the coil is not only two bars but more a window-like frame, which leaves only a space open for the neutron beam similar to the entrance windows of the resonator.
Due to the thickness of the foils, we can't contact the stage directly as at the prototype 2.0. We have to use contact plates in between. Due to the gross cutting of the plastic parts sometimes there is not enough space for both contact plates. This makes it harder to insert the stages into the resonator. Between the plates and the coil there is a small piece of isolating plastic foil to prevent

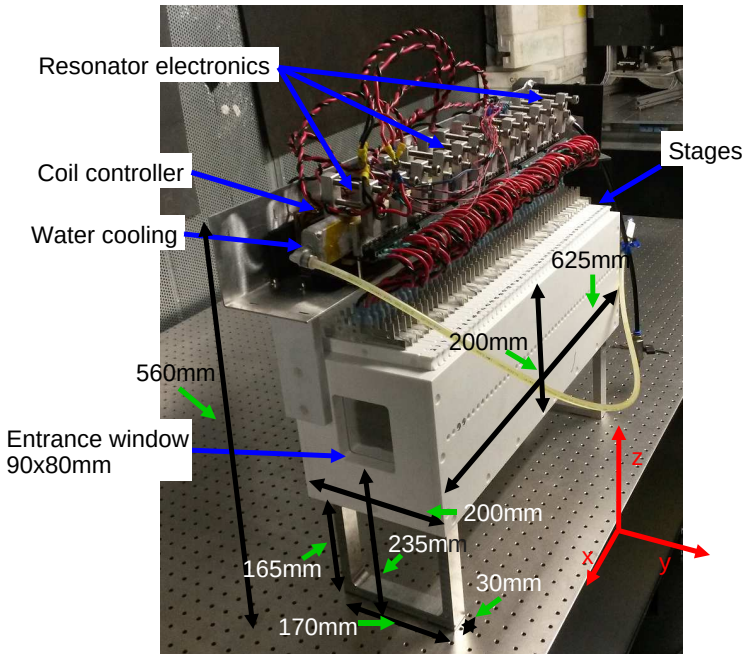

Figure 8: The prototype 3.1 with the VCN-electronic and the aluminum contact plates

a short circuit of the coil. One screw holds everything together. So it is very important that the hole for the screw in the isolating foil is smaller than in the coil and the plates. We tried this by stamping out the holes in the foils instead of drilling them what the construction team did. Furthermore, the isolating foils are not shaped equally and have no space in the plastic frame. Due to that it is hard to say if the insulator really prevents a short circuit.
Andrzej Pelczar the head of the electronic workshop of the Atominstitut did some tests with the coil stages. With an infra-red-camera he showed that the current runs mainly in the middle of the coil. Additionally, the contact between the aluminum contact plates and the aluminum foil of the stage is rather poor and not uniform over the entire area. The best contact is on the edge of the foils, because there is a double layer. Furthermore, the resistance of coil varies a lot due to the pressure applied on this contact, time, temperature, or disturbances like hitting the table.
To avoid the problem with the aluminum-aluminum contact, we changed the contact plates. We first tried to coat the aluminum plates with gold. This reduced the voltage drop in the contacts to a very constant level but the gold layer started to peel off. Consequently, we ordered new copper contacts plates. Due to delay we were not able to coat them with gold before the beam time in Grenoble 2014. Nevertheless, I changed all contacts plates from aluminum to copper. By measuring with a normal multimeter, we saw a reduced resistance of the contact. However, it is preferable to remove again all copper contact plates, coat them with gold and build them in again. This will be a very time-consuming work. To avoid a lot of extra work follow this instructions: To remove a contact plate, you have to loose the three upper screws and remove the middle one.

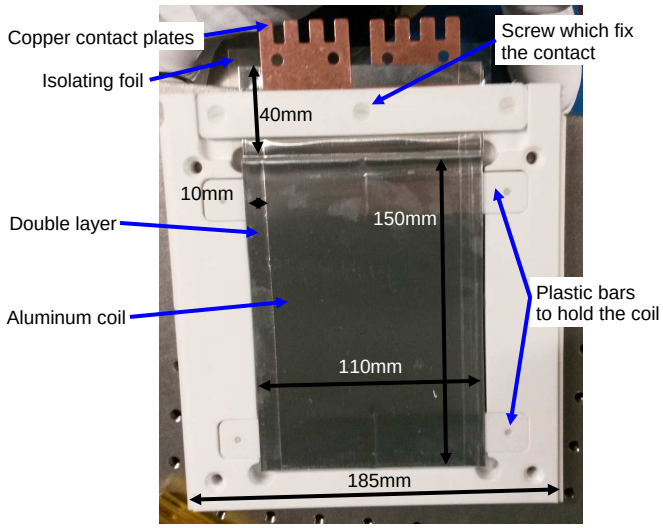

Figure 9: One stage of the prototype 3.1 with two copper contact plates

Then you can remove the contact plates. Now you can coat them with gold. It is important when you place the contact plates back into the stage that you screw the middle screw not to deep because otherwise it will scratch the coil of the next stage when you place the stage back into the resonator. During this procedure, I checked also all coils. When they were strongly deformed, I had to remove all screws and take the aluminum-coil itself. To straighten the coil again I used the same tools and the same procedure as for bending the coil for the first time. With great care I placed the coil back into the frame and fixed all screws again. The fact that not all screws of the plastic frame are on the same side of the stage complicates the flattening of the coil.

3.2 Magnetic environment

The resonator needs only a magnetic field in the z-direction as a guiding field. The other components of the magnetic field should be zero. Therefore, we use two pairs of Helmholtz coils, which produce the guiding field and a zero field in y-direction, and one solenoid to provide the zero field in the x-direction. Since 2014 we use also two fluxgates inside the box to monitor the magnetic field near the resonator. The LabVIEW program MCS (MONOPOL CONTROL SYSTEM) reads the fluxgates and adjusts the current or voltage limits of the power supplies of the connected coils with a feedback loop (see more in Section 4.4). This provides ideal conditions for the resonator.

3.2.1 Fluxgate SENSYS FGM3D

The fluxgate consists of the control unit SENSYS FGM3D TD and the magnetic field probe FGM3D/1000. This probe can measure the magnetic field strength in all three directions independently in the range of ± 1000 µT. The probe is connected to the 15-pin D-Sub socket of the control unit, which is further connected with the computer via USB.

At the moment we are using two fluxgates. We taped the probes below the entrance windows of the resonator with the orientation of the common coordinate system. The control units are in the edges of the big aluminum box. For the power supply we use a Voltcraft SNG-2250-OW (12 V & 1 A max) which is connected to the middle panel of the box with two Banana pins (Farnell element 14: black 169-8964 (GND), green 169-8968 1 BD (+12 V)). The control units are connected with a coaxial power connector (5.0/2.1 mm, GND outside) to cables which are attached to the middle panel as well.
A special program from SENSYS reads one fluxgate and displays the measured values. The program can stream these values (time of measurement, B_x, B_y, B_z, $|\mathbf{B}|$) into a virtual COM-Port. The program MCS reads the COM-Port. It is important that the MCS reads the cache of the interface faster than SENSYS-program writes the values into the cache. Otherwise, the SENSYS-program slows down until the cache is full and then the program freezes. In order to unfreeze it, we run a LabVIEW program that just reads the data of the COM-Port as fast as possible. To synchronize both programs, I use the time difference between the measurement and the readout of the COM-Port to adjust the reading speed of the MCS. Caution, the time of the measurement is converted in a time stamp, which is the number of ms that have passed since December 31st 1971, 11pm. The MCS synchronizes itself with the fluxgates. Adjusting the average sample rate in the SENSYS-program also changes the pace of transmitting.
In order to use two fluxgates, we have to open two SENSYS-programs which use two different COM-Ports.
During the beam time 2014 in Grenoble the usage of the fluxgates for monitoring and stabilizing the magnetic field inside the resonator improved usability significantly. Before that we only estimated the strength of the magnetic field during the experiments. These values relied on poorly measured parameters (Section 3.2.2). For all the future experiments, we should monitor and stabilize the magnetic field by fluxgates or gaussmeters. Additionally, more measuring points would help to detect gradients in the magnetic field induced by the surroundings and the spin flippers.

3.2.2 Guiding field

Tina Gerstmayr [44](p.26-27), Sarah Gumpenberger [43](p.34-35), Michael Bacak, Andreas Hawlik and Bernhard Hinterleitner [42](p.31-32) designed and constructed a larger pair of Helmholtz coils as the guiding field of the prototype 2.0 under supervision of Gösselsberger [47](p.99-100). Since then, we have used this pair of coils for every following prototype.
The wire is coiled around a hollow profile made of aluminum (Fig. 12). Inside the hollow profile there are three water pipes (Fig. Figure 10 on page 32), which can be connected to a water cooling system (aquaduct mark IV, aquacomputer). To maximize the heat transfer between the copper wire and the profile, the constructing team placed additional aluminum blocks on the wire to press it into the profile. The heat-production limits the maximum current running trough the coils to 10 A (300 W) which corresponds to a coil temperature of 70°C. I dismantled the ends of the wire to improve the contact to lever-lock Wago cage clamps (222-412). From these clamps normal wires (2.5 mm PVC-insulated-single-core copper wire for <24 A) connect the coils to the left panel of the Vacuum box. I connected the wires in the way that the direction of the

current is from red to white/black (cable/socket) and produces a magnetic field in the negative vertical direction (-z-direction) parallel to the magnetic field of the super mirrors.

In appendix A you can find more information about the measurements of

Table 3: Guiding field parameters

Parameter	Value
coil dimension	2 m x 0.25 m
length of 1 winding	4.42 m
number of windings W	159-200
used wire	DIN EN 60317-0-1 [47](p.158-159)
inner diameter	1.6 mm [47](p.158)
isolator	isolating lacquer (>10 MΩ)
outer diameter	1.69 mm [47](p.158)
resistance per meter R_{wire}	0.0085 $\frac{\Omega}{m}$ at 20°C [47](p.158)
resistance of the upper coil	$5.91 \pm 0.02\ \Omega$
resistance of the lower coil	$5.94 \pm 0.02\ \Omega$
total resistance R_{Guide}	$3 \pm 0.01\ \Omega$
produced B field per Ampere	$\approx 2.5\ \frac{Gauss}{A} = 250\ \frac{\mu T}{A}$

the relation between current and produced magnetic field and the number of windings W.

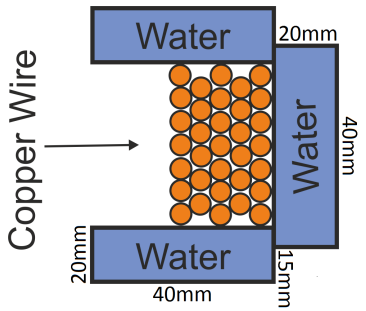

Figure 10: Cross-section area of the guiding field coils [43]

Table 4: Guiding field settings for prototype 3.1

Wavelength	B-field (B_0)	Current	Voltage	Power
70 Å	69.8 µT	0.289 A	0.86 V	0.25 W
60 Å	93.1 µT	0.38 A	1.15 V	0.44 W
50 Å	111.8 µT	0.46 A	1.38 V	0.64 W
40 Å	139.7 µT	0.58 A	1.7 V	1 W
30 Å	186 µT	0.77 A	2.3 V	1.8 W
20 Å	279 µT	1.15 A	3.46 V	4 W
10 Å	559 µT	2.31 A	6.9 V	16 W
5 Å	1.12 mT	4.6 A	13.83 V	64 W
3 Å	1.86 mT	7.7 A	23.05 V	177 W
2 Å	2.79 mT	11.5 A	34.6 V	400 W
1 Å	5.59 mT	23 A	69.2 V	1597 W

3.2.3 Protection against the magnetic field of the earth and other sources

Due to the VCN-configuration ($\lambda \approx 20$ Å $- 70$ Å), the magnetic field of the guiding field ($B_0 \approx 279$ µT - 70 µT) and the stages ($B_0 \approx 9.1$ µT - 2.2 µT) are very low and comparable with the magnetic field of the earth ($B_x \approx 21$ µT and $B_z \approx 44$ µT)[54](p.18). In the VCN-cabin at ILL, there are also other sources for disturbing magnetic fields: the walls of the cabin, which are made of soft magnetic iron and are easily magnetized by small magnets up to 50 µT, small magnets hanging on the walls everywhere or the huge crane on the ceiling of the reactor building. The biggest disturbance was the optical table on which we placed the MONOPOL-setup. The iron structure inside the table produced fields up to 300 µT. All these parasitic fields have in common that they are not homogeneous like the earth's magnetic field and have strong gradients, which complicates the shielding.
To solve this problem we used different methods. First we cleaned the surrounding area by removing all magnets close to the experiment. We removed magnetic spots in the walls by searching for them with a gaussmeter and demagnetized the spot mechanically by hammering with an aluminum bar on it. Moreover, we had to remove the heavy optical table and replace it with a self-made aluminum table made of X95 profiles (Fig. 11). To eliminate the remaining field, we have

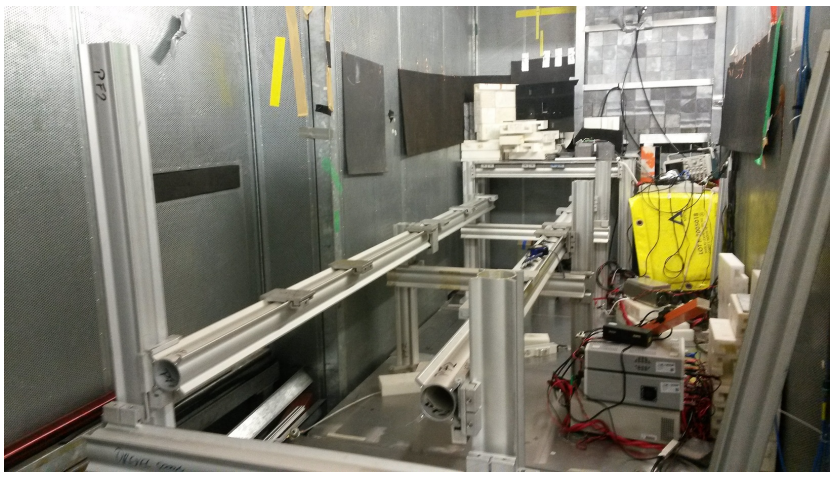

Figure 11: Aluminium table to carry the MONOPOL-experiment

two options. One is to produce a magnetic field equal in strength and in the opposite direction of the remaining magnetic field. The other is to build a high µ-metal shielding around the experiment, which bends the magnetic field lines outwards into the shielding [54](p.23).
During the beam time in 2013, the experiment team borrowed enough µ-metal from the Q-bounce group to cover the entire experiment. As a result, they had a nearly field free space in the experiment box. In 2014 the Q-bounce group were working in Grenoble at the same time and needed the shielding themselves. We could only use some old µ-metal plates and had to use the method of active compensation.
For this method, we used different coils for each directions. We used the guiding-

field coils for the z-direction, an already built Helmholtz-coil-pair for the y-direction and the new large solenoid for x-direction. All these coils produced nearly homogeneous fields and we stabilized the field strength with two fluxgates and the LabVIEW program MCS to $\vec{B} = (0/0/B_0)$. This setup of coils cannot compensate the gradients of the stray magnetic field. For this purpose, we used the spin flipper as a source of a magnetic gradient. We placed the resonator in an area where the gradient induced by the surroundings nearly cancels out the one from the flipper.
For future experimenting cycles with VCN: we have to avoid carefully stray magnetic background fields which may cause disturbances. In addition, coils which induce a magnetic gradient or even higher orders for compensation are possible to create a more homogeneous field in the beam. On the contrary, a strong gradient in the guide field can reduce the wavelength resolution of the resonator [17]. If we place all components on motion controllers, we can better adjust the resonator and the spin flipper for the gradient compensation, even if we operate in a helium atmosphere. The alignment between the fluxgates and the guiding field is very critical too. If we misalign them by one degree, 1.75% of the absolute guiding field strength will appear in the x or y component. This is more than the precision of the active stabilization in these directions. The MCS starts to compensate these contributions too.

3.2.4 The compensation-field coils in x-direction

Before the beam time in 2014, Erwin Jericha, Wilfried Mach and I developed and constructed a coil for the compensation of the magnetic field in x-direction (parallel to the neutron beam). We decided to build a large solenoid around the experiment along the inner surface of the box.
We built the solenoid in the following way: We bent stiff wires into u-like shapes and connected them to luster terminals which we glued close to the top of the inner wall of the box. In addition, we fixed these wires with tape on the wall of the box to keep the right spacing between the wires. We connected additional wires to the luster terminal to form the top of the solenoid which now looks like a cage around the experiment (Fig. 12). To access the experiment again, we just remove the top wires by opening the luster terminals. It is important after reassembling the solenoid to check if all wires are well connected, by checking the resistance of the solenoid.
On both ends there are additional windings, which can be separated to form two additional solenoids - the so called endcaps. We need the endcaps to produce a more homogeneous field in the volume close to the end of the solenoid, where we placed the spin flippers. The windings of the endcaps are marked with black tape. During operation in 2014, we connected the endcaps serially to the main solenoid because we had too few power supplies to have one channel free to supply the endcaps.

Table 5: x-compensation field solenoid parameters

Parameter	Value
length of the solenoid	1.35 m
length of the endcap	50 mm
size of one winding	0.58 m x 0.58 m
spacing between the Windings	25 mm
spacing at the Endcaps	1 mm
number of windings $W_{x-solenoid}$	55
number of windings $W_{x-endcap}$	4
used wire	H07V-K VISIBOX and H07V-U Blue 5015 1x2.5mm^2, RS 1924531, CCCN 85444995
used luster terminals	Legrand 0 342 11: RS 279-8793
resistance $R_{x-solenoid}$	>2 Ω
resistance $R_{x-endcap}$	0.4 Ω
produced B-field per ampere	$0.441\frac{G}{A} = 44.1\frac{\mu T}{A}$ and $0.0093\frac{G}{A} = 0.93\frac{\mu T}{A}$
needed power supply for solenoid	1 A & 2.2 V

3.2.5 The compensation-field coils in y-direction

This pair of Helmholtz-field-coils were designed by Robert Raab [53](p.55-62) in CST EMS and built by Michael Bacak, Andreas Hawlik and Bernhard Hinterleitner [57](p.12).
The wire is wound around a rectangular hollow profile. Both coils are screwed on the supporting structure of the guiding field (Fig.12). The connections for the power supply are similar to the one of the guiding field.
The coils can only compensate the earth's magnetic field or other homogeneous magnetic fields in the y-direction (perpendicular to the guiding field and the neutron beam). The compensation in the y-direction is important because the small magnetic fields of the resonator (B_1) have the same direction.

Table 6: y-compensation field coils parameters

Parameter	Value
size of the coils	2.015 m x 0.36 m
thickness of the aluminum sheet	2 mm
dimensions of the hollow profile	14 mm x 14 mm
gap of the hollow profile	10 mm
spacing between the coils	0.34 m
resistance R_{y-comp}	0.615 Ω
number of windings W	≈ 30
produced B-field per Ampere	$0.35(1)\frac{Gauss}{A} = 35(1)\frac{\mu T}{A}$
needed power supply	5 A & 3.2 V

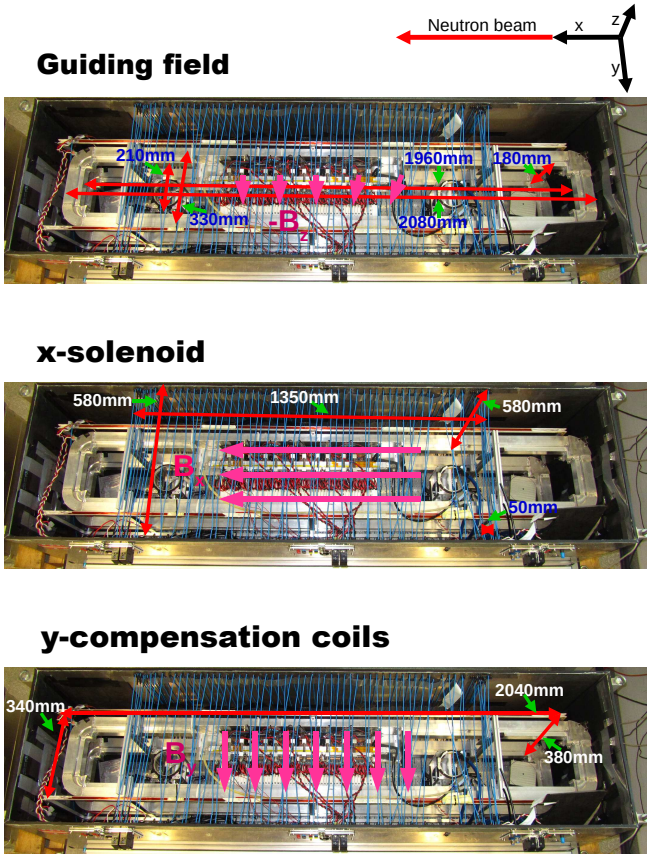

Figure 12: A summary of all used coils

3.2.6 Passive magnetic field shield

Bernhard Berger [54](p.24-35) simulated the passive shielding made of materials with a very high permeability µ with the software COMSOL. Due to the high permeability, the magnetic field lines bend into the shielding and leave a nearly field free space in the shielded region. Berger showed that it is possible to shield the experiment with four plates placed around the experiment. For the beam time in 2013, the MONOPOL-team borrowed four suitable µ-metal plates from an experiment of Hanno Filter and Tobias Jenke. These plates were a specially treated 80% NiFe-alloy sheets from the company SEKELS [63]. This alloy has a permeability of $\mu_r = 50000 - 140000$ but due to mechanical stress it can be reduced to $\mu_r = 150$. That is why we have to handle it with care. The team at that time constructed a special frame made of item profile and fixed the µ-metal plates with c-clamps on it [57](p.7-11).
Berger measured the strength of magnetic field components inside the box at ILL during the beam time 2013. He measured around 1-2 µT in every direction with the shielding instead of maximum 40µT without. This was good enough to only shield the experiment passively [54](p.32-35).

During the beam time 2014 we didn't have these plates. Instead, we only had some pieces of old µ-metal. They only improved the shielding a little bit. Therefore, we used an active shielding.

3.3 Spin flippers

We used two 0.03 mm thick aluminum current sheets as the broadband-spinflipper [53](p.72) which change the spin of the neutrons in a non adiabatic process [54](p.6)(Section 1.4.1).
Robert Raab designed these current sheets for a 6x6 cm^2 large VCN beam [53](p.62-67). The first current sheet was assembled for the beam time in 2013. We call this spin flipper "(old) current sheet 2013". The compensation coil of the current sheet 2013 is recycled from the old spin-flipper which was used for the prototype 1.0 [40](p.11-31). This spin flipper had a very small cross section and was used in a smaller guiding field. Raab developed both current sheet designs with the usage of CST-EM and SPARTAN. He also measured and optimized the settings of the current sheet [53](p.77-80).
In August 2014, the workshop of the Atominstitut built a second current-sheet spin flipper with the same design as the current sheet 2013. We call the new spin flipper "(new) current sheet 2014". I wound 100 windings on the compensation coils with a special winding machine which is situated in the technology laboratory of the ATI. Raab did the same for the current sheet 2013 in 2011 [40](p.29-31). Furthermore, I exchanged the aluminum contact plates with copper plates. In addition, I assembled new wires for the power supply of the current sheet (Fig. 13). These 35 mm^2 copper wires were part of an audio cable set (Dietz 20135). They withstand currents of more than 100 A. At one end, I split the wire in four equal parts and soldered a crimp receptacle on each end (Te Connectivity 62998-2, RS 719-7022) for the contact with the fringes of the contact plate. To improve the safety, I isolated the bare cables with shrink tubes and tape.
We are very certain that the workshop used different isolating plastics, which hold the current sheet. The current sheet 2013 withstands an applied current of 100 A for longer than a week. During the beam time 2014, we used the current sheet 2014 for the first time. After some days of applying a current of 100 A to the sheet, the plastic melted and the current sheet ripped in two pieces (Fig. 13). After that incident, we measured the spin flip efficiency carefully at different current values (see measurements in Section 6.2.1). We concluded that 50 A is sufficient. In the future we can only use very heat resistant plastic as an isolator and supporting structure.
I measured the produced B-Field of the compensation field close to the current sheet (Fig. 14) with the newly bought fluxgate and the LabVIEW controlled HAMEG HMP2030-power supply. I did the same measurement with both current-sheet spin flippers in the same geometry. Both seemed to be very similar. During the beam time 2014 we measured a big difference in the ratio between the compensation-coil current and guiding field strength at the best flip efficiency. In addition, I measured that the compensation field coils did not produce a homogeneous field in the region of the neutron beam. The compensation-field coils are not a Helmholtz configuration because the coil diameter is much smaller than the distance between the coils. This can be the result of reusing the compensation coils of the spin flipper from the prototype 1.0.

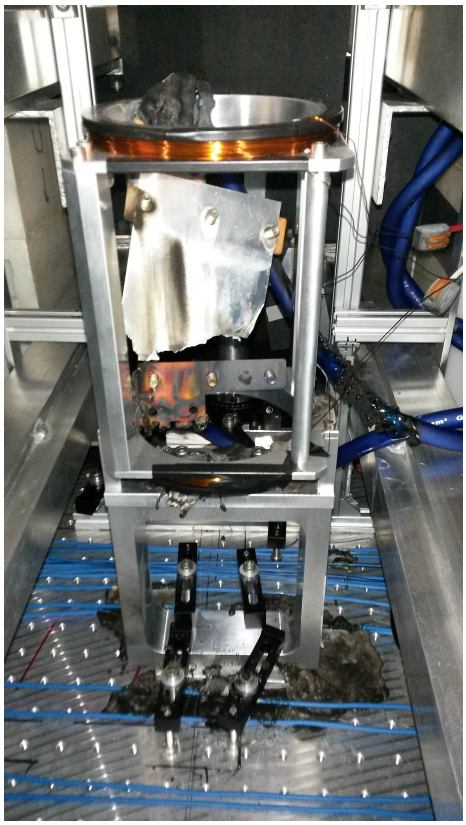

Figure 13: Spin flipper 2014 after melting of the plastic parts due to heating up of the current sheet

The spin-flip efficiencies of both spin flippers are very sensitive to the position of the current sheet. In 2014 we gained more flip efficiency in comparison to 2013 by adjusting the position of the current sheet manually as well as possible. A motion control system for the spin flippers would further improve the flip efficiency and reduce the time for calibration of the current sheet.

Table 7: Current sheets

Spin flipper	Old/2013	New/2014
number of windings of the Compensations coils	100 [40](p.11-15)	100
B_x	-37.85 $\frac{\mu T}{A}$	-34.127 $\frac{\mu T}{A}$
B_y	-1.11 $\frac{\mu T}{A}$	-1.438 $\frac{\mu T}{A}$
B_z	198.8 $\frac{\mu T}{A}$	194.03 $\frac{\mu T}{A}$
|B|	197.5 $\frac{\mu T}{A}$	189 $\frac{\mu T}{A}$
$R_{currentsheet}$	0.26 Ω	0.28 Ω
$R_{compensationcoils}$	1.2 Ω	1.16 Ω
Wire	r_w=0.8 mm [40](p.13)	Isodraht Multogan 2000 MH G1 (DIN EN 60317-29)

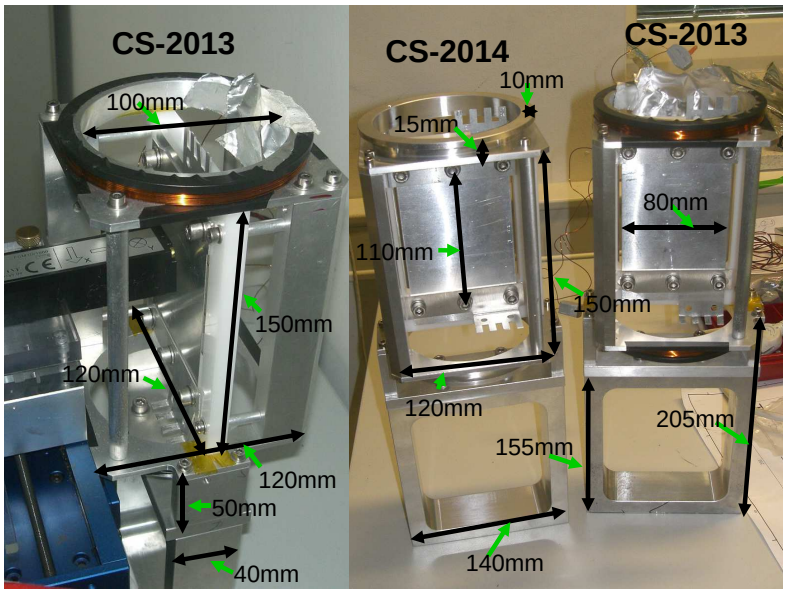

Figure 14: Left: current sheet 2013 during a B-field measurment. Right: both current sheets short after the construction of the current sheet 2014 before the winding of the compensation field coils. Both spin flippers still had aluminum contact plates.

3.4 Super mirrors

We borrowed two super mirrors from a Japanese group. These mirrors are round polished plates consisting of a Fe/SiGe multilayer structure [54](p.56). The mirror itself is fixed on a special metal structure. Strong ferromagnets are placed below and above the mirror on the supporting structure. They produce a magnetic field in the z-direction parallel to the guiding field. This field aligns all the magnetic moments in the ferromagnetic layers of the mirror. Neutrons are scattered differently due to their magnetic moment (see more Section 1.3). The reflected and the transmitted beam are polarized. The degree of polarization in the reflected beam is 95.9% (more details in Section 6.2.2). An even higher degree of polarization will further increase the signal-to-noise ratio and consequently the usability of the MONOPOL-setup.
We used the super mirrors not only as polarizers and analyzers but also to guide the neutron beam through the experiment. Finding the perfect adjustment of the mirrors is very important. The count rate in particular strongly depends on the adjustment. In 2014 we had a count rate more than 10-times higher than in 2013 due to a more precise adjustment (Section 6.1.1). In the future we should consider setting the super mirrors on movable tables to adjust the neutron beam automatically and with a higher precision. These tables should be movable at least in x- and y-directions and turnable around the vertical axis. A movability in z-direction is not that important but still preferable.
In 2014 Mach did not perfectly align the analyzer with the neutron beam. A small fraction of the beam passed the analyzer without hitting the mirror. We call this beam “monitor beam”. The intensity of the monitor beam depends on

the power level of the reactor and the absorption in the experiment. We call the reflected beam of the analyzer "test beam". The test beam depends also on the resonator settings and the current sheet settings. In the analysis of the measurements, I always used the monitor beam to rescale the test beam or to subtract the background (TOF). The concept of a monitor beam improves the usability of the resonator extraordinarily.

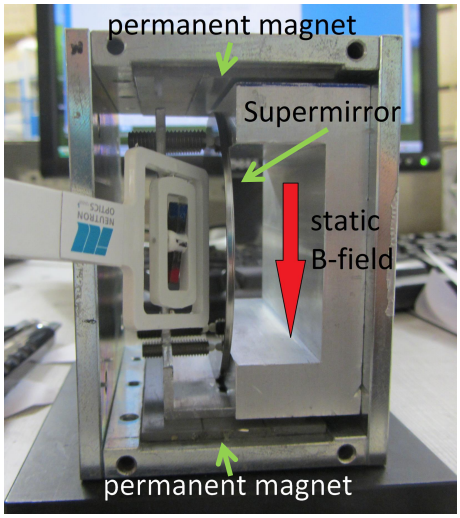

Figure 15: Japanese super mirror ©2014 Wilfried Mach

3.5 Chopper

During both beam times in Grenoble we used the same disk-chopper from the Japanese group of Dr. Hino [53](p.70) [54](p.56). The chopper is always situated in front of the MONOPOL-setup, close to the end of the neutron beam pipe which guides the VCN into the cabin (Figure 6 on page 27). Hanno Filter characterized the chopper very well [65]:

Table 8: chopper parameters

Parameter	Value
size of the disk	2.015 m x 0.36 m
thickness of the disc	5 mm
material of disk	aluminum with gadolinium lacquer
frequency	10-30 Hz
duty cycle	3.63%
opening time at 10 Hz	2 ms
fall/rise time at 10 Hz	1.44 ms

3.6 The box

During the phase of MONOPOL 3.1 all components were optimized for a VCN beam. Air (in specific nitrogen) strongly absorbs VCNs. Only less than 25% of the neutrons reach the detector (Figure 17 on page 42). Therefore, the team at this time constructed an airtight chest to contain most of the experiment (Figure 16 on page 41). This chest we call simply "the box". The main purpose of the box was to be able to change the gas around the experiment, for example to helium. This noble gas has a much lower neutron absorption rate than air [57](p.13-16). An additional advantage of the box is that the MONOPOL-setup became easier to transport.
The box itself is made of aluminum [54](p.52) [57](p.22-23). The wall thickness is 1 cm and the thickness of the bottom is 2 cm. On each narrow side there is one entrance window for the neutron beam, which is made of aluminum foil. On the front side there are three panels with many feed through for different proposes. A detailed list you can find in the appendix B. The cover plate is made of acrylic plastic and is fixed with 10 toggle catches. Roman Gergen did the CAD-design of the total box.
The box contains the resonator, the guiding-field coils, the compensation-field coils, the spin flippers and two super-mirrors (Figure 5 on page 26). To fix this equipment in the box, there is an array of screw holes in the floor of the box with a spacing of 2.5 cm.
The new thermal white beamline at the TRIGA-reactor at the Atominstitut is optimized for the dimensions of the box even though there will be only air in the box.

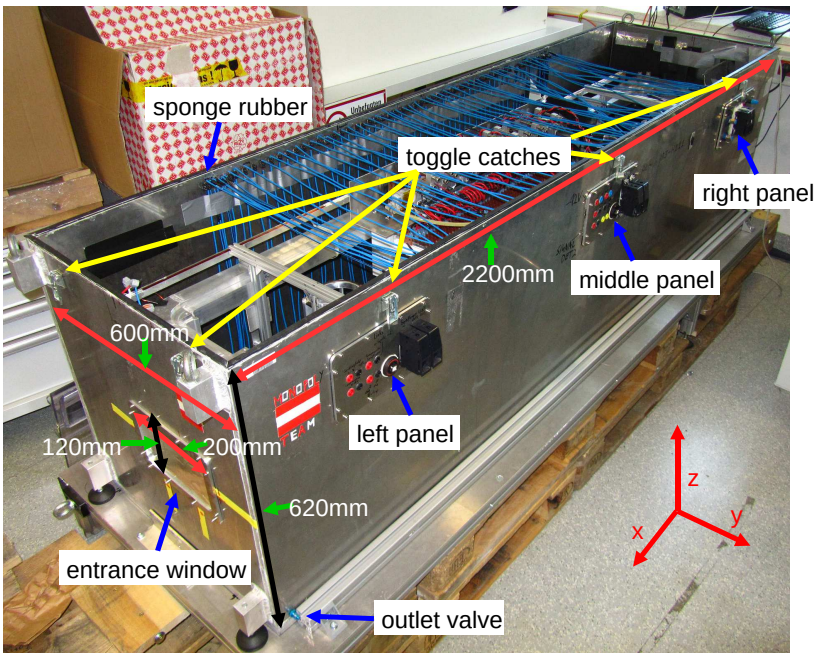

Figure 16: The aluminium box containing the MONOPOL-setup.

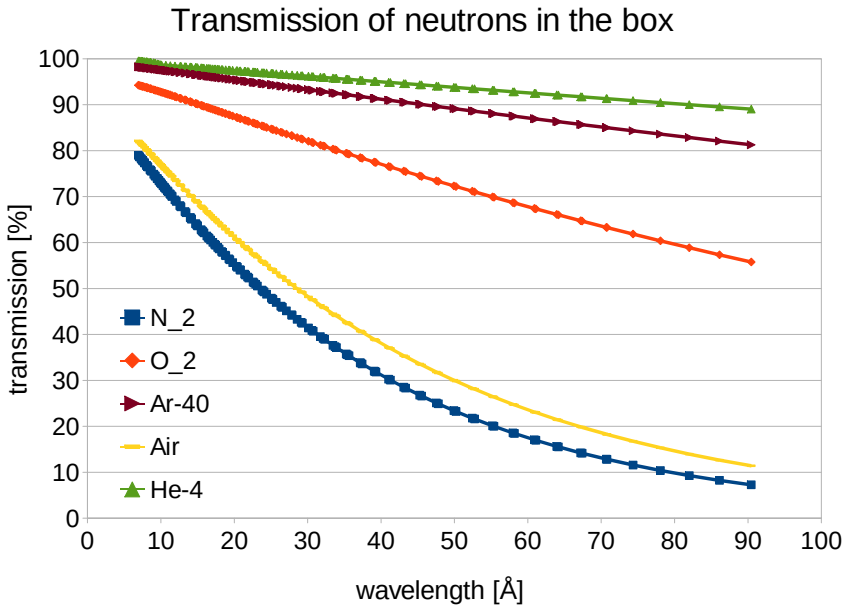

Figure 17: Transmission of neutrons in different gases at normal air pressure [64].

3.6.1 Steps to achieve airtightness

The box is designed to be airtight. For changing the gas mixture, the box has an inlet valve on the right panel and an outlet valve on the bottom left of the front side. During the first test cycle in Grenoble 2013, the experimenter vented the box with helium which supplanted the normal air due to a slight overpressure through the outlet valve. They achieved the overpressure by guiding the gas from the outlet valve with a pipe into a bottle filled with water. The overpressure and the gas flow depend on the adjusting of the immersion depth of the pipe and the opening of the valve of the helium bottle. It takes more than 4 days to achieve a stable helium-atmosphere inside the box. It would be much faster if we could evacuate the box to a pressure below 10 mbar and then vent it with helium. For this purpose the box would have to be vacuum tight. There are three weak spots that prevent us doing so: leakage of the panels and the cover plate and the mechanical stability of the entrance windows for the neutron beam. Probably the electronic inside the box can be damaged by too much under pressure. Our improvements were to diminish the leakage in the following ways:
We replaced all three panels with more vacuum tight versions to have enough feed-through for all new components. We only used sockets which were gas-tight or sealed them well enough by mounting adhesive. The old panels only had holes for the high current cables. After putting them through, the holes were sealed with silicone. This was air tight enough but extremely sensitive to mechanical stress on the cables. We also replaced the gasket between the box and the cover plate respectively the front panels. Instead of normal window seals we used sponge rubber which we glued on the aluminum box with mounting adhesive.

This worked quite well for the front panels but the cover plate still had a huge leakage. The three toggle catches on each long side of the box deformed the plastic cover in such way that large gaps between the cover plate and the box appeared between the toggle catches. We control this problem by gluing a second layer of sponge rubber on the edge of the box and placing lead blocks on the cover to close the gaps again (Figure 18 on page 43).

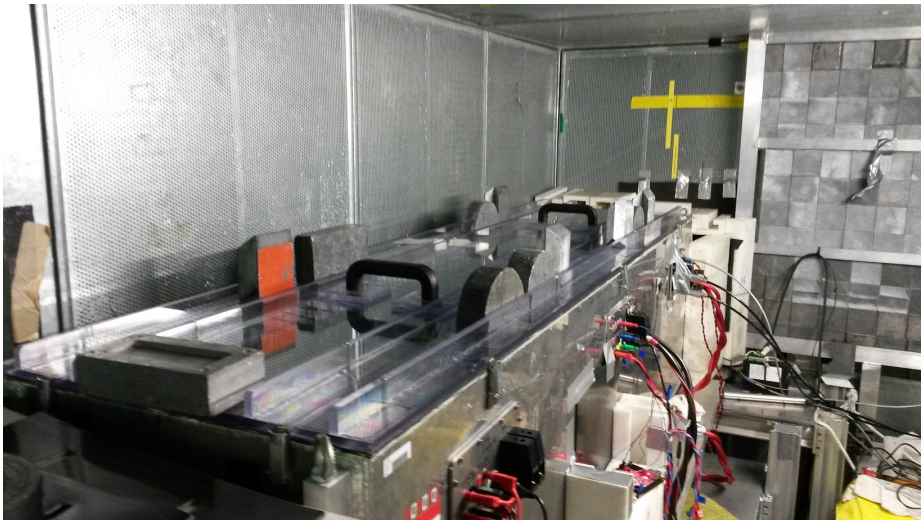

Figure 18: MONOPOL with closed cover plate standing in the VCN-cabin at the ILL in Grenoble.

A better method would be to place more toggle catches on the long sides of the cover plate. In addition, it is possible to replace the sponge rubber with vacuum-tight plastic gaskets. Then the box would certainly be vacuum tight. Therefore, the plastic gaskets must be perfectly shaped and we have to make small grooves in the box to hold the plastic gaskets in place.
We didn't take care of the last weak spot: the mechanical properties of the entrance windows. We didn't test if they could withstand the pressure difference between normal air pressure and vacuum. Elsewise, we had to reinforce the windows but more material in the window would decrease the transparency for VCN. A beam shutter which can move close to the window would hinder in this closed position the window to implode during an evacuation and would also improve operation safety.
We bypassed the problem of the long time needed for changing the gas mixture differently, by having a monitor beam. This beam always has the spectrum of the present gas mixture. By normalizing the test beam by the monitor beam we are independent of the gas mixture. We still used the slow helium venting during the beam time 2014 in Grenoble in order to increase the intensity.
To learn about the plug-in connectors in the three panels and the other used components read appendix B.

3.7 Periphery

Additionally to all the previously described components, we used two computers, several power supplies and a neutron detector to operate the MONOPOL (Figure 19 on page 45).
The neutron detector is a ^{3}He gas detector with a two dimensional spatial resolution of 128 x 128 pixels. We operated it with one computer ("detector PC"). This computer and the detector are part of the inventory of the VCN-cabin. The detector PC has signal inputs and outputs. We connected a trigger signal (Chopper signal or PWM pulse) to start the measurements and used an output to trigger all other components if one measurement was finished and a new measurement started. The other components changed their settings for the new measurement due to that signal. Hence, we could automatically run multiple measurements with different parameters in a row for a long period of time, during the night for example.
The detector-control program was able to record the spatial neutron distribution even with a time resolution of 0.1 ms. This is essential for TOF-measurements. During the analysis of the data, we separated the monitoring beam and the test beam by only summing up the neutron counts of the pixels which were irradiated by the beam. Therefore, the background of randomly scattered neutrons was rather low. Wilfried Mach further decreased this fraction of noise in the measurements by placing neutron absorbers around the beam and the detector. Ultimately the background from the stray field was negligible and the dominant contribution was from the not perfectly polarized neutron beam.
We used the second computer for all other tasks. The LABVIEW-program MCS (Section 4.4) controlled all power supplies via GPIB and the fluxgates via USB. We operated the central master controller of the resonator with a web interface via USB and ETHERNET. We brought this computer with us and we call it "MONOPOL PC".

3.7.1 Needed power supplies

Guiding field: 1.5 A($\pm$1 mA) and 5 V($\pm$1 mV) & (20-60 Å) (HMP 2030)
Compensation field in y-direction: 5 A($\pm$1 mA) & 3.2 V($\pm$1 mA) (HMP 2030)
Compensation field in x-direction: 1 A & 2.2 V (HMP 2030)
2x Spin flipper current sheet: 100 A (TTi QPX600DP)
2x Spin flipper compensation field coil: 2 A & 3 V (HMP 4040)
Resonator stages: 5 V & $<$ 200 A
Coil controller: 5 V & 1.2 A (HMP 4040)
Coil controller OPA: $\pm$7 V & 0.1 A (Kepco Bop 20-5D)
You can find more detailed information about the power supplies used in appendix C.

3.8 Electronic control of the resonator

At the moment we are operating the resonator itself with the 'MONOPOL PC'. Furthermore, we have to adjust the setup by hand and we have to use the 'DETECTOR PC'. The MONOPOL PC is the starting point of two separate controlling systems: the MONOPOL CONTROL SYSTEM (Section 4.4) and the MONOPOL-ARM (Figure 19 on page 45). In addition, we use many programs

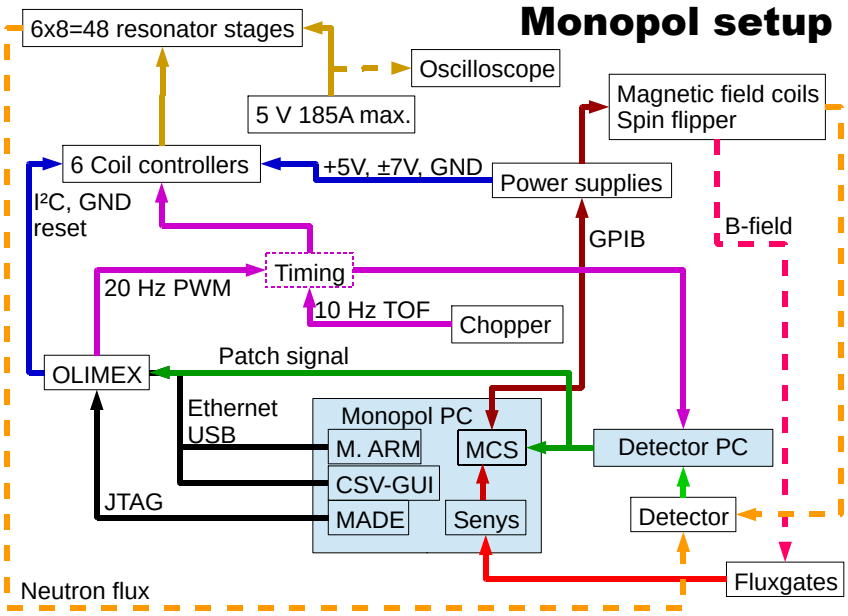

Figure 19: A schematic drawing of all main electronic components of the MONOPOL setup.

for the preparation of the experiments (CSV-GUI, ...) and the upgrade of the MONOPOL-ARM system (MADE,...). See more about these software packages in Section 4.

The MCS consists of a large LabVIEW-based program which controls all connected power supply units and the flux gates. It is responsible for setting the magnetic field around the resonator and the power supply of the resonator itself. The MONOPOL-ARM is a web-interface that controls the resonator. This controlling system is based on the architecture proposed in the master thesis of Sebastian Nowak [36](p.44)[37]. The user stores the measurement protocols (csv-files called recipes) on the SD-card of the Central Master Controller (CMC) and operates CMC via ETHERNET by using a web interface. The central master controller sends all the information to 1-6 different responsible coil controllers via an I^2C-Bus: the current settings, the relay settings, the shunt resistor settings, pulse starting time and pulse length of every stage. Each coil controller operates 8 stages. They apply the correct voltage to the appropriate OPA, which controls the current through the connected stage coil. Furthermore, the relay setting determines the direction of the produced magnetic field and a shunt resistance setting limits the current through the coil. With an additional PWM line the central master controller sends time marks to the coil controllers. They use it as synchronized start pulses for their operation. This is necessary for the Traveling-Wave-Mode. We can also activate the stages in a steady state mode via the web interface and the CMC.

We didn't have the possibility to monitor the VCN-electronic. Particularly, we wanted to know if the current in every coil was correct and if some stages switched off by malfunction. Therefore, we wired a small cable parallel to the

high current wire of the resonator stages. On the small wire we placed a high frequency current probe. We also used this probe for the calibration. Before every measurement we could check with an oscilloscope connected to that probe if the resonator was programmed correctly and turned on. Every future resonator electronic should be capable of monitoring the stage currents during the measurements and reporting malfunctions.

3.8.1 Central Master Controller

Stefan Seifried implemented the central master controller during his Bachelor's thesis [48]. He also developed a programming environment for the used OLIMEX-board called Eclipse M.A.D.E.. Stefan Baumgartner made further improvements during his master thesis [55] which led to more usability.
We used an OLIMEX LPC-2378 development prototype board (Figure 20 on page 47) [35](p.11-22). This development board has a 32-Bit ARM7TDMI micro controller (NXP LPC2378 FBD144) and many interfaces (RS232, USB, I^2C, SD/MMC Card slot, 100MBit ETHERNET, standard JTAG). We used the USB port for the power supply, the ETHERNET and the JTAG to connect the board to the MONOPOL PC. We only needed the JTAG-connections when we installed a new software on the OLIMEX-board.
There are many connections to the resonator, which are all attached to the middle panel of the box: Common ground, the I^2C Bus to program the coil controllers [35](p.34-42)[48](p.53-57), the PWM/Interrupt signal for timing and the reset line to restart the coil controllers before they are reprogrammed. This is important because the coil controllers often have malfunctions if they are reprogrammed without reseting them.
In 2014 Stefan Baumgartner also implemented the batch line besides the reset line to improve the usability. The batch line is connected to the DETECTOR-PC. If the CMC receives the signal of the measurement's restart, it resets all coil controllers and reprograms them according to a new recipe. If the cover of the MONOPOL-box is open you can hear this process. At first, you hear one loud switching click when all coil controllers are reset at the same time and the relays switch to the default position. Afterwards you hear six quiet switching clicks when the coil controllers are programmed sequentially and the relays switch into the desired direction. With this technique it is possible to do up to 10 measurements in a row. Afterwards we have to restart the OLIMEX-board by unplugging the USB-power supply or press the reset button on the circuit board itself. Otherwise, it will not work properly.
At the moment, we have two new OLIMEX-boards fully operational (bought Aug. 2014) and two damaged old boards. The one that was originally used before 2014 has a damaged SD-card slot and the old reserve board sometimes has problems identifying the plugged-in SD-card.

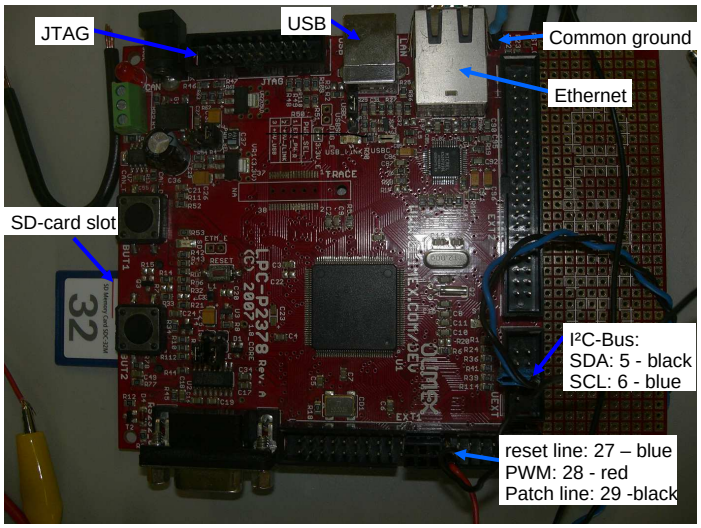

Figure 20: OLIMEX-board (old version)

3.8.2 Coil controllers

The coil controllers are situated directly above the resonator stages to minimize the cable length between controllers and the stages. Therefore, these controllers are limited in space (9.5 cm = length of 8 stages). The important parameters are the maximum and minimum current and the response time. All parameters depend strongly on the neutron energy (Table 9 on page 47). For a VCN beam we only have currents up to 1 A, a necessary time resolution of 5 µs and pulse lengths of the traveling wave above 1 ms. This simplifies the constructions of VCN-coil-controllers a lot. Therefore, more important is a stable current flow during one pulse [54](p.21).

Table 9: Coil controller parameters for one out of 48 stages

Energy	Wavelength	Speed	Traveltime for a=12 mm	Rectangular	Gaussian Center	Edge
thermal	1 Å	3954 $\frac{m}{s}$	3.03 µs	20 A	60 A	1 A
thermal	2 Å	1977 $\frac{m}{s}$	6.07 µs	10 A	26 A	0.6 A
thermal	3 Å	1318 $\frac{m}{s}$	9.1 µs	7 A	17 A	334 mA
cold	5 Å	791 $\frac{m}{s}$	15.2 µs	4 A	9.8 A	218 mA
cold	10 Å	395 $\frac{m}{s}$	30.3 µs	2 A	4.7 A	108 mA
cold	20 Å	198 $\frac{m}{s}$	60.7 µs	1 A	2.3 A	54 mA
VCN	30 Å	132 $\frac{m}{s}$	91 µs	660 mA	1.5 A	35 mA
VCN	40 Å	98.9 $\frac{m}{s}$	121 µs	500 mA	1.1 A	26 mA
VCN	50 Å	79.1 $\frac{m}{s}$	152 µs	400 mA	900 mA	20 mA
VCN	60 Å	65.9 $\frac{m}{s}$	182 µs	330 mA	760 mA	17 mA
VCN	70 Å	56.5 $\frac{m}{s}$	212 µs	270 mA	650 mA	14 mA

Bernhard Berger [54](p.37-50) and Stefan Baumgartner built the VCN-coil-controllers. There are 6 coil controllers and each controls 8 stages. Each unit is made of two circuit-boards. We call the vertical board “resonator logic platine”

and the horizontal board "power supply platine". Both circuit-boards are connected by four 2x7 pin sockets. All four connections are identical and always transmit the signals for two stages.
In the middle of the resonator logic platine there is the ATMEGA165P micro controller which needs +5 V as a power supply. This micro controller receives the resonator settings from the central master controller via the I^2C-Bus. The micro controller redirects the current values to a digital/analog converter (MCP4728-E/UN) which transforms it into 8 DAC-signals [54](p.45). These DAC-signals are sent constantly to the OPA2228P. The timing signal, the shunt setting and the relay setting is supplied directly from the ATMEGA-chip.

There are four OPA2228P on the power supply platine and each controls two

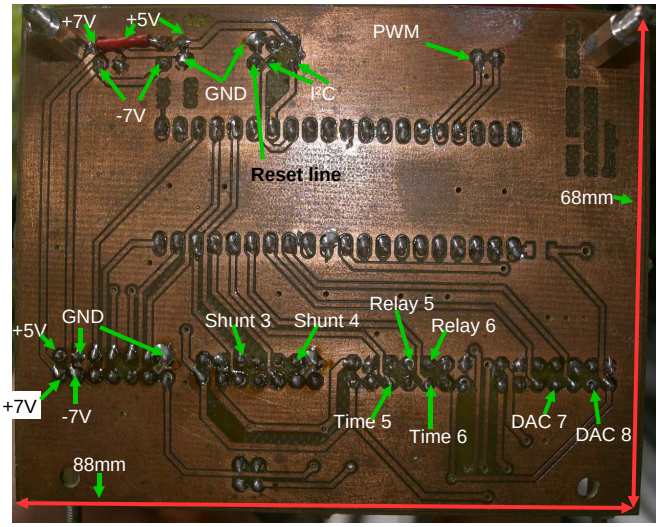

Figure 21: View of the VCN-coil-controller

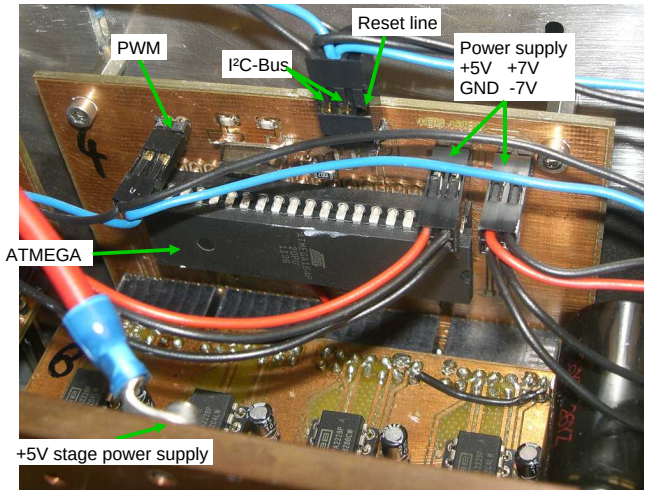

Figure 22: View on reverse side of the resonator logic platine

stages. They control the current through the stage coils according to the designated DAC-values. The MOSFETs (PSMN2R7-30PL) actually switch the current on and off according to the timing signal of the ATMEGA-chip. The relays (P2 12053, V23079-A1001-B301) are set once during the programming of the recipe to a fixed position. This setting defines the direction of the current through the coil, which defines the direction of the produced magnetic field $\mathbf{B}_1$. Therefore, we can change the stage size by combining some stages together only by using a different recipe. On the power supply plantines there are two parallel shunt resistors (3.3 kΩ & 470 Ω). They are the main voltage drop of the stage current. By changing the shunt setting, we can disconnect the smaller shunt resistor. This also changes the current through the stage at the same DAC-value. Therefore, we can use the VCN-electronics in two current ranges (0-1 A & 0-4 A) with different current resolutions.
The main power supply of the stages is directly connected on copper plates which are screwed on the MOSFETs and the resistors. A water cooling pipe is clamped between these plates. Therefore, the copper plates are not only responsible for the power distribution but also for the heat transfer from the electronics to the cooling system. To prevent a short-circuit one side of the cooling pipe is isolated with Kapton tape.

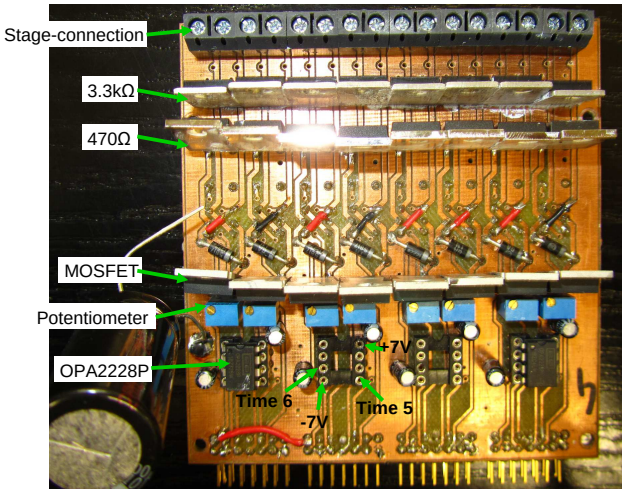

Figure 23: View on the power supply platine

The limitations of these VCN-electronics are: the maximum operation time which is only 2^{15} µs = 32.768 ms long per pulse. The stages of one coil controller can only be activated from the left to the right (in the flight direction of the neutron). The maximum current is 3-4 A (depends on the cooling capacity). The minimum time resolution for low currents is below 10 µs. At large currents this electronic produces high current overshoots during switching. It takes more than 15 µs to achieve a stable current. The overshoot can be reduced by resetting a potentiometer but then the rise time of the current pulse increases. Furthermore, we can only adjust the potentiometer for one current level. During the calibration of the resonator, I optimized the coil controller for a DAC-value of 2000 which correspond to a wavelength of 35 Å.
The major disadvantages of the VCN-coil-controller are the lack of reliability

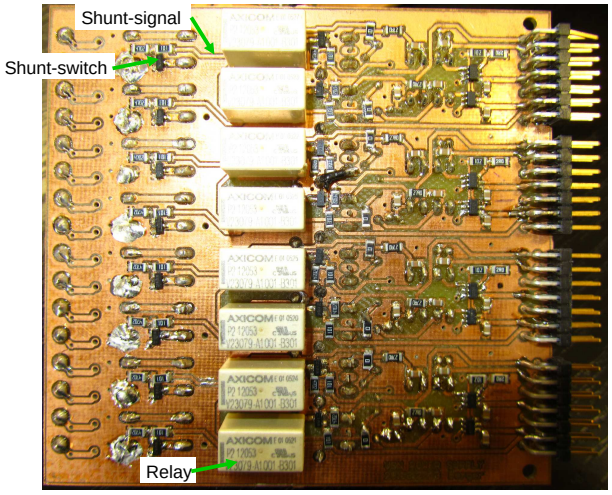

Figure 24: View on reverse side of the power supply platine

and of monitoring possibilities. During the transportation to and from Grenoble many of the soldered connections broke open. Stefan Baumgartner and Bernhard Berger repaired many during the first beam time by soldering new wires on the controller to bypass the open connections [54](p.48).
During the second beam time many stages had malfunctions again. I was able to repair some but four stages remained broken. Therefore, we connected the stage coils differently to the coil controllers in order to be able to use one resonator consisting of 44 neighboring stages. I connected small wires to the not used electronic channels otherwise the coil controllers would not work properly. In addition, the coil controllers need an "occupational therapy" for their malfunctioning electronic channels. In the recipes (csv-files) I always inserted lines corresponding to the unused channels with a very small none zero DAC-value, an opening time between the opening times of its neighboring channels, the common pulse length and a switch for the relay in order to hear the switching clicks louder. This is very important otherwise the VCN-electronics will do aimless actions with the electronic channels we really need, like turning them on and off randomly and hence increase the noise.
In addition, the geometry of the VCN-coil-controllers is very impractical for repairing. We always had to disassemble the electronics just to dismount the damaged coil controller. To dismount and to mount this coil controller again, we had to loosen and tighten tiny screw nuts in nearly inaccessible corners.

In the appendix D you can find a list of all components which were used to build the VCN-coil-controllers.

In the future a new electronic should be implemented. The head of the electronic workshop Andrzej Pelczar has already designed and built a prototype. This electronic is designed for thermal neutrons. It will have no troubles with overshooting during switching due to a special design. In addition, he has added many monitoring possibilities. At the moment two students are testing the prototype.

4 Software

A lot of different programs to simulate or control the Badurek resonator exists. To simulate and design the resonator, we used CAD-programs, CST, SPARTAN and COMSOL:
With CAD-programs it is possible to design the MONOPOL-setup and its components in order to craft it. Roman Gergen mainly did the design of the MONOPOL. He also possesses many CAD-files of the MONOPOL-setup. In addition, Bacak, Hawlik and Hinterleitner drew the VCN-configuration in the CAD-program Inventor [57].
Robert Raab and many others designed the geometry of the resonator, the spin flippers and all other field coils with CST. This program simulates the current flow through all coils and calculates the produced magnetic fields [33, 44, 43, 42, 40].
The software SPARTAN [31, 32] uses the results of CST and simulates how the spin of the neutrons behave in this magnetic field configuration [43, 42].
COMSOL Multiphysics is a software package which can simulate many physical problems like the heat production of coils [26, 42].

For controlling the MONOPOL we have to use many different programs. This fact makes it really complicated to use the MONOPOL-setup. In the future one program should do all the work.
The GUI-CSV writer calculates the settings of the resonator and writes it in a csv-file (recipe). The MONOPOL-ARM webserver on the OLIMEX-board programs and controls all of the coil controllers. We operate this web server by using a web browser on the MONOPOL PC. The firmware NR-KOMPLETT is installed on ATMEGA micro controllers which operate the coil controller and consequently set the stage current.
Besides all of that, we control all of the power supplies and the fluxgates with the LabVIEW-program MCS (MONOPOL CONTROL SYSTEM).
A detailed description of the programs used, their drawbacks and their possible improvements you can find in the following subsections.

4.1 GUI-CSV writer

This software was written by Anton Buder [51]. Stefan Baumgartner made the last improvements on 20.6.2013 before the beam time in Grenoble 2013 [56].
The software can calculate the setting of the resonator in the Traveling-Wave-Mode for a given wavelength, shaping, sub-shaping, number and thickness of the stages, offset and pulse length. The output is a csv-file, a so called *recipe*. This recipe consists of lines with five numbers each. Every line stands for a stage. The order is the same as the direction of travel of the neutrons. The five numbers are: the DAC-value, the time in µs counting from the trigger pulse (PWM/chopper) to when the stage should be turned on, the time as long as the stage has to stay turned on (pulse length), the position of the relay and the setting of shunt resistors.
In order to create the correct magnetic field in the stage coils for given wavelength you have to calibrate the resonator. At the moment you have to measure the current with a current probe by at least three different DAC-values for both shunt positions for every stage and write it in a calibration file (.dat) in GUI. In

addition you have to measure a general conversation factor between current and produced magnetic field. I measured the calibration with a .bat-file (see more in Section 4.2) for 9 different DAC-values (5 high shunt, 4 low shunt) after fixing the potentiometer of the electronic to eliminate the overshoot at a DAC-value of 2000. With the help of the batch-file I clipped the current probe on a wire of one stage and measured all calibration points. I always saved the values of the oscilloscope. I did this for all 48 stages. In addition, I learned which electronic channel of the coil controllers were working properly or had a malfunction.
In the future the calibration should be also done between the DAC-value and the produced magnetic field. Then we would know not only the difference between the electronic channels but also between the coils of the stages. So we take into account the different contacts of the aluminum foil and the gold/copper contact plates and also the different geometries of the foil due to mechanical deformation.

A major drawback in usability with the current version of GUI is that we can not easily change the configuration of the resonator. If we want to electronically split the entire resonator in small resonators, remove some coils or change the wiring between coil controllers and the coils of the stages, we have to create a new calibration file in GUI and also rework all the produce recipes by hand. We had to do this time consuming work often during the beam time in Grenoble in 2014 in order to exploit the limits of the MONOPOL-setup and use the VCN-electronics with all its malfunctions.

This type of program for calculating the resonator setting is always needed. Therefore, the existing program should be improved in order to gain more usability or a new program should be written as a part of general resonator controlling program. It still should have all the functions of the old CSV-GUI plus a lot of new functions listed below. For this task a student of the faculty of computer science would be useful.

4.1.1 Possible improvements:

The calibration-file (.dat) should be written in ASCII-code not in HEX to more easily change the order of coils or delete one coil if it is damaged. At the beam time 2014 in Grenoble we only used 44 stages out of 48 because four electronic channels were not functional and it took a long time to create a calibration file with 44 stages with the existing file for 48 stages.
In order to really enhance the software and get rid of the drawbacks, it should be possible to have only one calibration file for the entire resonator and all its electronic channels. Then it should be possible to decide which channel is used and which channel is connected to which coil. With a graphical layout we would gain a lot of usability. It should be as easy as defining a shaping to split the resonator in more complete independent parts as we did 2014. For example we split the resonator in four 11-stages-long resonators with different shaping or different pulse length (Section 6.4). In 2014, I achieved this by having four different calibration files producing four different recipes and joining them together. In addition, I had to insert lines for the four turned-off stages in order to create one working recipe.
In order to better see what is going on in the resonator, a graphical visualization of the recipe in slow motion would be nice.

At the moment the CSV-GUI only can produce recipes for the Traveling-Wave-Mode and not for the Conventional-Mode or a quasi static mode, which is needed if you use a chopper and you want to have a longer resonator opening time than the chopper. It is useful for studying the difference between the modes if it is possible to change the mode inside the program.
Also the CSV-GUI is more flexible than the electronics allow. A general current limit for the stages already exists but during measuring Darwin plots (Section 6.4) we discovered that the coil controllers have also other limits: the offset and the pulse length cannot exceed $2^{15} = 32768$ because the old VCN-coil controllers and the MONOPOL-ARM only support signed I16 and every larger number will be reduced by just using the last 15 digit. The old electronic modules use shift registers for handling the eight stages. Therefore, it is not possible to turn on or off the last stage of a module before the first stage. The electronic turns on/off the first stage as it should be. When it is ready to turn on/off the last stage and recognizes that the time for switching is already past, the electronic does something completely random. We had to take this into account in our recipes and we lost a lot of flexibility. Consequently, it is not possible to split the resonator into more than one and start with the last resonator if the sub-resonators share a coil controller. In the future the CSV-GUI should take all these limitations of the electronics into account and also save it in the calibration file.
An informative method of testing the resonator is to use a chopper in front of the MONOPOL. We can study the wavelength spectrum of the neutron with a TOF-methode (Section 6.3). In order to synchronize the centers of the 5 ms neutron pulse of the chopper and the 2 ms long traveling wave of the resonator (Section 6.2.8), we had to measure the distance between the chopper and the first used stage-coil of the resonator and had to calculate the flight time of the neutrons for each used wavelength with excel. In addition, we had to measure the time difference between the trigger signal and the opening time of the chopper. For more usability all this should be possible in the CSV-GUI by just setting the distance and the chopper offset and the GUI being able to calculate the timing offset of the resonator by itself. It would be useful to be able to separately de-tune the synchronization of the pulse centers. With this method it would be possible to split one resonator electronically in two parts and create two pulses within the chopper pulse by just detuning both parts in different directions. This built-in synchronization with a chopper also allows multiple pulses with different wavelengths from a pulsed neutron source.
In the current CSV-GUI version we can only use one opening time for all stages. A gradient in the opening or closing time in both directions would be useful to manipulate the edges of a resonator pulse by changing the velocity distribution. This is very important for very short pulses close to the minimum (the flight time through one stage coil). The resonator spin flips neutrons with a certain velocity distribution due to its number of stages (Section 1.7). The wave-like turning on and off of the resonator is synchronized to a center velocity. Therefore, faster neutrons which enter the resonator in the beginning of the traveling wave will interact with magnetic fields of turned on stages and after some time when it takes over the traveling wave it will sense turned off stages. So the spin-flip is incomplete and these neutrons will not contribute to the analyzed neutron pulse. Neutrons which have the center velocity or are slower will always see turned on stages in the beginning of the traveling wave and they will contribute

to the analyzed neutron pulse. Similarly, at the end of the traveling wave slower neutrons will fall behind and will not contribute to the neutron pulse. If it is possible to detune the turning on and off of the stages, we will have the same traveling wave for a given wavelength but a gradient in the opening time of the stages. For very short pulses this means that a negative gradient (the opening time of the stages becomes smaller) will reduce the intensity of the neutron pulse by narrowing the velocity distribution contributing to the pulse. A positive gradient (the opening time of the stages becomes longer) will increase the intensity of a pulse by allowing faster or slower neutrons to contribute more to the final neutron pulse. At the moment it is not really possible to study this effect, because you have to change every offset and opening time of all stages manually in the csv-file.

4.2 Monopol-Arm

This software was produced by Stefan Seifried [48] in his development environment MADE [49]. Stefan Baumgartner and Bernhard Berger further developed this software [56] in order to use it with the VCN-coil-controllers. In addition, Baumgartner improved this software between the two test cycles in Grenoble (2013, 2014) due to the experiences during the first test cycle.
The software is directly installed on the central master controller (OLIMEX-board). If we want to upgrade the software, we have to install it via the JTAG connection. We have to do it twice or three times in order to install it once properly.
We store .csv-files or .bat-files on the SD-card of the OLIMEX-board. If we load a .csv-file, the CMC will program the coil controllers. In order to turn on the resonator, we have to choose a frequency of the PWM-signal and start the resonator via a web browser. A new method is to use the .bat-files. These files contain a list of csv-files which are also stored on the SD-card. If we start this bat-file, the CMC will program the coil controllers according to the first csv-file. If the CMC receives a signal via the batch line, it will reset the coil controllers and reprogram them according to the next recipe in the list. Note that the voltage in the batch line is always high and the signal is close to zero. Therefore, we can produce signals in the batch line only by grounding it by hand. Unfortunately, stress peaks in the electric circuit also can induce batch signals. We observed that the lamp of the VCN-cabin can induce these signals during switching on and off.
The CMC writes every batch process into a report-file with a time stamp (the time since starting the OLIMEX-board). This allows us to review all measurements done if they were synchronized between resonator, detector and MCS. In addition, we have to reset the CMC after every use of a bat-file in order to be able to communicate between the CMC and the MONOPOL-PC. The reason for this is due to the report file, which is written from the CMC on the SD-card. This violates the absolute usage rights of the MONOPOL-PC. Therefore, we have to reset the CMC in order to reestablish well defined usage rights of the SD-card on the OLIMEX-board.
We are very limited in the usage of the SD-card. The MONOPOL-ARM can only identify .csv-files or .bat-files which are not contained in any folder or have no filename that exceeds 8 characters. In addition, only 11 files can be identified. For this reason, we can only use a bat-file containing 10 csv-files.

4.3 Firmware of coil controller: NR-Komplett

This software was developed mainly by Stefan Baumgartner. It is the operating system of the ATMEGA-chips on the coil controllers. All time critical parts are programmed in assembler. A detailed description does not exist. Baumgartner's masters thesis will describe the working principles of this software [55].

4.4 Monopol Control System - MCS

For programing and monitoring all power supplies I wrote a large LabVIEW-program before and during the beam time in 2014. It also controls the fluxgates and actively stabilizes the magnetic field inside the MONOPOL-setup. The functions of the program increased with our demands during the measurement cycle. At the moment, the program is strongly oriented to the controlled components. Therefore, most parts of the user interface are occupied for controlling each channel of the connected power supplies and to readout the fluxgates. We can change the voltage and the current settings of each channel and turn on and off each channel separately or all together. The MCS automatically measures the voltage and current applied on the output of every channel and calculates the power and the resistance too. For some channels a safety feature also exists. The measured resistance is compared to a saved value. If both values differ strongly, the MCS will shut down this channel to prevent a possible short circuit. All measurements are frequently stored in a log file. This is helpful if a malfunction occurred during the night, a system crash of the MONOPOL PC for example.
In addition, it is possible to make sweeps by varying the current or the voltage of one channel. The MCS automatically stores every measurement in a separate file. We used this function to determine the resistance of the components or the ratio between produced magnetic field and the current. It is also possible to vary the guiding field and the spin flipper compensation field together, in order to find the perfect coupling between them (Section 6.2.1). Furthermore, it is possible to couple them during the normal operation. The guiding field can also be varied by inserting wavelength. The MCS calculates the corresponding magnetic field strength and stabilizes the magnetic field at the desired value with a feedback control. We can also change the wavelength with a constant increment. A small LabVIEW program, which observes the batch signals from the detector, can also induce a modification of the wavelength. We used this to automatically measure the spectrum with the MONOPOL-setup (Section 6.3). The resonator and the MCS changed their settings when a measurement ended and a new one started.
If the MCS is still needed in the future, the program has to be further developed. At the moment every change in the Monopol-setup (changing of the powersupply / channel, ...) has to be also done in the program itself. Therefore, the program has to gain more flexibility and also more usability. One approach is to build a user interface consisting of the main parts of the resonator. The user should be able to easily change the configuration of connection during operation. Furthermore, a fusion with the other controlling systems (ARM, GUI, ...) is preferable.

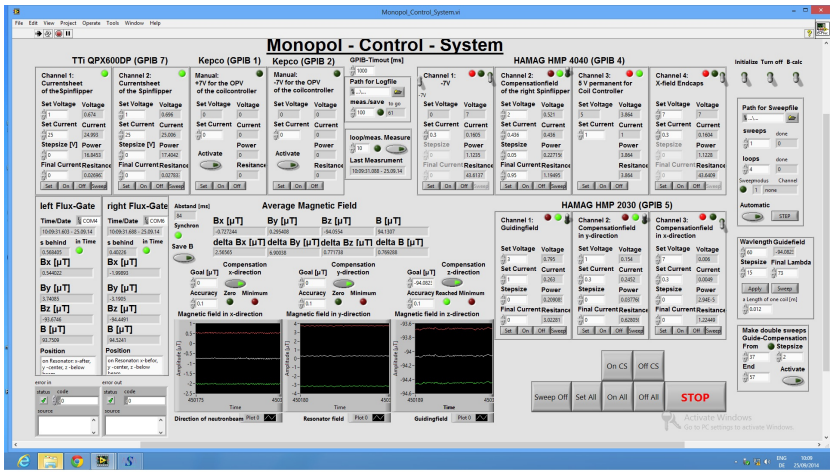

Figure 25: a screen shot of the MONOPOL CONTROL SYSTEM

5 List of possible improvements of the MONOPOL-setup

Badurek-resonator:
The contact plates can be coated with gold. A new more stable frame for the coil can be developed and constructed.
Magnetic environment:
Additional coils to compensate gradients in the magnetic stray fields or to produce a gradient in the guiding field to decrease the wavelength resolution.
Spin flippers:
Rebuild the current sheet 2014. Design new compensation field coils to produce a more homogeneous and larger field free region around the current sheet.
Super mirrors and chopper:
These equipment were borrowed from a Japanese group. In order to use the MONOPOL-setup at the TRIGA reactor in Vienna, we need super mirrors and a chopper which can handle a 6x6 cm^2 thermal neutron beam. In addition, the super mirrors should have a very high degree of polarization.
The box:
Gain vacuum-tightness to accelerate the gas replacement. In addition, if we place many components inside the box on step motor drivers, we can automatically adjust more precisely the setup.
Power supplies:
Supplant or repair damaged power supplies (KEPCO, TTI).
Coil controllers
New coil controllers for different energy ranges. It should be able to operate every stage independently in order to gain the most flexibility. In addition, many monitoring possibilities should be implemented.
Software:
Simplification of the programs needed. The goal is to have only one program which prepares, monitors and analyzes the measurements.

6 Measurment and results

6.1 Preparations

6.1.1 Adjustment of the neutron beam

First we searched for the neutron beam with the help of a neutron camera and marked the spot where the beam crossed the centerline of the box with a laser placed on the ceiling. In the designated spot we placed the super mirror at 9 degrees to the neutron beam. With the camera we checked if the reflected beam was approximately on the centerline (Fig. 26). If the camera was close enough to the mirror we could also see the reflected and the transmitted beam at the same time. Then the beam already went straight through the box and left it through the second entrance window. Behind this window the 2-d neutron detector already measured the beam. For the fine adjustment we moved the polarizer a little bit in every direction and rotated it. With the neutron detector we controlled if the beam was still parallel to the centerline and searched for the highest beam intensity. As soon as we found the optimal place we fixed the mirror to the box. At this stage we could already make a TOF-measurement with the chopper and saw the neutron spectrum which was only affected by the polarizer. In addition, we marked the beam line with a laser on the ceiling.

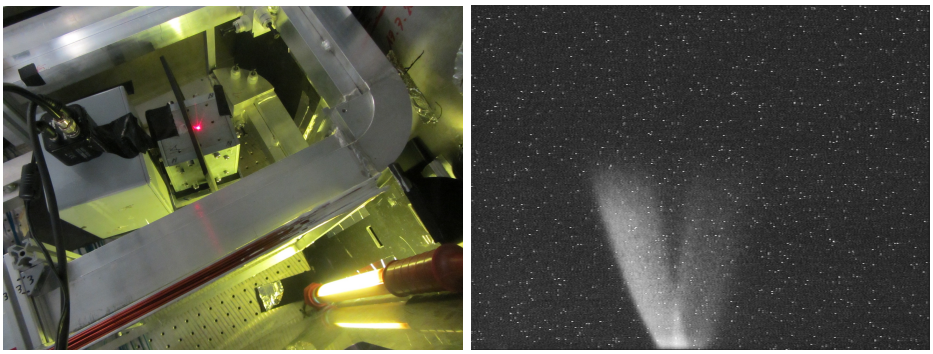

(a) Adjusting the polarizer super mirror with the help of a laser and a neutron camera

(b) View of the split neutron beam

Figure 26: Adjusting of the polarizer super mirror

The next step was to place the analyzer close to the end of the guiding field. We had the laser as a visualization of the neutron beam. This time we situated the mirror a little bit away from the center of the beam. Therefore, a fraction of the beam passed by the mirror without hitting it (Figure 27a on page 58). This was the so called “monitor beam”. The reflected beam was the analyzed beam or as we called it the “test beam”. Again we optimized the position of the mirror with the 2-d neutron detector. We wanted to have two well separated beams with a very high intensity in the analyzed beam and a suitable intensity in the monitoring beam.

The last step was to adjust the spin flippers. We used the laser again to place the spin flippers (Figure 27b on page 58). The spin flippers were very sensitive to their position relative to the neutron beam. Therefore, we measured the

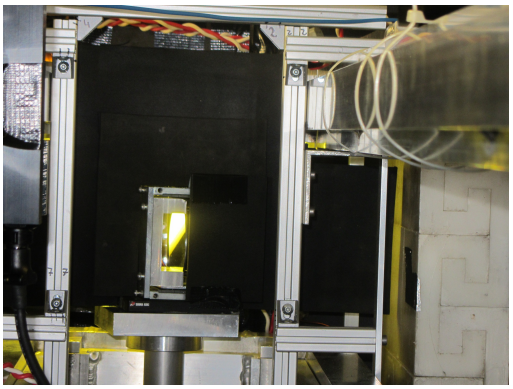

(a) Adjusted analyzer super mirror. It is possible to see optically, that a small fraction of the beam passes the super mirror without reflection as the monitor beam.

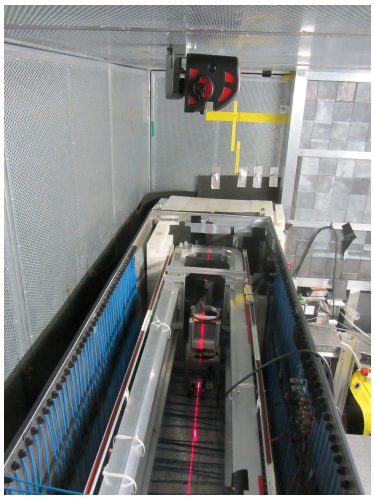

(b) A laser beam marks the flight pass of the neutron beam.

Figure 27: Adjusment of the MONOPOL-setup

spin-flip ratio with different currents in the compensation coils and searched for the best place by placing it by hand (*spin flip ratio* $N_{00}/N_{01} \approx 20-25$). In the future this should be done automatically, because it is very important to find a very high flipping ratio in order to reduce the background. One possibility is to place the spin flippers on motion drivers and connect them together with the detector and the power supplies in one program that is able to do an automatic calibration. Another way is to improve the spin flipper itself. Obviously, the compensation-field does not produce a very large field free region because it is to small and its geometry is not a Helmholtz configuration.

6.2 Measurements

6.2.1 Measurement of the optimal settings of the current sheet 2013

A very high spin flip ratio (N_{00}/N_{01}) represents a high spin flip efficiency of the current sheet and a low background. This noise results partly from a wrong adjusted compensation field of the current sheet (CF) in comparison to the guiding field (GF) (Section 1.4.1). Therefore, we measured automatically the spin flip ratio for many different values of the compensation field current at four different guiding field strengths and at a fixed current sheet strength (Figure 28 on page 59). At a given guiding field strength there exists an optimal compensation field current to achieve the highest spin flip efficiency of the current sheet. We extracted this value by fitting a quadratic polynomial into the measurements close to the expected value and calculating the turning point of this curve. In Figure 29 on page 59 you can find these values for all four different guiding field strengths. We fitted a linear curve into these values and used the gradient as a proportionality factor in the MCS-program. If we change the wavelength setting

and therefore the guiding field strength, the MCS-program automatically sets the compensation field to the optimal value (Section 4.4).

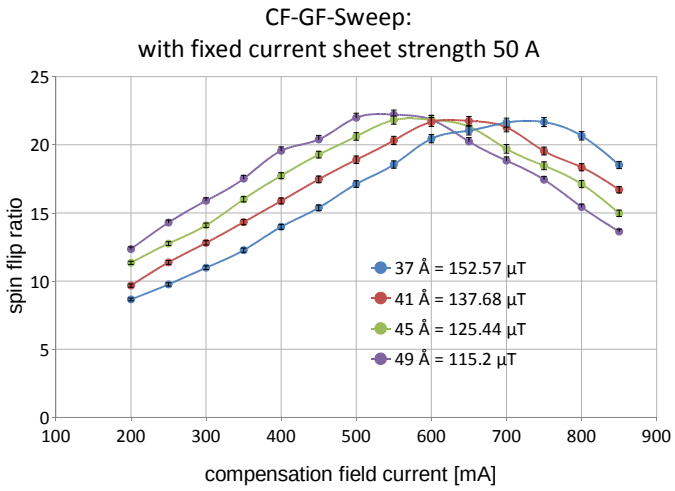

Figure 28: The spin flip ratio at different compensation field currents of the current sheet 2013 and different guiding field strengths.

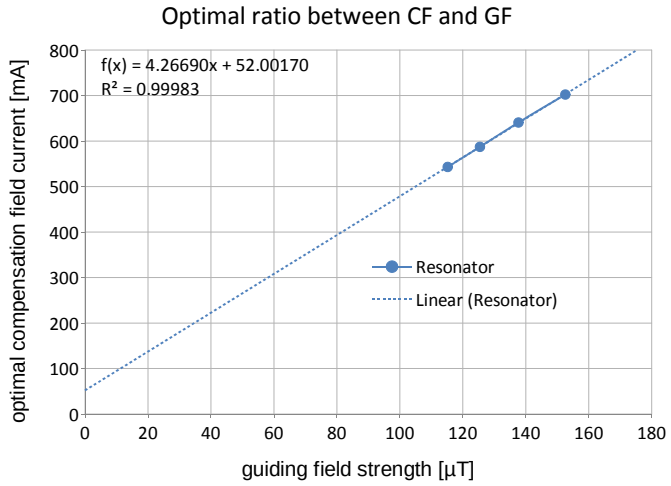

Figure 29: Dependence between the compensation field current of the current sheet 2013 and the guiding field strengths.

Due to the destruction of the current sheet 2014 (Figure 13 on page 38) we wanted to decrease the current running through the current sheet (CS). Therefore, we measured the spin flip ratio at a fixed guiding field strength and a fixed compensation field current and changed the current of the current sheet (Figure 30 on page 60). We concluded that we can reduce the current from

100 A to 50 A without decreasing in the spin flip efficiency. In addition, we gain operation safety because the aluminum sheet of the spin flipper is much colder due to the lower current. We also compared the compensation-field-current-depending spin flip ratio at different current-sheet currents (Figure 31 on page 60). We clearly see that a higher current sheet current decreases the noise from the inaccurate adjusted compensation field because the current sheet contributes more to the total magnetic field and the remaining z-field stays the same.

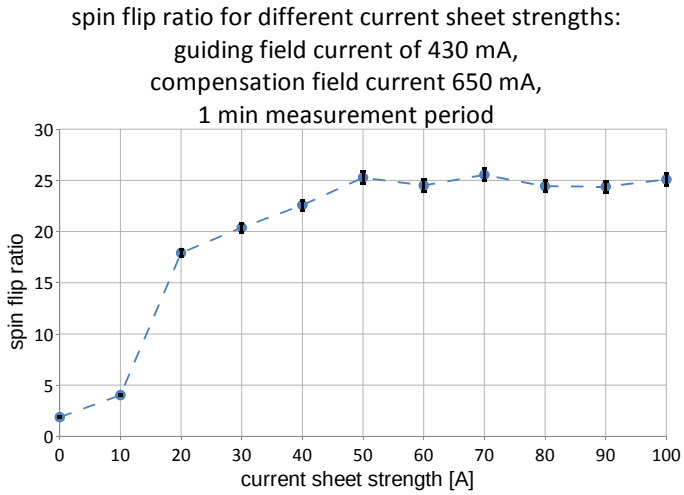

Figure 30: Relation between the spin flip ratio and the current running through the current sheet 2013.

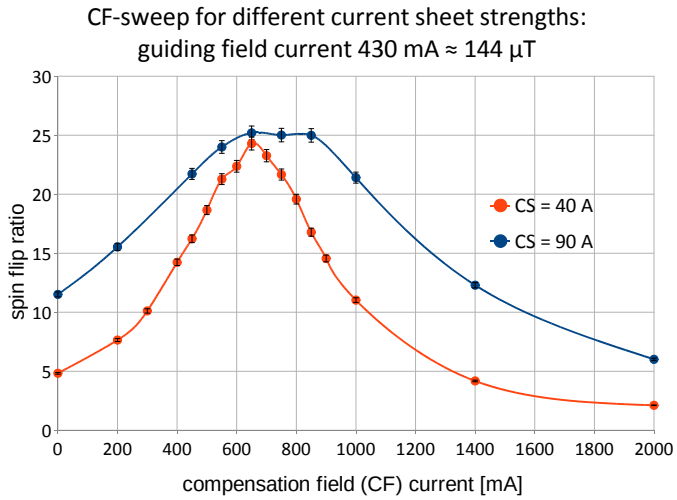

Figure 31: Relation between the spin flip ratio and the current running through the current sheet 2013 for different compensation field currents.

6.2.2 Measurement of the polarization and the spin flip efficiencies

Before we placed the resonator into the box, we measured the efficiencies of the spin flippers and the super mirrors. We used both spin flippers with a current of 100 A running through the aluminum sheet. The compensation fields currents were 0.91 A for the current sheet 2013 and 0.45 A for the current sheet 2014. The guiding field remained at 0.7 A. We always measured twice 600 s all four possibilities in air.

Table 10: Polarization and spin-flip-efficiency measurement

Measurement	1st Value	2nd Value
N_{00}	418749 cts	418833 cts
N_{10}	20803 cts	21102 cts
N_{01}	19330 cts	19430 cts
N_{11}	411771 cts	414869 cts

With these results we calculate the spin-flip efficiencies and the degree of polarization by inserting into the equations of Section 1.4:
Efficiency of current sheet 2013: 99 ± 0.33 %
Efficiency of current sheet 2014: 98.2 ± 0.32 %
Efficiency of the super mirrors combined: 92 ± 0.29 %
Efficiency of one super mirror: 95.9 ± 0.15 %

6.2.3 Measurement of the spectral spin-flip efficiency of the resonator and the current sheet

The resonator and the current sheet are both spin flippers. Their main difference is their wavelength dependencies. The current sheet is a broad band spin flipper. On the contrary, the resonator only spin flips neutrons with wavelengths close to the resonance wavelength. In order to verify this, we used a chopper for a TOF-measurement. Therefore, the measurement is a convolution between the opening function of the chopper and the neutron spectrum.
Figure 32 on page 62 displays all four different modes which are possible with the resonator and the current sheet (N_{00}, N_{01}, N_{10} and N_{11}) and a combination of these measurements in air with the displayed measurement period. We see that the resonator only flips neutrons around a certain wavelength and the current-sheet spin flips nearly every neutron except a small background. As expected, the combination $N_{11} + N_{10} - N_{01}$ is nearly the same as the measurement without any active spin flipper (N_{00}). We remeasured everything after we had vented the box with helium and gained a similar result (Figure 34 on page 63). In order to see better the spectral-dependency of the resonator, I subtracted a rescaled spectrum of the monitor beam. The scaling parameter is the total-counts ratio between the test beam and the monitor beam in wavelength regions far away from the resonance wavelength. I used this method of background reduction not only for these measurements (Figure 33 on page 62 and Figure 35 on page 63) but for all TOF-measurements.
Using these measurements (N_{00}, N_{01}, N_{10} and N_{11}) Figure 36 on page 64 presents the calculated wavelength-depending spin-flip efficiency of the resonator

(Section 1.4: (12)). These spectral spin-flip probabilities are still convoluted with the chopper-opening function. This is the reason, why the spin-flip efficiency at the resonance is not close to 1 and the wavelength resolution seems to be much wider than predicted.

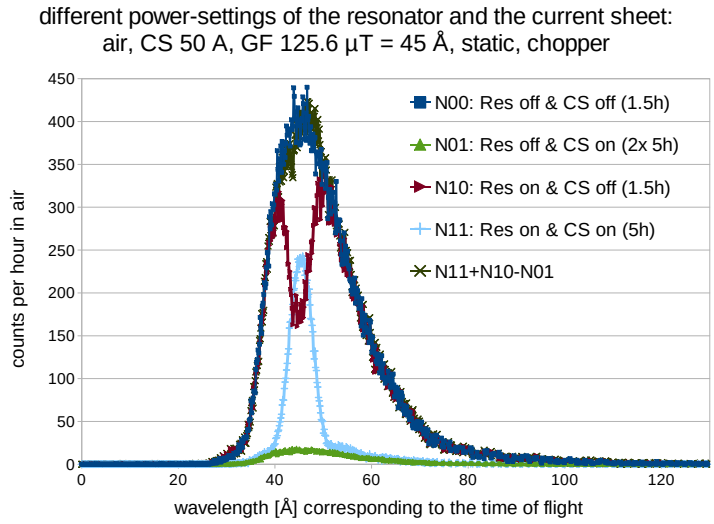

Figure 32: The measured spectra of all four spin-flipper modes in air (N_{00}, N_{01}, N_{10} and N_{11}) and a combination of these measurements.

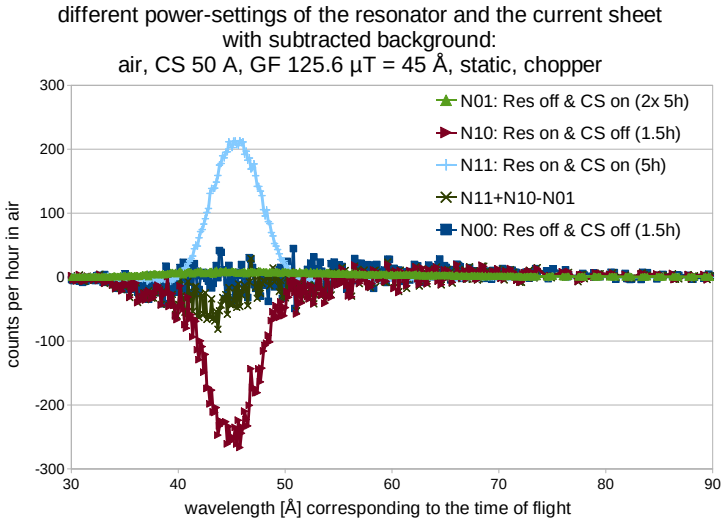

Figure 33: The wavelength-depending spin-flipper measurements with a subtracted background. You see only the wavelength-depending influence of the resonator.

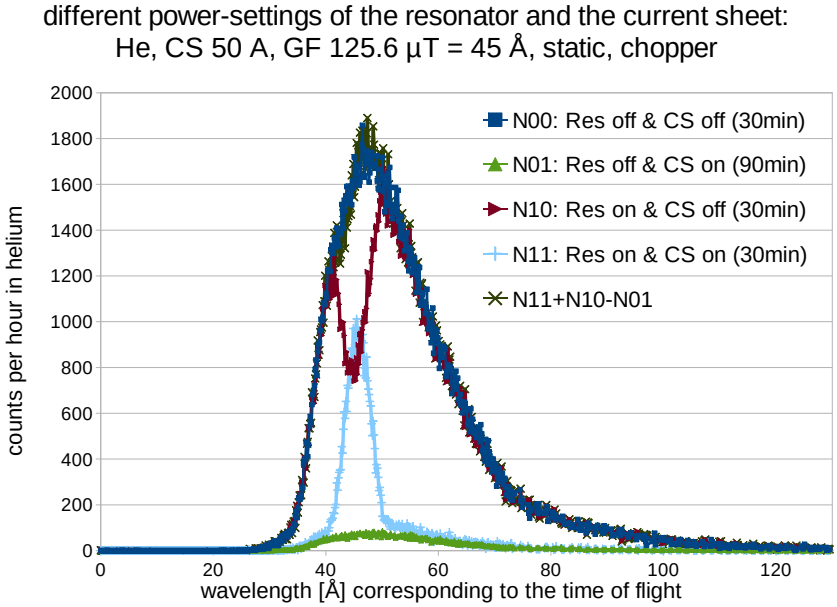

Figure 34: The measured spectra of the spin-flipper modes in a helium atmosphere. In comparison to the air-measurements the neutron count rate increased, in particular with higher wavelengths.

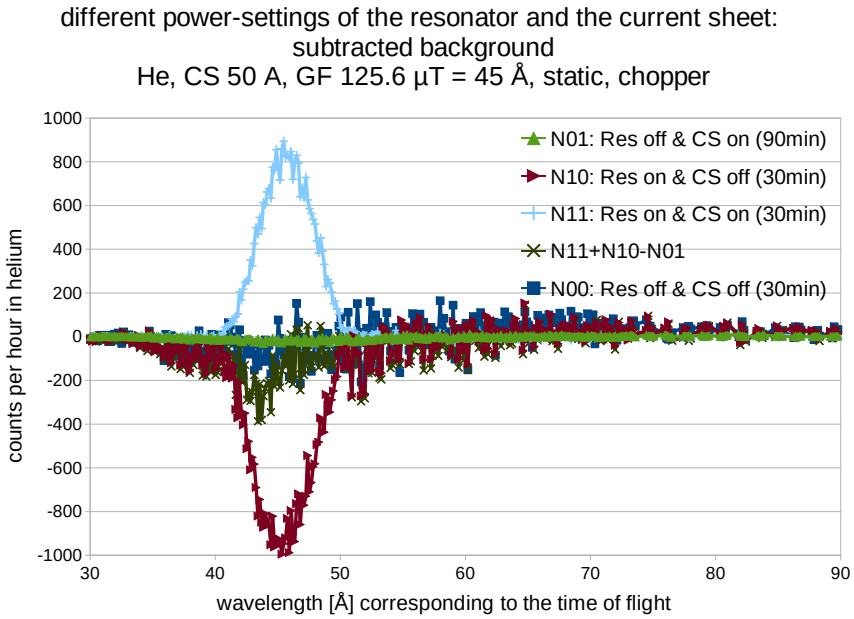

Figure 35: The wavelength-depending spin-flipper measurements with a subtracted background in helium. You can see the wavelength-depending influence of the resonator.

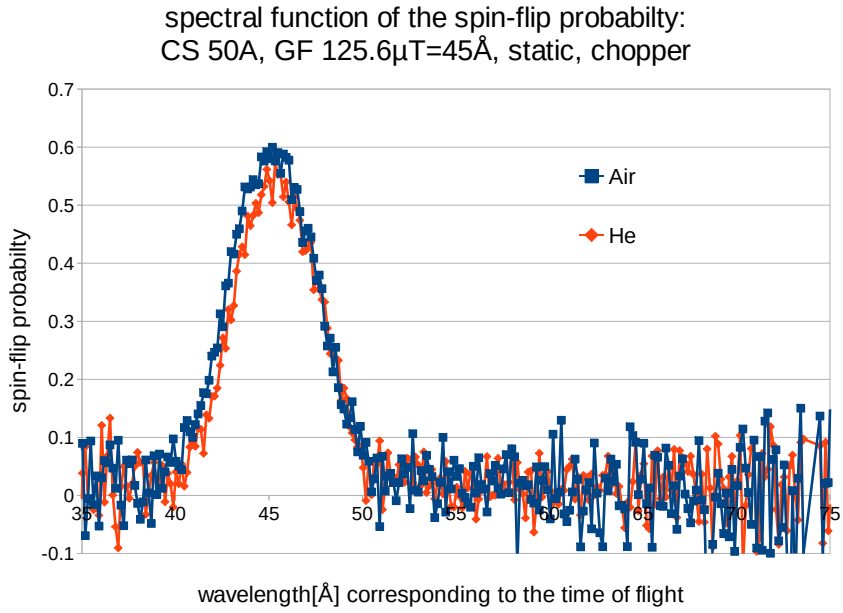

Figure 36: The spectral spin-flip probability measured in helium and air. Take into account that these probabilities are still convoluted with the chopper-opening-function. There is no difference between the measurements in air and in helium.

6.2.4 Testing different pulse settings of the resonator

In the beginning we tested different settings of the resonator. We used different modes: the traveling wave mode (TWM) and the conventional mode (labeled with *conv.*). Changing the time between turning on and off of the stages (*active-stage time*) varies the pulse length. In addition, we studied the influence of the shape of the B-field distribution in the resonator coils (Gaussian shaping is denoted as *Gauss*). In order to compare all the different measurements, I divided them with the average count rate of their monitor beam. Therefore, a different measurement period or reactor power level vanished in the common results.
The results were as predicted (Section 1.7.1): The pulse length can be reduced without decreasing the pulse height until the flight time of the neutrons is longer than the active-stage-time (Figure 37 on page 65). Due to the fact that a neutron pulse has a narrow wavelength distribution around the resonance wavelength, the pulse intensity decreases already at longer pulse length, because faster and slower neutrons drop out of the traveling wave of the resonator. We concluded that we can reduce the pulse length until 2 ms without losing pulse intensity.
The shaping of distribution of the stage magnetic field $\mathbf{B}_1$ is essential to the pulse intensity. An equally shaped distribution has less intensity than a Gaussian shaped distribution independent from the mode (Figure 38 on page 66, Figure 39 on page 66, Figure 40 on page 67). The conventional mode has much longer rise- and fall times than the TWM (Figure 38 on page 66). Therefore, the minimum pulse length is much longer than in TWM. Additionally the arrival times of the pulses are different. This is due to the fact that the switching times of the last stages depend on the mode. In the conventional mode they are activated immediately in the beginning of the resonator pulse. On the contrary, in TWM the stages are activated when the traveling wave arrives at the end of the resonator.

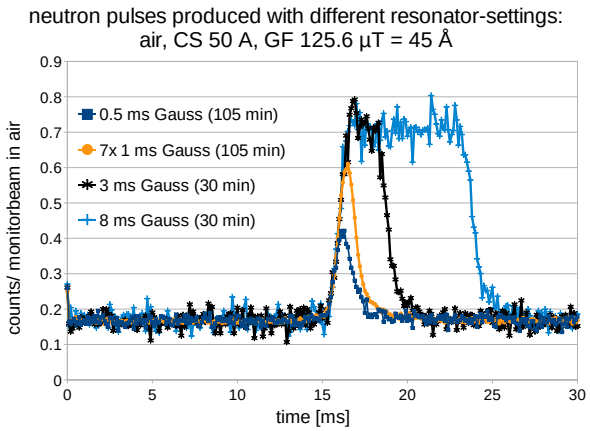

Figure 37: We varied the active-stage time from 0.5 ms to 8 ms. We always used Gaussian-shaped TWM-pulses. Due to a computer crash we measured 7 times at a resonator setting of 1 ms active-stage time for a measurement period of 105 minutes each.

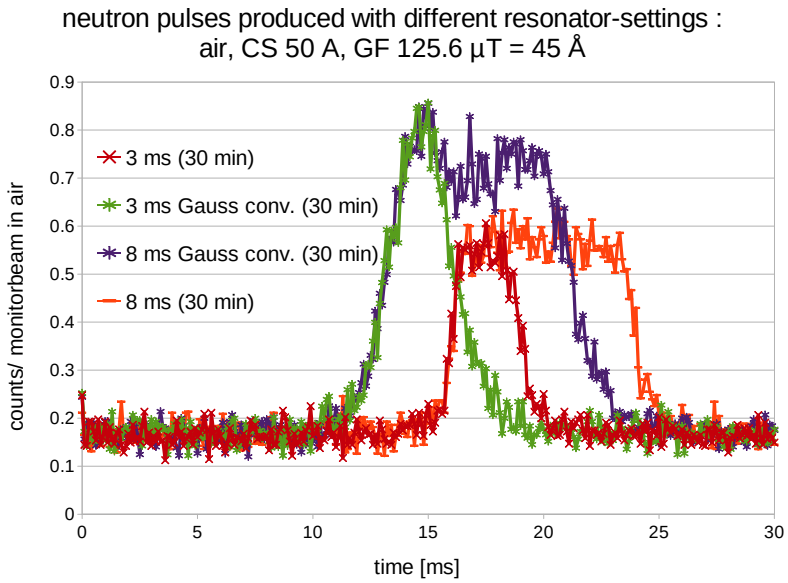

Figure 38: The difference between a Gaussian-shaped conventional pulse and equally shaped TWM-pulse are the different rise and fall times and the different arrival times of the pulse in the detector.

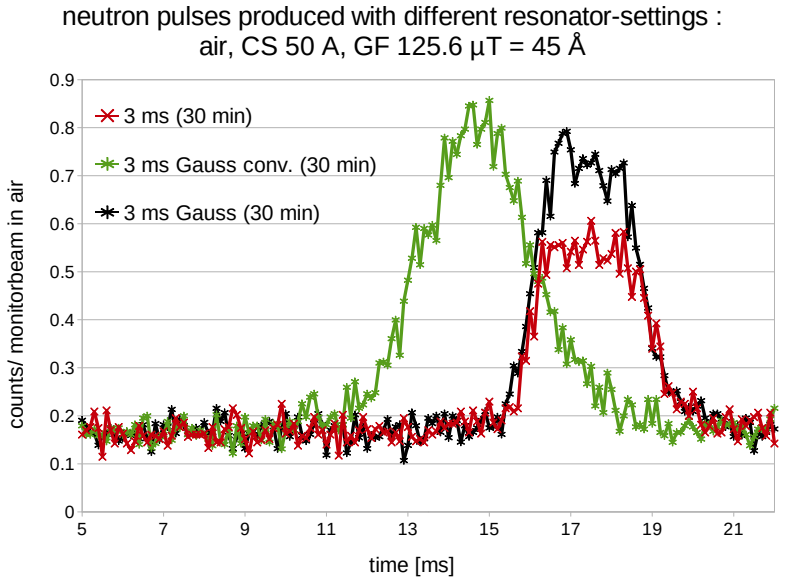

Figure 39: A compilation of different pulses with the same pulse length of 3 ms. You can see the influence of the different settings.

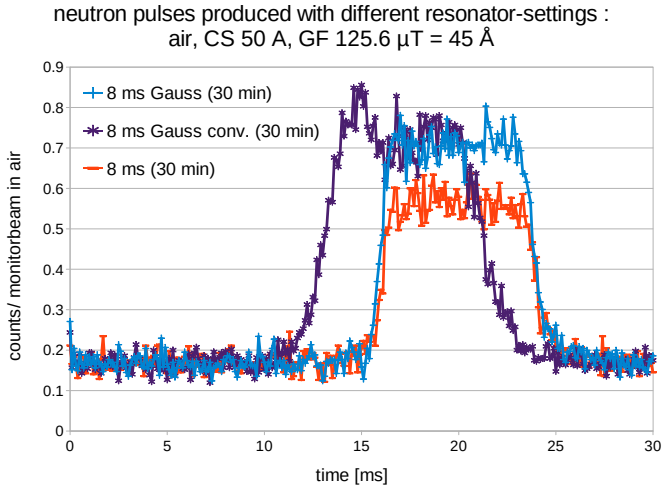

Figure 40: A compilation of different pulses with the same pulse length of 8 ms.

6.2.5 Different shaping of the stage magnetic field distribution

The advantage of the Badurek resonator isto change the magnetic field distribution (shaping) of the stages without changing the geometry (Figure 41 on page 67). With the software CSV-GUI it is possible to create a Gaussian shape. We can vary a parameter between -5 and 15, where negative values are anti Gaussian shaped, zero is equally shaped and positive values are Gaussian shaped.

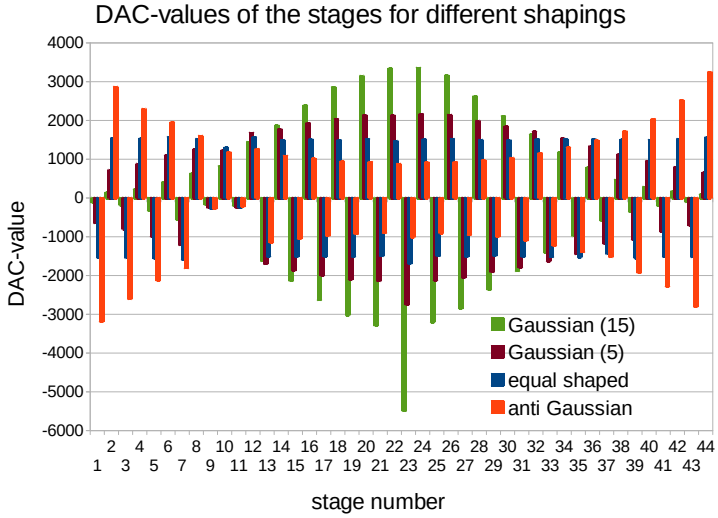

Figure 41: The DAC-Values of different resonator shaping. The reason for the low DAC-values of stage 9 and 11 are damaged shunt resistors.

In addition to the testing with TWM pulses, we measured different shaping with a static resonator and a chopper (Figure 42 on page 68). If we subtract the background, we observe that the shaping is essential to the wavelength resolution (Figure 43 on page 68). In addition, the pulse total count rate increases with a stronger Gaussian shaping.

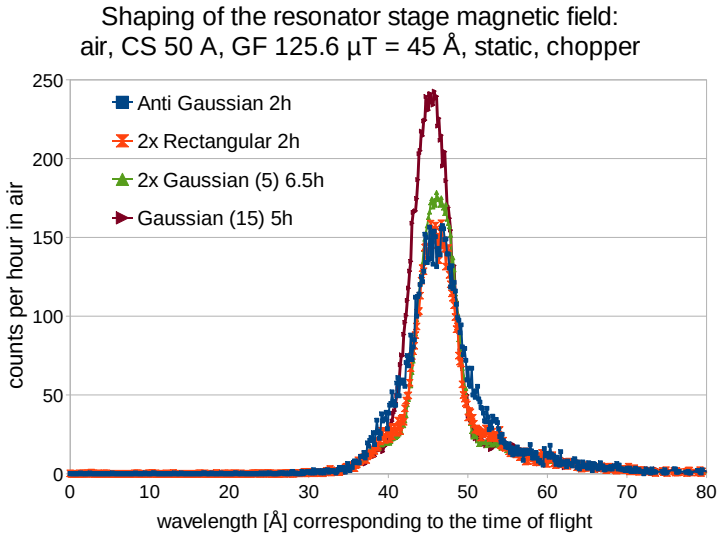

Figure 42: Measurement of different resonator shapings. Due to the static mode of the resonator the convoluted chopper-opening function widens the pulse.

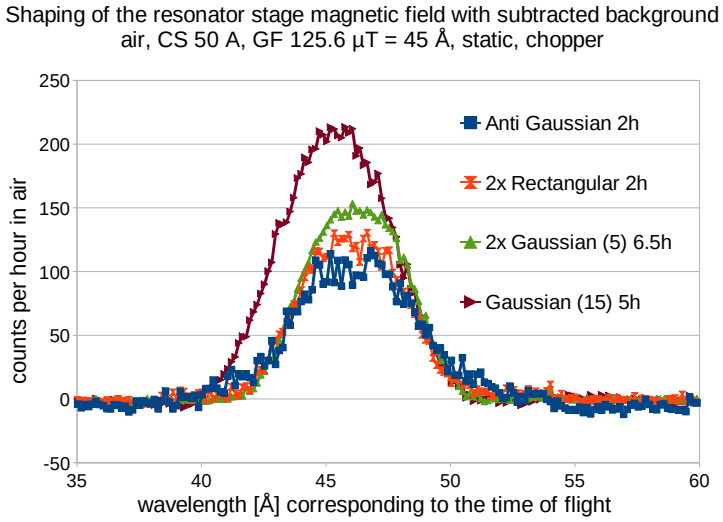

Figure 43: Measurements of different resonator shapings with subtracted background. A higher parameter for the Gaussian shape increases the pulse height.

6.2.6 Variation of the resonator lengths

We varied the size of the resonator just by using different recipes. We chose four different settings: 11, 22, 33, 44 stages and compared them. We did not combine stages together. This is denoted with (1/0). We measured this variation with and without the chopper. The TOF-measurements (Figure 46 on page 70 and Figure 47 on page 71) show that the energy spread is indirect proportional to the coils used (Section 1.7, equation (23)).
TWM-measurements had similar results (Figure 45 on page 70 and Figure 45 on page 70). We observed an additional effect that the background level is sometimes higher after the pulse than before. This is due to the VCN-electronic. We deactivated some stages in the resonator because they had broken electronic channels in their VCN-coil controllers. Therefore, we created recipes out of 44 stages and inserted 4 lines for the disabled stages. When the timing of the inserted lines were not between the preceding and the subsequent stage, the coil controllers had problems turning on and off the stages at the correct time. Sometimes they stayed switched on and made a noise in the background. This problem is much worse if we use even less stages.

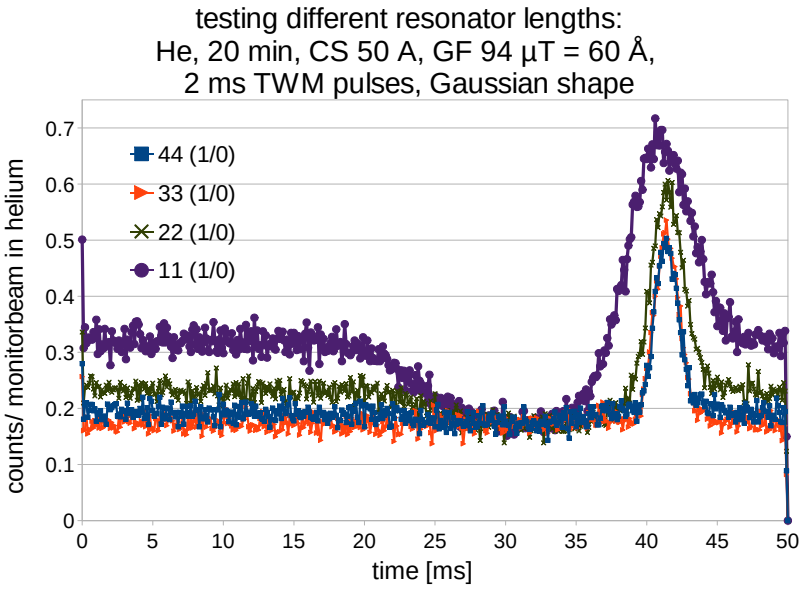

Figure 44: We used different resonator lengths L to produce Gaussian-shaped TWM-pulses with different wavelength resolution. The strong variation in the background can be produced by the malfunctioning of VCN-coil controllers

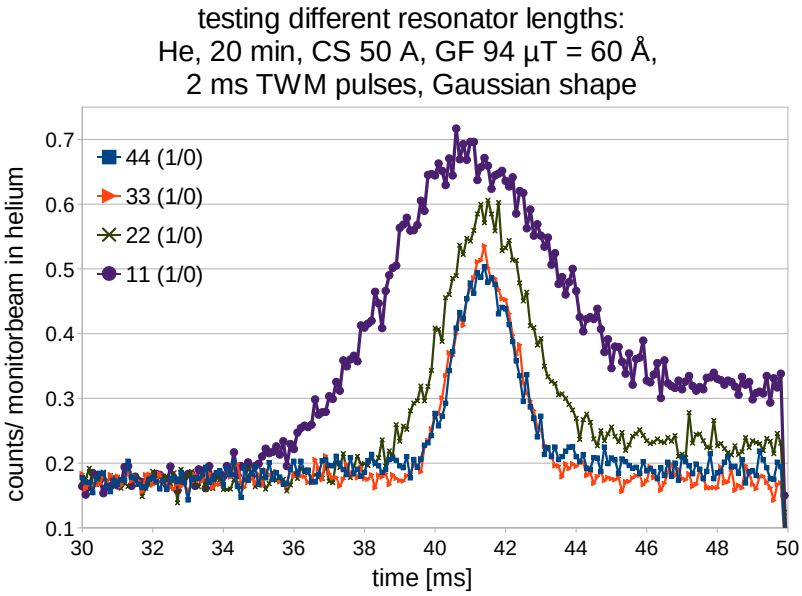

Figure 45: Close up of the Gaussian-shaped TWM-pulses with different wavelength resolutions.

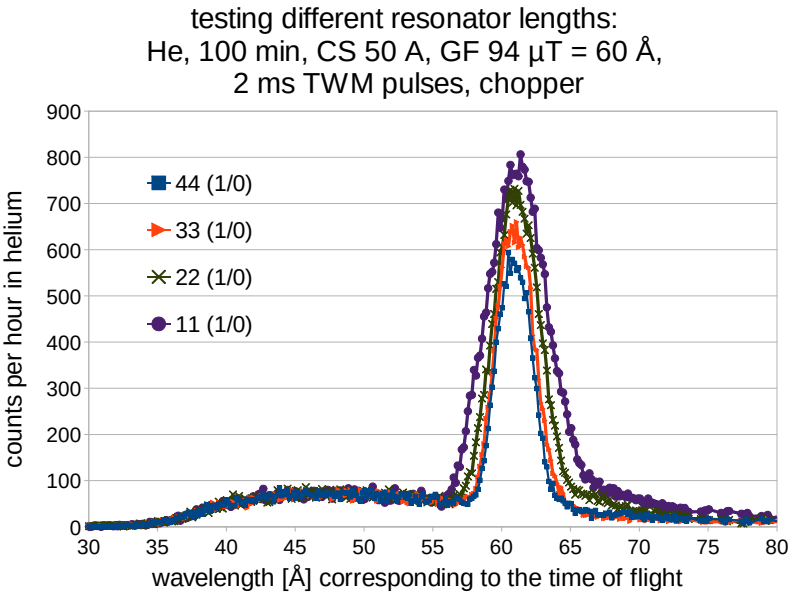

Figure 46: TOF-measurements of Gaussian-shaped TWM-pulses produced by resonators with different lengths.

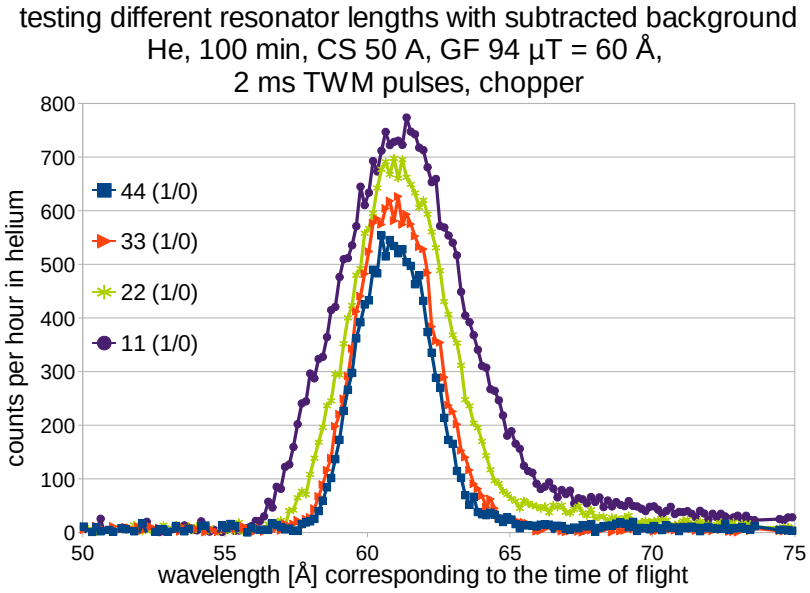

Figure 47: The TOF-measurement with subtracted background. We can see the different wavelength resolution, even tough, this function is still a convolution between the pulse spectrum and the chopper-opening-function.

6.2.7 Resonator sweeps at fixed guiding field

In this set of measurements we adjusted the resonator to different wavelengths but kept the guiding field constant to 125.6 µT. This field strength selects neutrons with a wavelength of 45 Å. The resonator produced pulses with wavelength settings between 37 Å and 53 Å (Figure 48 on page 72). We expect that the resonator always spin flips neutrons with the same wavelength of 45 Å due to the fixed guiding field. The different arrival times of the pulses are due to the fact that the resonator turns the coils on and off faster if the adjusted wavelength is shorter. Between the fastest setting (37 Å) and the slowest (53 Å) there is a time different of 2 ms in the last stage. Even though, the first stage is always switched on and off at the same time. In addition, the velocity spread of the spin flipped neutrons also changes. If the resonator works too fast then the faster neutrons have a better chance to stay in the TWM-pulse and slower ones will more likely drop out. This fact increases or decreases the pulse intensity at the beginning and the end of the pulse. For 45 Å we expect that the shape of the TWM-pulses is nearly trapezoidal.
The measurement with 43 Å is different to all other measurements. This appears in all measurements with this setting, even though, we used completely different recipes or we remeasured carefully. There could be some kind of resonance in the electronic. A strong evidence are these measurements because we only varied the resonator setting and fixed all other parameters.
In addition, you can see that the level of the monitoring beams rose. This is due to the fact that before the measurement we floated the box with helium and it slowly supplant the air. We can still compare all measurements because we always normalize the test beam with the monitoring beam but we have to take into account that the beam spectrum slowly change to higher wavelengths and therefore the pulse intensity seems to decrease.

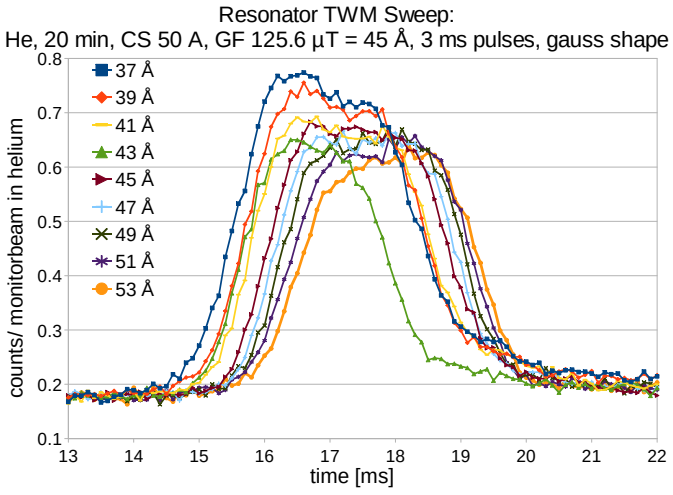

Figure 48: A close up of varying the adjusted wavelength of the resonator at a fixed guiding field strength. The pulse shape variation and the different arrival times are obvious.

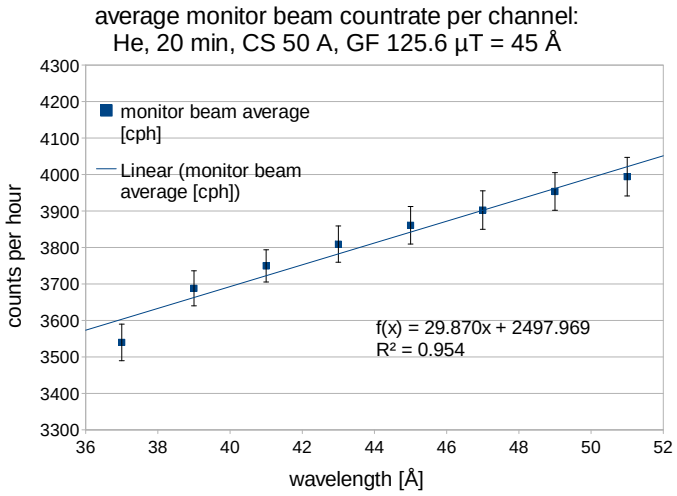

Figure 49: Rising of the intensity during the measurements due to filling the box with helium.

6.2.8 Synchronization of the chopper and the resonator

We want to use the chopper and the resonator at the same time in order to make TOF-measurements of the resonator. The neutron pulse of the chopper is 5 ms long. The pulse length of the resonator is variable. We can reduce it until 2 ms without decreasing the maximal intensity (Figure 37 on page 65). Therefore, the resonator can produce shorter neutron pulses than the chopper. With this in mind, we can reduce the background of the very short resonator pulses by chopping the beam. This only works if the resonator wave is inside the chopper's neutron pulse. We achieve this by using the chopper signal to start the pulse of the resonator instead of the PWM-signal of the central master controller. In addition, we need a fitting offset of the resonator pulse. This offset is composed of the velocity-depending neutron flight time between the chopper and the first stage (1.37 m) and a constant time due to the cable length, the processing time of electronic and the time difference between the chopper signal and when the beam can really pass the chopper. Therefore, we measured the setup with different offsets at the same guiding field strength (corresponding to a fixed wavelength). We will obtain the perfect offset when the resonator forms the highest neutron pulse (Figure 50 on page 74 and Figure 51 on page 74): The *peak area* is the total count rate in a neutron pulse after we subtracted the background. We fitted a quadratic regression in the peak areas of the neutron pulses. The calculated turning points are 14022 µs in helium and 13997 µs in air (Figure 52 on page 75). We compared these values with the expected neutron flight time (15.6 ms) and gained the value of a constant time shift (-1.4 ms). In order to verify our approach, we did the same measurements at different wavelengths (37 Å & 53 Å) and gained the same results (Figure 53 on page 75).
From all these measurements we gained the result that we always have to subtract 1.4 ms from our calculated neutron flight time in order to synchronize the resonator with the chopper.

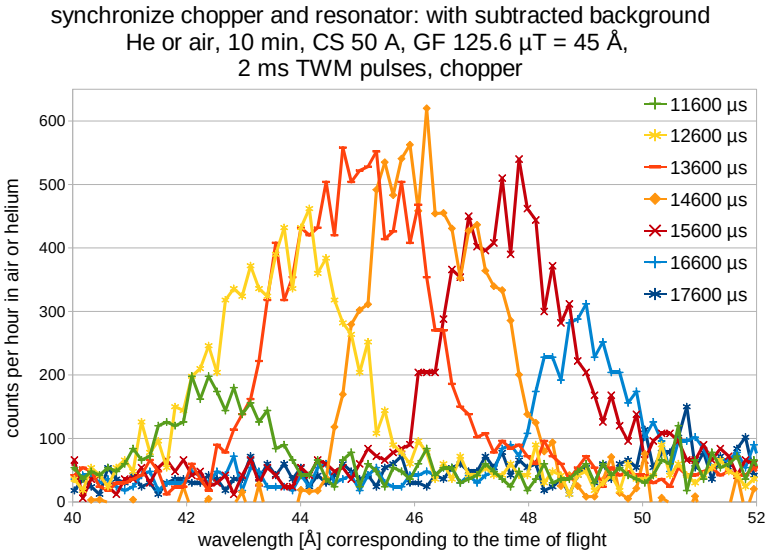

Figure 50: Different offsets in air and 45 Å with a subtracted background. The pulse shape represents a convolution between the chopper-opening-function and the resonator-TWM-pulse shape.

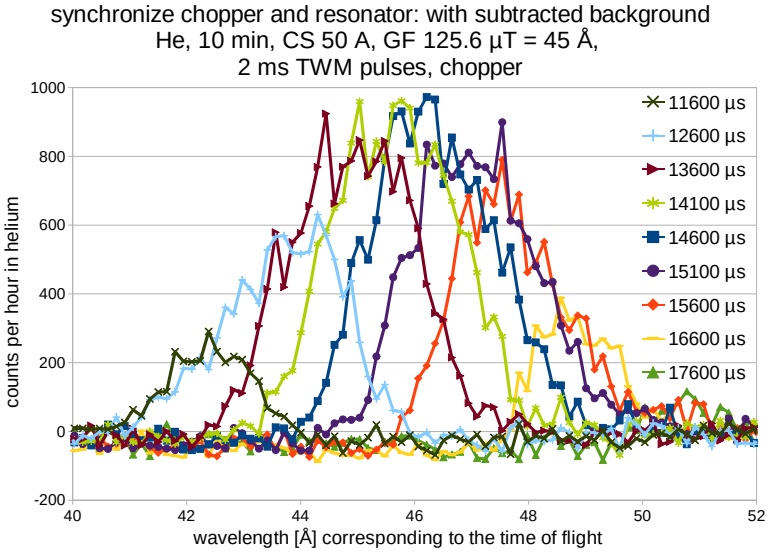

Figure 51: Remeasuring the dependences of the offset in helium (45 Å, with subtracted background). The results are similar to the measurements in air except a high count rate.

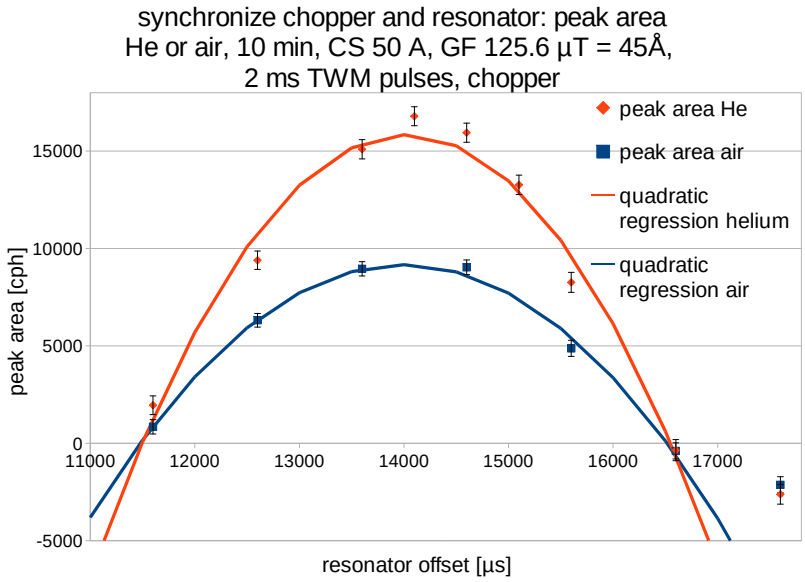

Figure 52: The peak area of the neutron pulses already with subtracted background for the measurements in helium and air. These

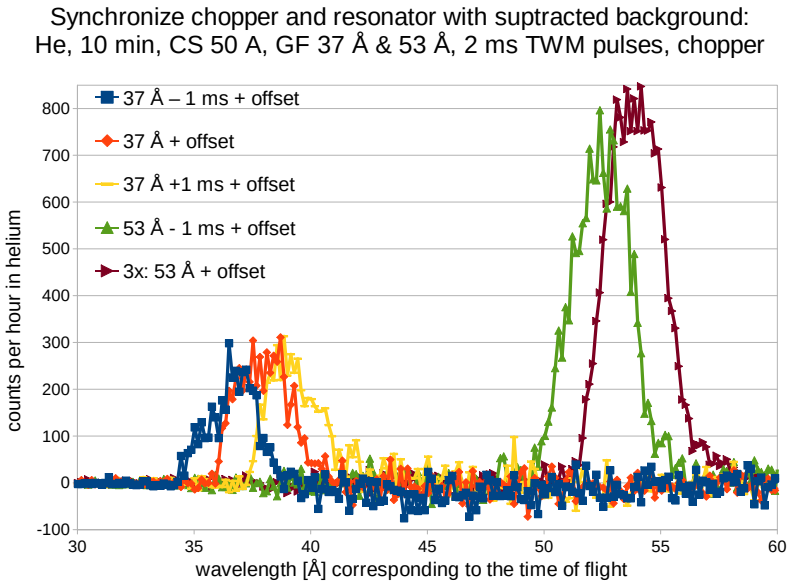

Figure 53: Verification of the expected offset at 37 Å and 53 Å measured in helium.

6.2.9 Overlaping of two TWM-pulses in helium

During these measurements we split the resonator into two parts with special recipes. The first 22 stages formed the first resonator and the other 22 stages the second Badurek-resonator. Both resonators produced neutron pulses. The first one started always 10 µs behind the PWM-signal. We varied the beginning of the second resonator. During the first measurements both pulses were matching. Hence, both resonators spin flip the same neutrons. Later on, we delayed the second resonator more and more so that the resonators affected different sections of the neutron beam. We expected that during the time when both pulses matches each other we would have the least intensity and when they mismatched we would have the full intensity of two pulses. In Figure 56 on page 77 you can see that the intensity dropped down by 31 %. This means that 31% of the effected neutrons are spin flipped twice by the resonator.

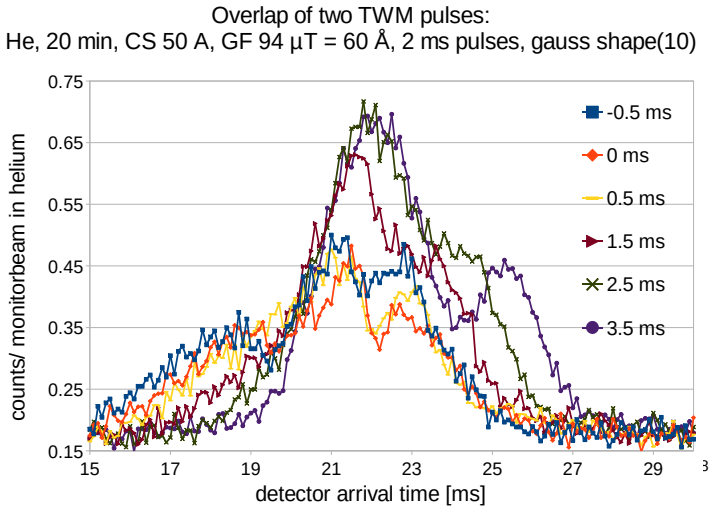

Figure 54: Detailed view of the measurements of two overlapping 2 ms TWM-pulses, we can see a strong decrease of the neutron pulse intensity if both traveling waves matches.

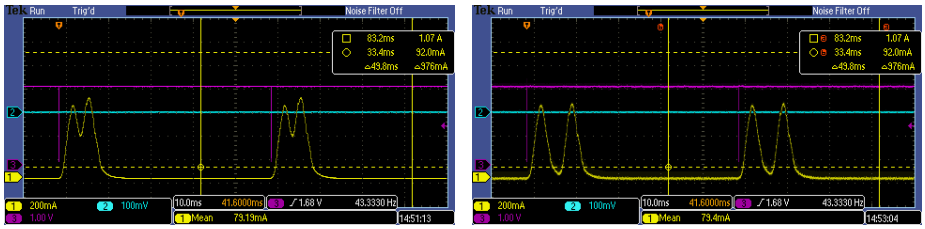

(a) matching traveling waves (b) mismatching traveling waves

Figure 55: Stage current measured with a current probe during the measurement of a bipartite resonator.

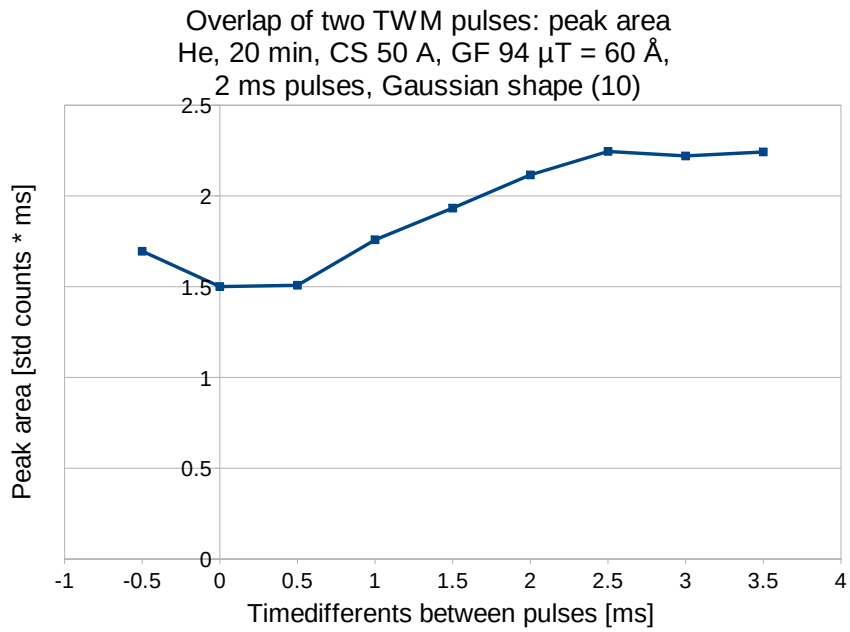

Figure 56: Measured peak area of two overlapping 2 ms TWM-pulses (total counts). A strong decrease occurs at the matching of the pulses due to double spin flips.

6.3 Spectra of the VCN-beam

During every TOF-measurement we measured the spectrum of the VCN-beam as a convolution with the chopper function (Section 1.5). I added up all of these measurements and gained a very precise spectrum of the monitor beam, a spectrum of the background of the test beam (only the section without the influence of the resonator) and a spectrum without any active spin flippers from the spectral-spin-flip-efficiency measurement for air (Figure 57 on page 78) and helium (Figure 58 on page 78).

The monitor beam has more neutrons with shorter wavelengths in comparison to the test beam. This is due the wavelength depending reflection of the analyzer super mirror. In addition, the test beams have an increased intensity of neutrons with longer wavelengths (Figure 59 on page 79). The current sheet have a higher efficiency for longer wavelengths too.

The huge count rate difference between the air spectrum (low level) and the helium spectrum is only partly due to the different absorption but also because of a power increase of the reactor during the time when we measured in air. If we compare the monitor beams after the power level rise (high level) and the helium venting (Figure 60 on page 79), we gain informations of the helium percentage inside the box (Figure 61 on page 80). Our result is that only 52% of the air is supplanted with helium.

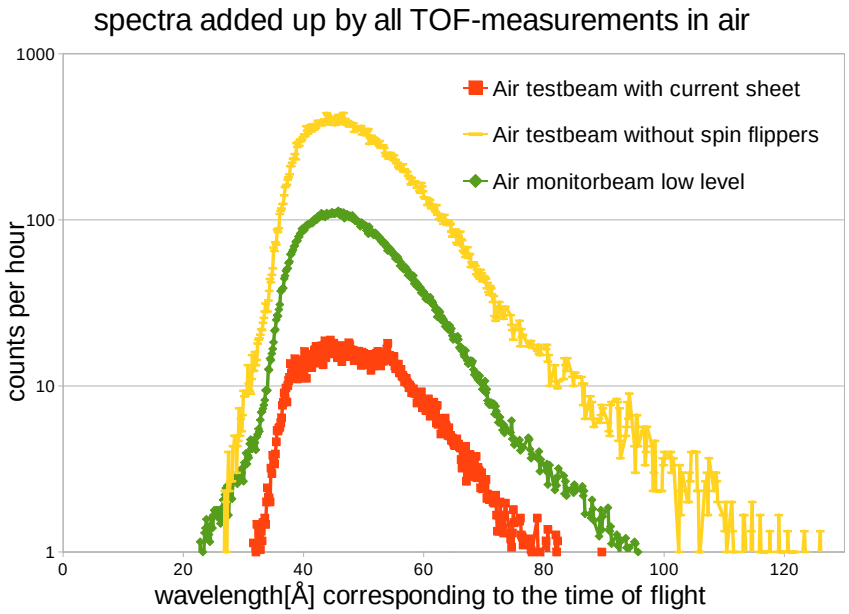

Figure 57: The VCN-spectra in air, before a power level rise of the reactor

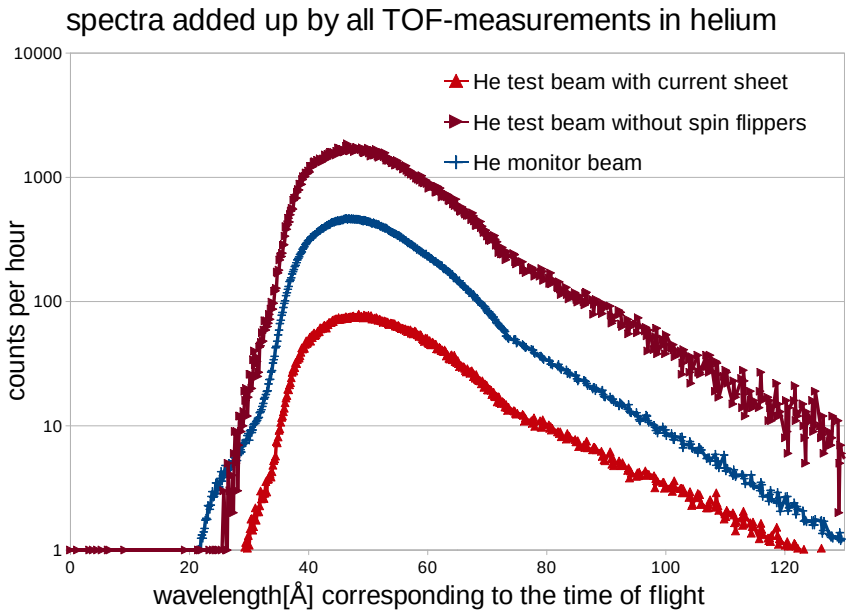

Figure 58: The VCN-spectra in helium

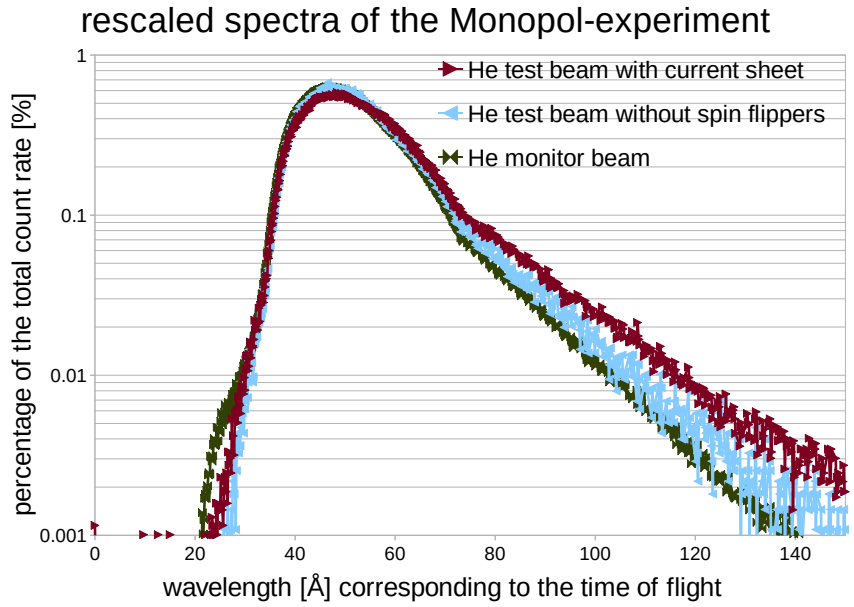

Figure 59: The rescaled VCN-spectra in helium. All spectra are divided per their total count rate.

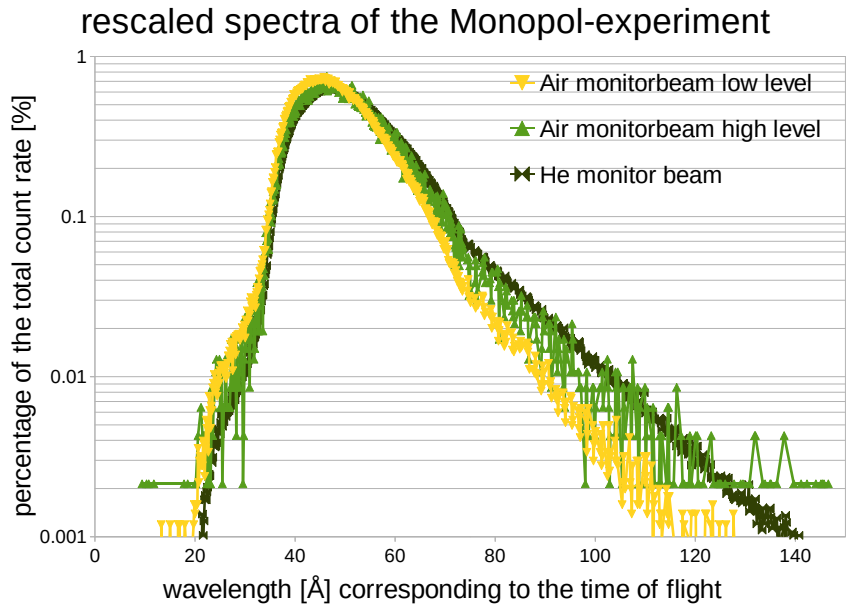

Figure 60: The rescaled spectra of the monitor beams in air (low and high power level) and helium. All spectra are divided per their total count rate. In helium the neutron absorption is lower than in air, therefore the spectrum in helium has a higher fraction of neutron with longer wavelengths.

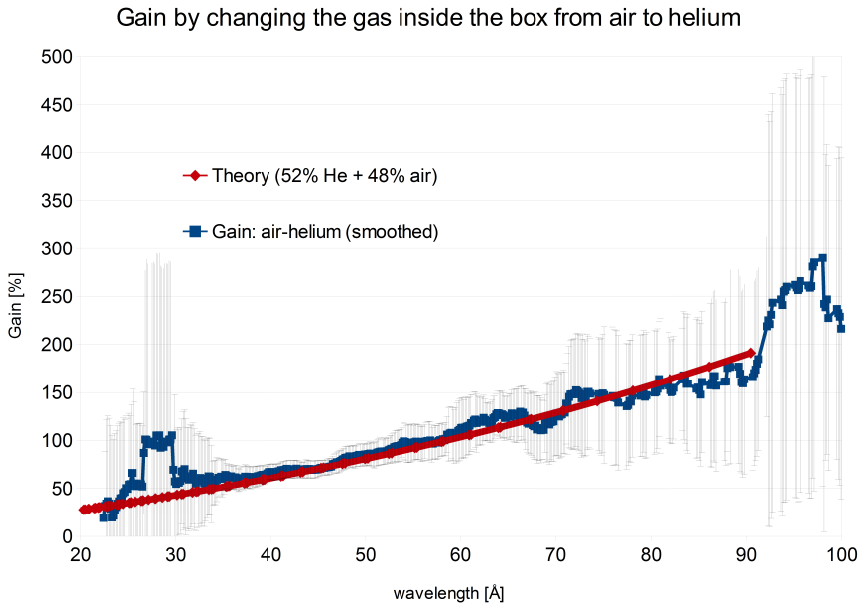

Figure 61: The gain in count rare due to supplanting air (78.08% $^{14}N_2$ + 20.95% $^{16}O_2$ + 0.93%^{40}Ar) with helium.

6.3.1 Spectrum measured with the chopper and the resonator in helium

We measured this spectrum with the synchronized chopper and the resonator. In addition, the resonator and the MCS changed their setting simultaneously according to the detector signal. We did 17 measurements between 37 Å and 69 Å during two nights (Figure 62 on page 81). With these measurements we can recreate the original spectrum using the intensity of pulses with already subtracted background (Figure 63 on page 82) or use the peak area, which is the total count rate of one neutron pulse (Figure 64 on page 82).

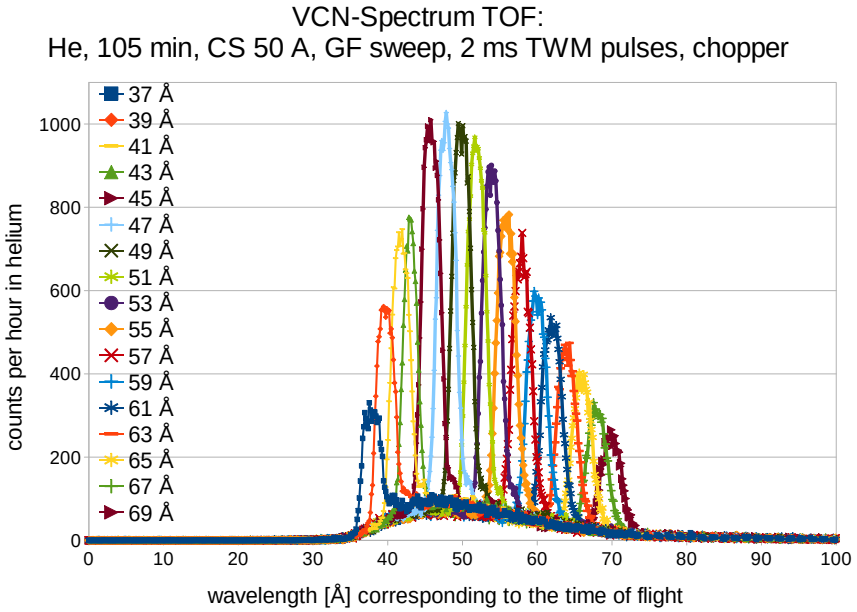

Figure 62: Spectrum of the VCN-beam in helium measured by the resonator with 2 ms TWM-pulses and the chopper. The background from the spin flippers and the super mirrors is well observable.

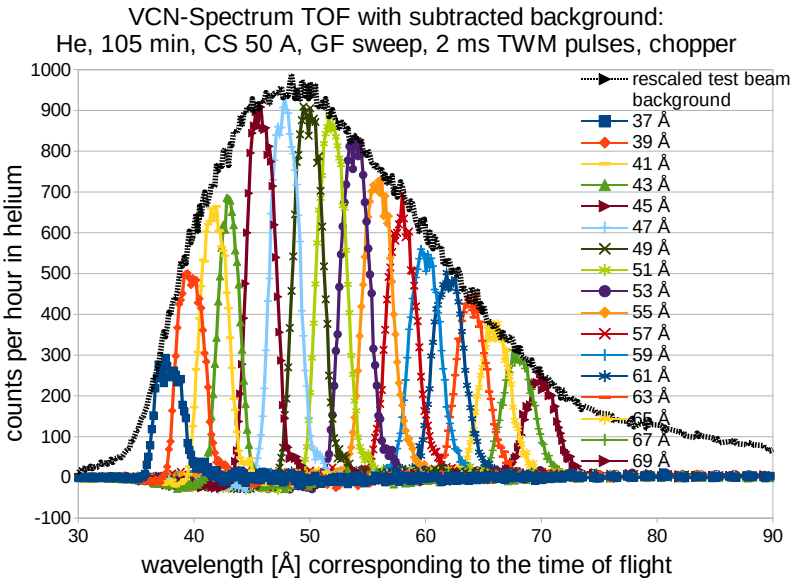

Figure 63: Detailed spectrum of the VCN-beam in helium with subtracted background measured by the resonator with 2 ms TWM-pulses and the chopper. A rescaled spectrum of the background in the test beam envelopes all pulses.

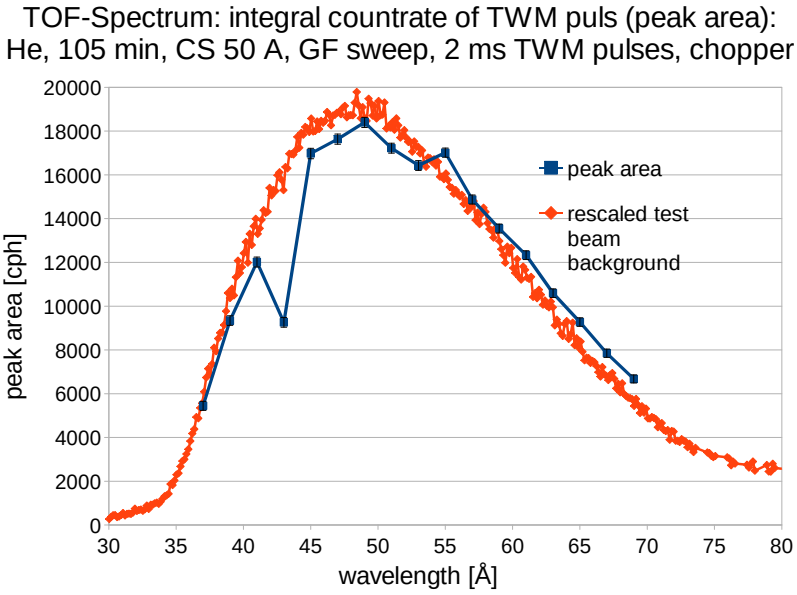

Figure 64: The peak area already with subtracted background measured by the resonator with 2 ms TWM-pulses and the chopper. The first strong deviation from the spectrum at 43 Å is due to the VCN-electronic. The second deviation is between 53 Å and 55 Å because the first nine measurements were done in a different night.

6.3.2 Spectrum in TWM and helium

We produced this spectrum in a helium atmosphere and without a chopper (37 Å- 69 Å). Only the Badurek-resonator scans the spectrum of VCN. We synchronized the detector, the resonator electronics and the MCS. Therefore, we were able to make more measurements in a row, always fitting the parameters of the resonator (guiding field and the compensation field of the spin flipper) according to the chosen wavelength.
In the results (Figure 65 on page 83) we can already see the wavelength dependences (the arrival times of the pulses and the pulse intensities). I reconstructed a spectrum of the VCN-beam using the pulse intensities. I calculated the peak areas of the neutron pulses by subtracting the background counts from the total counts. The unit of the peak area is *standard counts* which is the counts divided the average counts of the monitor beam.
With this method we gained a spectrum of the neutron beam using only the resonator (Figure 66 on page 83).

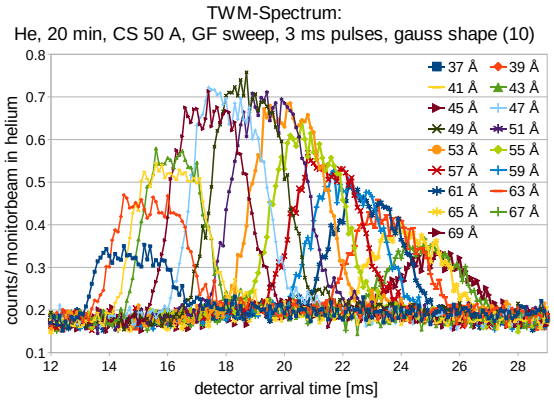

Figure 65: 3 ms TWM-pulses for different wavelength settings (37 Å - 69 Å).

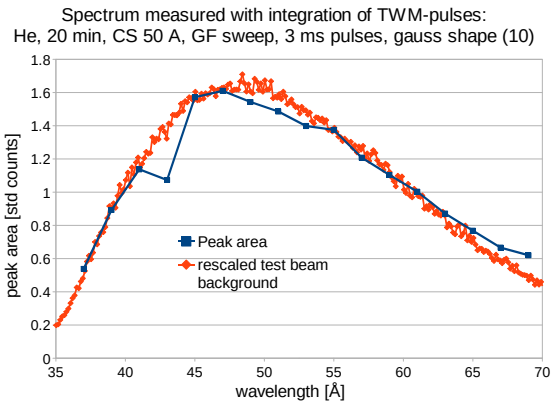

Figure 66: The peak area of 3 ms TWM-pulses which correspond to the spectrum of VCN-beam in helium.

6.4 Darwin plots

In 2014 we invented a new method of testing the flexibility of the Badurek-resonator. We split the resonator in small independent resonators by using only special recipes. We created a different recipe for every small resonator. Due to different offsets the small resonators manipulate different parts of the neutron beam. In addition, we varied some parameters (length of the traveling wave, shape of the spatial magnetic field, ...) in these recipes. We merged them in one recipe together and applied it on the prototype 3.1. Per duty cycle every small resonator creates one neutron pulse. Instead of making more measurements with different parameter settings and merging the results together in one diagram, we only measured once and observed the effect of varying one parameter immediately in one figure. This figure we call "Darwin plot", like the famous graphic of the evolution of mankind.
While trying to accomplish Darwin plots, we learned a lot about the potential and limitation of our system. We recognized that the electronic can only switch the coils on and off in the same order as the neutrons fly. Hence, we can only turn on the last resonator after all other resonators. In addition, the electronic only can manipulate the neutron beam up to 2^{15} µs after the PWM-pulse. Every larger time interval was reduced by deleting all digits before the last 15. Furthermore, the CSV-GUI was not constructed for this purpose. Therefore, we worked for a long time in order to create useful recipes (See more about these problems in Section 4.1).

6.4.1 Timing-Darwin

The active-stage time varies between the four sub-resonators (Figure 68 on page 85 and Figure 69 on page 85). We expected a similar result as if we would make four different measurements (Figure 37 on page 65).The pulse hight should increases with longer stage-active time. In the attached current probe we monitored the stage current (Figure 67 on page 84) which was important to accomplish these Darwin plots.

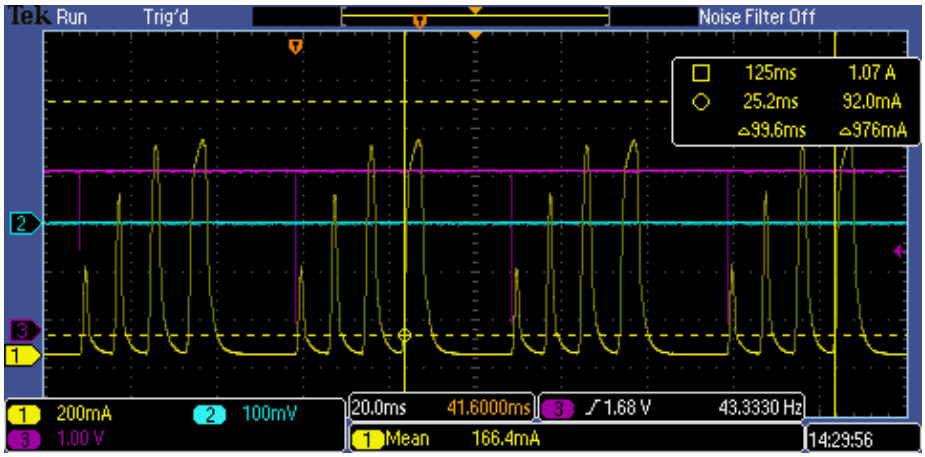

Figure 67: Current through the stage coils during the Darwin-plot for different timing measured with a current probe

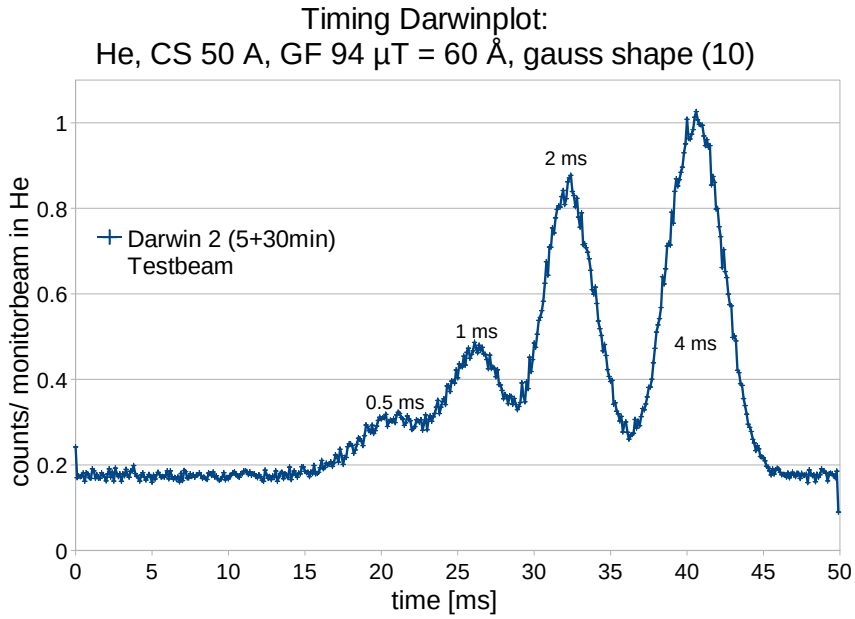

Figure 68: Measurement of the Darwin plot for different timing (number 2)

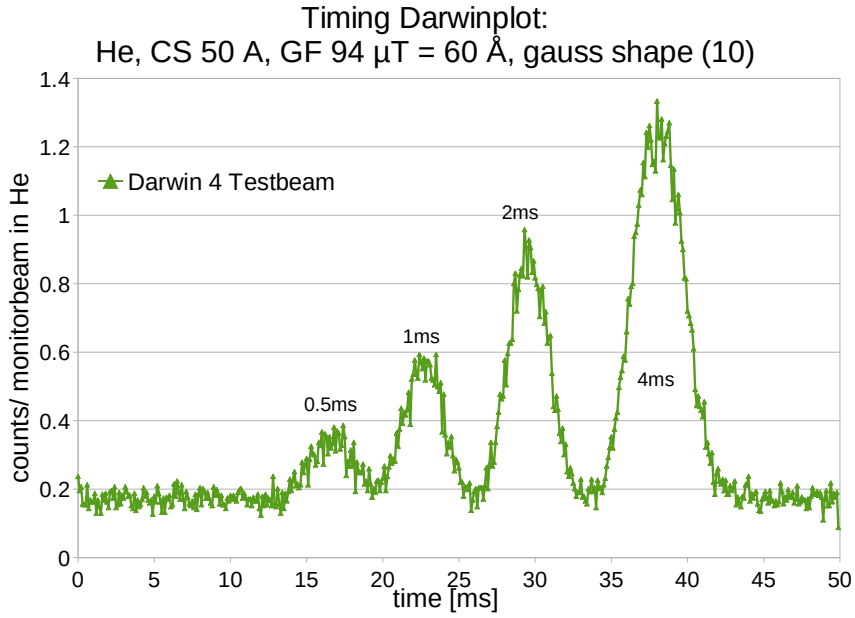

Figure 69: Measurement of the Darwin plot for different timing (number 4)

6.4.2 Shaping-Darwin

In the shaping-Darwin plot we fixed the active-stage time and varied the shaping of the magnetic field in the stages (Figure 71 on page 86). We expected that the pulse height increases the more we Gaussian shape the magnetic field distribution of the resonator.

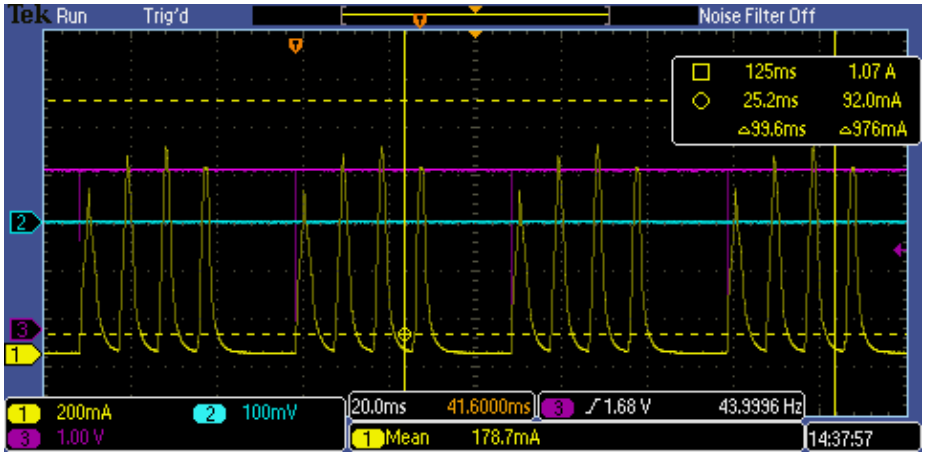

Figure 70: Current through the resonator coils during the Darwin plot for different shaping measured with a current probe

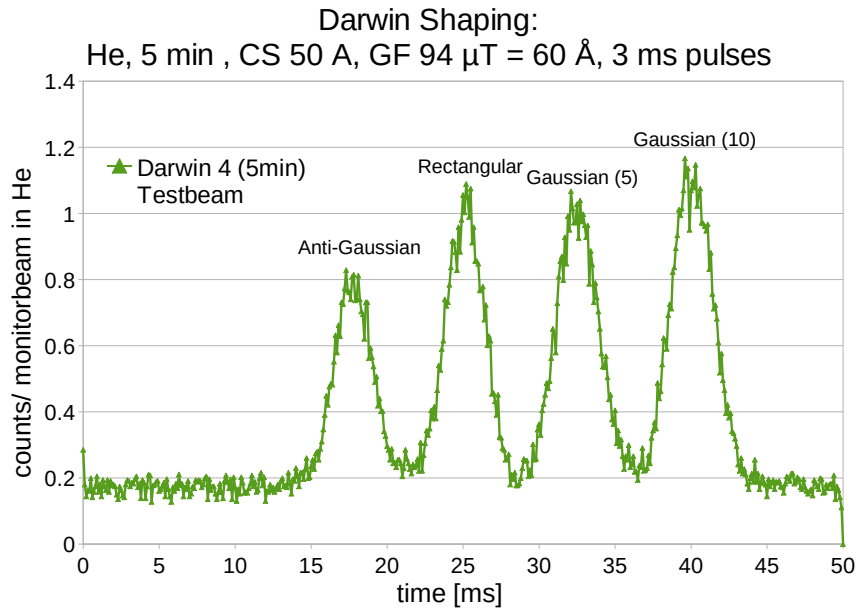

Figure 71: Measurement of a Darwin plot with different shaping of the subresonators (Darwin 4)

7 Conclusion

The current MONOPOL-setup is a fully operational Badurek-resonator for VCN (>30 Å). We were able to diminish many drawbacks and improved the setup (monitor beam, batch line, active magnetic field stabilization, ...). However, we are well aware of the remaining disadvantages and their possible solution. In this thesis, I depicted them always when I presented the component. One major drawback of the MONOPOL-setup I want to present again: the efficiencies of the polarizer and the analyzer is crucial for the Badurek resonator. In order to achieve a very high signal to noise ratio, we really need nearly perfect super mirrors.
The MONOPOL-setup is ready for the next step. Soon a new resonator electronic and a new beam line at the TRIGA-reactor in Vienna will be implemented. With these opportunities we can test a Badurek resonator in a thermal white beam for the first time. The MONOPOL-setup can prove its abilities also for thermal neutrons. An application as a beam preparing device is possible for many major experiments (PERC,...). Furthermore, with the gathered knowledge it is possible to build a Badurek resonator in serial-production as the forth MONOPOL generation.

A Measurements of guiding field coils paramters

A.1 Relation between current and produced B field

I measured the total guiding field in one point with a FW Bell 7010 Gaussmeter during a voltage-sweep done by TTi QPX 600DP. With these measurements I calculated the relation for the parallel connected coils as 242 µT·A^{-1}. The constructors measured 450 µT·A^{-1} [42](p. 34, 37) and 510 µT·A^{-1} [46]. They also used the MONOPOL-setup and the dichromatic beam line of the TRIGA reactor to calculate the value 537 µT·A^{-1} [44](p. 42). During the beam time 2014 in Grenoble, we measured values between 250 - 290 µT·A^{-1}. We could explain the big difference between the measured values, if the constructors used a different setup (the coils connected serially or measured only one coil).
The fluxgate monitoring needs this value only as parameter of the feedback loop in the MCS. An inaccuracy only influences the time which is needed to reach the destined strength.

A.2 Number of windings W

There are only different estimations for the number of the windings, but the number is not important for the experiment.
The team who built the coils estimated 200 windings [42](p. 31). I remeasured the different methods to estimate W, which the constructors used too:
The crudest estimation is to approximate W geometrically.

$$W = w \cdot n = \frac{w \cdot T}{d} = \frac{17 \cdot 14\ mm}{1.65\ mm \cdot \frac{\sqrt{3}}{2}} \approx 144 \cdot \frac{2}{\sqrt{3}} \approx 166 \tag{24}$$

w' is the average number of windings per layer, n the number of layers, T the thickness of all layers and d the thickness of one layer equal to the diameter of the wire times $\frac{\sqrt{3}}{2}$. I use the factor because the wires lie between the wires of the layer below.
Additionally, I estimated W with the measured resistance R_{coil}:

$$R_{coil} = \frac{\rho_{copper}}{A} l = R_{wire} \cdot l \ \rightarrow\ l \approx \frac{5.93\ \Omega}{0.0085\ \frac{\Omega}{m}} \cong 697.6\ m \rightarrow W \approx 158 \tag{25}$$

In order to really estimate the number of windings very accurately, we have to measure the magnetic field distribution produced by both coils and compare it with a simulation of these coils, like Raab did for the small guiding field of the prototype 1.0 [41].

B Used components of the box

B.1 List of all plug-in connectors of the three feed-trough-panels

Left panel:

8 Banana sockets (4 red-black pairs):
2 for the guiding field (12 A & 36 V)
1 for the compensation field of the left spin flipper (20 A & 30 V, common ground with the guiding field)
2 for the compensation field in y-direction (5 A & 3.2 V)
2 for the left endcap of the compensation field in x-direction (1 A & 2.2 V)
1 for the compensation field in x-direction (1 A & 2.2 V)
2 WGK 95 SW high current feed through for the left current sheet (100 A & 1 V)
1 USB feed through for the left flux gate
In the future we need more Banana sockets to avoid having one common ground for two coils. There is also space for plug-ins for future stepper motors which can move or rotate the built-in components or a shutter in front of the entrance windows.

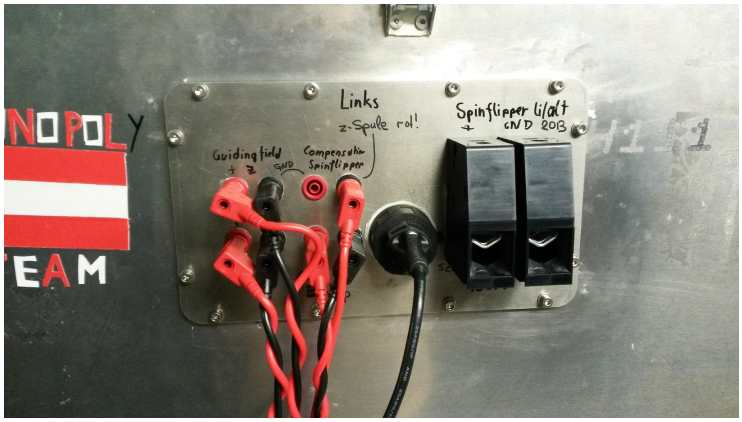

Figure 72: left panel of the MONOPOL-box

Middle panel:

12 Bananasockets:
2 (red-blue) +7 V / -7 V (≈ 0.2 A) power supply of the coil controller's OPV
2 (red-black) +5 V / GND (1 A max) for the ATMEGA-chip of the coil controllers
2 (red-black) +12 V / GNDas power supply for both flux gates
2 (red-blue) for the reset line (red +5 V) and the interrupt line (blue) between OLIMEX-board and coil controllers
2 (black-black) for the I^2C-Bus form the OLIMEX-board to the coil controllers)
1 USB feed through for the right flux gate
2 WGK 95 F VP SW high current feed through for the resonator-stages (5 V- 185 A max)

If we want to use the MONOPOL for thermal neutrons, the current needed for the stages could exceed 250 A. In this case, we need different feed through or more of the used ones. An alternative is to use the resonator in normal air only with no cover plate. Then we can attach the cables directly to the stages. In addition, the cooling is much easier too.

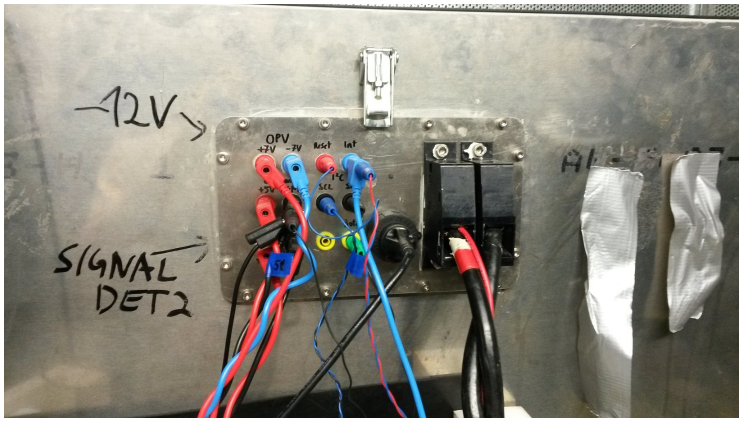

Figure 73: middle panel of the MONOPOL-box

Right panel:

2 connections for the water cooling of the stage's power supply
2 WGK 95 SW high current feed through for the right current sheet (100 A & 1 V)
4 Banana sockets (2 red-black pairs):
2 (red-black) for the compensation field of the right spin flipper (20 A & 30 V)
2 (red-black) for the end caps of compensation field in x-direction (the black is also used for the compensation field in x-direction itself (1 A & 2.2 V)).
1 inlet valve for helium or vacuum
In the future we need additional Banana sockets to separate the end caps of the x-solenoid from the main part. There is also space for plug-ins for future stepper motors.

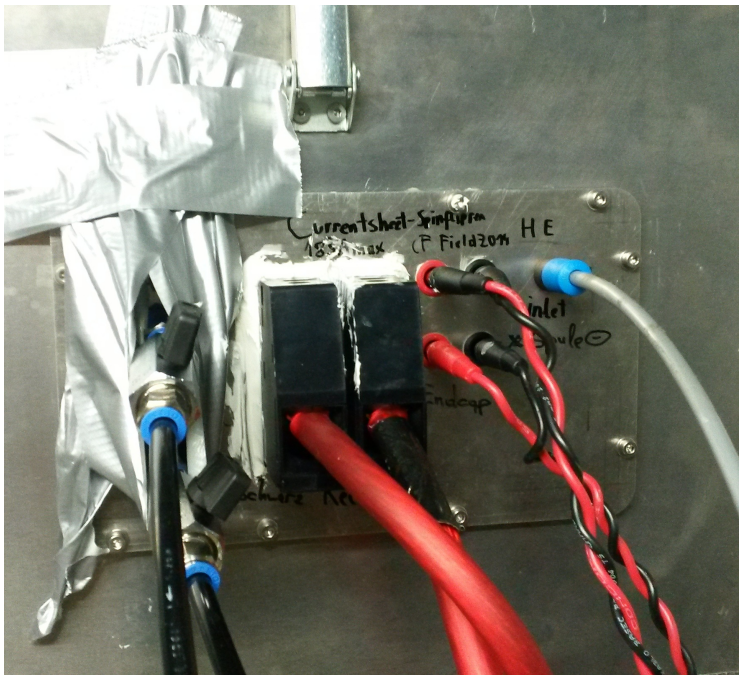

Figure 74: Right panel of the MONOPOL-box

B.2 List of all used components

Used sockets

Banansockets 'Einbaubuchsen' SLB4-G 4mm M4:
8x red: RoHS 404-244, CCCN 85369010, Herst.Teile-Nr. 23.3020-22
8x black: RoHS 404-200, CCCN 85369010, Herst.Teile-Nr. 23.3020-21
2x blue: RoHS 404-216, CCCN 85366990, Herst.Teile-Nr. 23.3020-24
2x Yellow: RoHS 404-266, CCCN 85366990, Herst.Teile-Nr. 23.3020-23
This 4 mm Banana-sockets are glued with a mounting adhesive in a 12.2 mm hole in the panel and fixed from the inside with a M12 screw nut. At the inside we fix the cables with screw nuts on a M4 threaded bolt. These sockets can handle currents up to 1000 V and 32 A.

High current: OMNIMATE Power-Serie WGK (185 A max)
4x WGK 95 SW
2x WGK 95 F VP SW, Best.-Nr. 1250660000

usb feed through:
2x PX0840/B/5M00 from Bulgin, RoHS 468-6377

"Schottverschluss" for water cooling:
FESTO SCM-1/4, Mat.-Nr.:9971, Serie: E708, RGP8-35
Push-in fitting (Adapter Steckschraubverbindung):
FEST QS-1/4-8, Mat.-Nr.: 153005, Serie E3
Valve (Ventile): RoHS 486-277, 1/4 inch, CCCN 84818081

Used kables

Banana 4 mm test lead (32 A - 600 V):
5x red 2 m: RoHS 7865368, CCCN 85369010, Herst.Teile-Nr. 66.9407-200-22
0x black 0.5 m: RoHS7865387, CCCN 85369010, Herst.Teile-Nr.66.9408-050-21
1x blue 2 m: RoHS 7865371, CCCN 85369010, Herst.Teile-Nr. 66.9407-200-24
0x yellow 2 m: RoHS 7865362, CCCN 85369010, Herst.Teile-Nr.66.9407-200-23
1333168, 6491X-2.5 mm BLACK, 133-3168 Farnell
6491X-2.5 mm Red, 120-2725 Farnell
6491X-2.5 mm white, 117-7774 Farnell

Used screws

hexagon socket head cap screws: A4, M4 x 12 mm, DIN 912
M4 Washer: Supplier No. 121976, Item: 125-4-4.3

Old panels

A-2.109-B: Buchse, 4 mm, panel, black, 1698951 Farnell
A-2.109-G: Buchse, 4 mm, panel, green, 1698955 Farnell
A-2.109-BL: Buchse, 4 mm, panel, blue, 1698952 Farnell
A-2.109-R: Buchse, 4 mm, panel, red, 1698950 Farnell

Used cable lug

19324-0016, ring, 2.5-6 mm^2, M10, 229-5579 Farnell

C Used power supplies

Hameg HMP 2030
Power output: 0-32 V and 0-5 A with max. 80 W
Accuracy: <2 mA, 0.05% + 2 mV
3 separated channels and full remote controllable via LabVIEW and GPIB 5 (HO740 interface)
Hameg HMP 4040
Power output: 0-32 V and 0-10 A with max. 80 W
Accuracy: <0.05% + 2 mA, 0.05% + 2 mV
4 separated channels and full remote controllable via LabVIEW and GPIB 6 (HO740 interface)
Kepco BOP 20-5D:
Power output: manual ±20 V; ±5 A (Current Mode and Voltage Mode)
Remote controllable via LabVIEW and GPIB 1 orGPIB 2 (Bit 4886 interface card) only for positive voltage and current in Current Mode possible.
Accuracy: >10 mV & > 10 mA
TTi QPX600DP:
Power output: 0-60 V (0.1% ±2 mV) or 0-80 V (0.1% ±4 mV), 0-50 A (0.3% ±20 mA), max power 600 W
2 separated output-channels and full remote controllable with LabVIEW possible using GPIB 5 or GPIB 29.

D Components of the VCN-coil-controllers

The number in the column needed denotes the number of needed components on the resonator logic platine and the power supply platine respectively. Additionally, many parts are stored in closets in the PERC-laboratory.

Table 11: VCN coil controller components

Component	needed	stored
ATMEGA 164P		1
ATMEGA 164PA-PU, 1748515 Farnell		5
base for ATMEGA 2x20 pins	1/0	1
TXC G 20.0 Ek5L	1/0	2
MCP4728-E/UN: DAC 12Bit, Quad, 10MSOP, 1800217 Farnell	2/0	8
Condensator: C0805C102K5RACTU,0805, 1nF, 50V 141-4660 Farnell		≈ 50
Condensator: MULTICOMP MC0805B473K250CT MLCC 0805, X7R, 25V, 47nF, 1759160 Farnell		≈ 90
Condensator: MULTICOMP MCCA000322 MLCC 0805, NPO, 50V, 22pF, 1759195 Farnell	2/0	> 100
Condensator: MULTICOMP MCCA000386 MLCC 0805, X7R, 50V, 100nF, 1759265 Farnell		> 100
Condensator AVX TAJA106K006RNJ Tantal, SMD 10µF 6V , 197014 Farnell	2/0	≈ 90
switch: SN74LVC1G3157DBVR, SPDT ANA, SMD, 1470910 Farnell	8/0	21
OPA228PA, 109-7467 Farnell	0/4	4
base for OPA 2x4 pins	0/4	15
Condensator 10 µF 25 V, 9452486 Farnell, MCMR25V106M4x7	0/8	≈ 27
Potentiometer: T63YB, 1249, 5K	0/8	22
MOSFET: PSMN2R7, 30PL, PBm 110 3 C2, 9429	0/8	18
Schottky Diode: 1A 95-10, 1458990 Farnell 1N5817G	0/8	≈ 31
Condensator 22000 µF, 10V	0/1	3
Relay: Axicom, P2 12053, V23079-A1001-B301, 117-5082 +421-9960 Farnell	0/8	15
Copper plate for heat transfer	0/1	2
Aluminium plate for heat transfer	0/1	2
MOSFET: PMV31XN, N, SDT-23, 108-1481 Farnell	0/16	92
Power resistor: MHP 50, OR47 F, 12 50	0/8	26
Power resistor: 220 35, 3R30, 236	0/8	14
hexagon socket head cap screws DIN 912 A4 M2, 5x6		≈ 150
05.12.053: bolts, M2,.5X5-NI, 1466814 Farnell		≈ 40
05.12.123: spacer, M2,.5X12-NI, 1466844 Farnell		≈ 37
M2.5 Hex Full Nut Steel Z/C Din934 M2, 141-9446 Farnell	4/4	≈ 60
M2.56 CSSTMCCZ100 screwsDin 84 M2, 141-9411 Farnell	0/0	100
amplifier: MCP6N11-010E/SN, 800 µA, 8SOIC , 206-5864 Farnell	0/0	2
analog switch: TS5A3357DCUTG4, 1XSP3T, SMD, US8-8, 1379265 Farnell	0/0	9
Schottky diode: VS-STPS20L15DPBF, 20A, 15V, 1013333 Farnell	0/0	2
Schottky diode: VS-80CPQ020PBF, 2x40A, 20V, 1013352 Farnell	0/0	1
transistor: MPS2907AG, 1611212 Farnell	0/0	5
transistor: 2N3904BU, NPN 200mA T0-92 RM, 1700648 Farnell	0/0	9
green LED: 703-087, 3mm, 211-2096 Farnell	0/0	≈ 50
red LED: HLMP-Y301-F0000, 3mm, 186-3178 Farnell	0/0	> 50
2.54 Pitch sil vertical pc tail pin header assembly: M20-9990846, 102-2257 Farnell		> 10
MULTICOMP MCCMA51-S-DC12V-C RELAIS, AUTO,SPDT,12VDC,0.8W , 200-8759 Farnell		

References

[1] K.A. Olive et al.(Particle Data Group), *2014 Review of Particle Physics*, Chin. Phys. C , 38, 090001 (2014).

[2] NIST, *CODATA*, http://physics.nist.gov/cgi-bin/cuu/Category?view=html&All+values.x=80&All+values.y=11' (2015).

[3] A. Furrer, J. Mesot, T. Strässle, *Neutron Scattering in Condensed Matter Physics*, World Scientific Publishing Co. Pte. Ltd., Singapore (2009).

[4] W. G. Williams, *Polarized Neutrons*, Clarendon Press Oxford (1988).

[5] triga-reactor at the Atominstitut Wien, http://ati.tuwien.ac.at/reaktor (2015) .

[6] Institut Laue Langevin, http://www.ill.eu (2015).

[7] A. Schebetov, B. Peskov, N. Pleshanov, V. Pusenkov, V. Syromyatnikov, V. Ul'yanov, *Neutron optical devices of PNPI* .

[8] C. Klauser, J Chastagner, D. Jullien, A. Petoukhov, T Solner, *High precision depolarisation measurements with an opaque test bench*, J. Phys.: Conf. Ser. 340 (2012) 012011.

[9] G. M. Drabkin, Zh. Eksp. Teor. Fiz. 43 (1962) p.1107 [Sov. Physi. JETP 16 (1963) p.781]

[10] G. M. Drabkin, V. A. Trunov, V. V. Runov, *Static magnetic field analysis of polarized neutron spectrum*, Sov. Phys. JETP 27(2) (1968) p.194-196.

[11] M. M. Agamalyan, G. M. Drabkin, V. T. Lebedev, *Monochromatization of polarized neutrons by the method of spatial spin resonance*, Zh. Eksp. Teor. Fiz. 73 (1977) p.382-386 [Sov. Phys. JETP, 46(2) (1978) p.200-202].

[12] M. M. Agamalian, j. Schweizer, Ya. M. Otchik, V. P. Khavronim, *Optimization of the Drabkin Monochromator*, Nucl. Inst. and Meth. 158 (1979) p.395-397.

[13] M. M. Agamalyan, V. V. Deriglazov, *Spatial spin resonance in amplitude-modulated magnetic fields*, Zh. Eksp. Teor. Fiz. 83 (1982) p.303-309 [Soviet Physics JETP, volume 56(1) (1982) p.166-169].

[14] M.M. Agamalyan, G.M. Drabkin, V.I. Sbitnev, *Spatial spin resonance of polarized neutrons. A tunable slow neutron filter*, Phys. Rep. 168(5) (1988) p.265-303.

[15] B. Alefeld, A. Kollmar, G. Badurek, G. M. Drabkin, *Space-time focusing of polarized neutrons*, NIM Phys. Res. A 306 (1991) p.300-304.

[16] G. Badurek, A. Kollmar, A. Seeger, W. Schalt, *Use of a Drabkin spin resonator in inverted geometry neutron time-of-flight spectroscopy*, NIM Phys. Res. A 309 (1991) p.275-283.

[17] S.V. Grigoriev, V.V. Runov, A.I Okorokov, A.D. Tretyakov, O.A. Gubin, G.P. Kopitsa, M.K. Runova, *Spatial spin resonance of polarized neutrons in amplitude-modulated magnetic fields*, NIM Phys. Res. A 389 (1997) p.441-446.

[18] S.A. Klimko, S.V. Grigorievm V.V. Runov, A.I. Okorokov, *Monochromatization of a polarised neutron beam by means of spatial spin resonance*, Phys. B 283 (2000) p.397-399.

[19] A.A. Parizzi, W.-T. Lee, G.P. Felcher, F. Klose, *Decoupled Moderators -Do we always need them? or: A New Approach for Pulse Shaping*, arXiv:physics/0105026 (2001).

[20] A.A. Parizzi, W.-T. Lee, F. Klose, *Modeling the neutron spin-flip process in a time-of-flight spin-resonance energy filter*, App. Phys. A 74 (2002) p.1498–1501.

[21] A.A. Parizzi, F. Klose, V. Christoph, *Neutron polarization evolution calculations along the SNS magnetism reflectometer beam line*, Phys. B 356 (2005) p.156–162.

[22] D. Yamazaki, K. Soyama, T. Ebisawa, S. Tasaki, M. Furusaka, M. Arai, *Development of Drabkin energy filters for JSNS project*, Phys. B 335 (2003) p.282-285.

[23] D. Yamazaki, K. Soyama, T. Ebisawa, K. Aizawa, S. Tasaki, *Pulse shaping by means of spatial neutron spin resonance*, NIM Phys. Res. A 529 (2004) p.204-208.

[24] D. Yamazaki, K. Soyama, T. Ebisawa, M. Takeda, R. Maruyama, S. Tasaki, *Chopper mode of Drabkin energy filters for pulsed neutron sources*, Phys. B 356 (2005) p.174-177.

[25] M. Furusaka, *Current activities and plans for polarized neutron instruments of the JSNS/J-PARC project*, Phys. B 356 (2005) p.79-85.

[26] Tobias Denkmayr, *New RF Gradient Spin Flipper for ANTARES*, project report (2012).

[27] G. Badurek, E. Jericha, *Upon the versatility of spatial neutron magnetic spin resonance*, Phys. B 335 (2003) p.215-218

[28] G. Badurek, Ch. Gösselsberger, E. Jericha, Design of a pulsed spatial neutron magnetic spin resonance, *Physica B* 406 (2011) p.2458-2462

[29] C. Gösselberger, H. Abele, G. Badurek, E. Jericha, S. Nowak, G. Wautischer, A. Welzl, *Design of a novel pulsed spin resonator for the beta-decay experiment* PERC, Physics Procedia 17 (2011) p.62-68.

[30] C. Gösselberger, H. Abele, G. Badurek, E. Jericha, W. Mach, S. Nowak, T. Rechenberger, *Neutron beam tailoring by means of a novel pulsed spatial magnetic spin resonator*, J. Phys.: Conf. Ser. 340 (2012) 012028.

[31] Andreas Welzl , *SPARTAN: Software zur simulation des Neutronen-Spin-Flips*, bachelor's thesis, Vienna Universtiy of Technology (2010).

[32] Andreas Welzl, *SPARTAN II: Software zur simulation des Neutronen-Spin-Flips*, project work, Vienna Universtiy of Technology (2011).

[33] Gregor Wautischer, *Spatial neutron magnetic spin resonance*, project work, Vienna University of Technology (2010).

[34] David Birschitzky, *Neutronenspin - Resonanz*, bachelor's thesis, Vienna University of Technology (2011).

[35] Bernhard Rauer, *Projektarbeit-Hadronenphysik*, project work, Vienna University of Technology (2011).

[36] Sebastian Nowak, *Wellenselektion von Neutronen mittels dynamischer Magnetfelder*, master thesis, Vienna University of Technology (2011).

[37] Sebastian Nowak, *Monopol Resonatorsteuerung Version Herbst 2011*, documentation report (2011).

[38] Michael Klopf, *Projektarbeit-Neutronenphysik*, project work, Vienna University of Technology (2011).

[39] Wilfried Mach, Tobias Rechenberger, *Technische Verbesserungen eines Neutronenresonators zur Wellenlängenselektion von polarisierten Neutronen*, project work, Vienna University of Technology (2011).

[40] Robert Raab, *Computerunterstützte Verbesserungen eines Neutronenspinflippers*, project work, Vienna University of Technology (2011).

[41] Robert Raab, *Ausgewählte Experimente mit polarisierten Neutronen und Vergleich Messung zu Simulation*, project work, Vienna University of Technology (2011).

[42] Michael Bacak, Andreas Hawlik, Bernhard Hinterleitner, *Optimierung eines Neutronenresonators für einen großen Strahlquerschnitt*, bachelor's thesis, Vienna University of Technology (2012).

[43] Sarah Gumpenberger, *Implementation of a spatial magnetic spin resonator for neutron spectroscopy applications*, master thesis, Vienna University of Technology (2012).

[44] Tina Gerstmayr, *Ein magnetischer Wanderwellenresonator zur zeitlichen und spektralen Präperation polarisierter Neutronenstrahlen*, master thesis, Vienna University of Technology (2012).

[45] Maximilian Franz Zach, *Design of a pulsed spatial neutron magnetic spin resonator - Entwilckung eines räumlich gepulsten Magnetfeld eines Neutronenspinresonators*, draft of a master thesis, Fachhochschule Technikum Wien (2012).

[46] C. Gösselberger, M. Bacak, T. Gerstmayr, S. Gumpenberger, A. Hawlik, B. Hinterleitner, E. Jericha, S. Nowak, A. Welzl and G. Badurek, *Wavelength-selected neutron pulses formed by a spatial magnetic neutron spin resonator*, Phys. Procedia 42 (2013) p.106-115

[47] Christoph Gösselsberger, *Entwicklung eines Wanderwellen-Neutronenspinresonators*, PhD thesis, Vienna University of Technology (2012).

[48] Stefan Seifried, *Central Master Controller for a pulsed spatial neutron magnetic spin resonator*, bachelor's thesis, Vienna University of Technology (2012).

[49] Stefan Seifried, *Dokumentation von Monopol IDE (MADE)*, documentation, Vienna University of Technology (2012).

[50] Anton Buder, *Neutron Resonator Software*, bachelor's thesis, Vienna University of Technology (2012).

[51] Anton Buder, *Monopol CSV Software*, project work, Vienna University of Technology (2013).

[52] Stefan Kugler, *SpinflipControl Software zur Ansteuerung eines Neutronen-Spinflippers*, project work, Vienna University of Technology (2013).

[53] Robert Raab, *Weiterentwicklung eines Wanderwellen-Neutronenspinresonator für sehr kalte Neutronen*, master thesis, Vienna University of Technology (2013).

[54] Bernhard Berger, *Experimentelle Umsetzung der Geschwindigkeitsselektion mittels Spinresonanz für sehr kalte Neutronen(VCN)*, master thesis, Vienna University of Technology (2013).

[55] Stefan Baumgartner, *in Arbeit*, master thesis, Vienna University of Technology.

[56] Stefan Baumgartner, Bernhard Berger, *Resonator Manual*, manual, Vienna University of Technology (2013).

[57] Michael Bacak, Andreas Hawlik, Bernhard Hinterleitner, *Magnetische Abschirmung und Umrüstung eines Neutronenresonator auf sehr kalte Neutronen*, project work, Vienna University of Technology (2013).

[58] Dominic Blöch, Matthias Schmidtmayr, *Aufbau und experimentelle Realisierung eines Neutronenresonators für sehr kalte Neutronen*, bachelor's thesis, Vienna University of Technology (2014).

[59] Florian Peter Pribahsnik, *Simulationen eines Neutronenmonochromators*, project work, Vienna University of Technology (2014).

[60] Maja Sajatovic, Matthias Scheiner, *Simulation des Zeitverhaltens eines Badurek-Resonators für sehr kalte Neutronen*, bachelor's thesis, Vienna University of Technology (2014).

[61] Michael Bacak, *Design der Strahlabschirmung für einen weißen Neutronenstrahl am TRIGA MARK II Forschungsreaktor der TU Wien*, master thesis, Vienna University of Technology (2015).

[62] Andreas Hawlik, *Strahlpräparation eines weißen Neutronenstrahls am TRIGA Mark II Forschungsreaktors der TU Wien*, master thesis, Vienna University of Technology (2015).

[63] SEKELS GmbH, *Broschüre Magnetischer Abschrimungen*, http://www.sekels.com/downloads/ (2014).

[64] National Nuclear Data Center, *Evaluated Nuclear Data File (ENDF)*, http://www.nndc.bnl.gov/exfor/endf00.jsp (2014).

[65] Hanno Filter, *Vermessung des Choppers*.

List of Figures

1 Principle of the current sheet [40] 14
2 Diffraction of neutrons or X-rays in a crystal [40] 16
3 Using a Drabkin resonator as beam monochromator [28][33] . . . 18
4 Working principle of the Badurek resonator [27] 19
5 The MONOPOL-setup during storage after the beam time 2014. Some parts are missing because they were borrowed or stored separately. 26
6 The MONOPOL-setup during operation in 2014. ©Mach 27
7 The calculated transmission through a resonator due the Beer-Lambert law. The values of the total neutron cross-section are taken from ENDF [64]. 28
8 The prototype 3.1 with the VCN-electronic and the aluminum contact plates 29
9 One stage of the prototype 3.1 with two copper contact plates . . 30
10 Cross-section area of the guiding field coils [43] 32
11 Aluminium table to carry the MONOPOL-experiment 33
12 A summary of all used coils 36
13 Spin flipper 2014 after melting of the plastic parts due to heating up of the current sheet 38
14 Left: current sheet 2013 during a B-field measurment. Right: both current sheets short after the construction of the current sheet 2014 before the winding of the compensation field coils. Both spin flippers still had aluminum contact plates. 39
15 Japanese super mirror ©2014 Wilfried Mach 40
16 The aluminium box containing the MONOPOL-setup. 41
17 Transmission of neutrons in different gases at normal air pressure [64]. 42
18 MONOPOL with closed cover plate standing in the VCN-cabin at the ILL in Grenoble. 43
19 A schematic drawing of all main electronic components of the MONOPOL setup. 45
20 OLIMEX-board (old version) 47
21 View of the VCN-coil-controller 48
22 View on reverse side of the resonator logic platine 48
23 View on the power supply platine 49
24 View on reverse side of the power supply platine 50
25 a screen shot of the MONOPOL CONTROL SYSTEM 56
26 Adjusting of the polarizer super mirror 57
27 Adjusment of the MONOPOL-setup 58
28 The spin flip ratio at different compensation field currents of the current sheet 2013 and different guiding field strengths. 59
29 Dependence between the compensation field current of the current sheet 2013 and the guiding field strengths. 59
30 Relation between the spin flip ratio and the current running through the current sheet 2013. 60
31 Relation between the spin flip ratio and the current running through the current sheet 2013 for different compensation field currents. 60

32 The measured spectra of all four spin-flipper modes in air (N_{00}, N_{01}, N_{10} and N_{11}) and a combination of these measurements. . . 62
33 The wavelength-depending spin-flipper measurements with a subtracted background. You see only the wavelength-depending influence of the resonator. 62
34 The measured spectra of the spin-flipper modes in a helium atmosphere. In comparison to the air-measurements the neutron count rate increased, in particular with higher wavelengths. . . . 63
35 The wavelength-depending spin-flipper measurements with a subtracted background in helium. You can see the wavelength-depending influence of the resonator. 63
36 The spectral spin-flip probability measured in helium and air. Take into account that these probabilities are still convoluted with the chopper-opening-function. There is no difference between the measurements in air and in helium. 64
37 We varied the active-stage time from 0.5 ms to 8 ms. We always used Gaussian-shaped TWM-pulses. Due to a computer crash we measured 7 times at a resonator setting of 1 ms active-stage time for a measurement period of 105 minutes each. 65
38 The difference between a Gaussian-shaped conventional pulse and equally shaped TWM-pulse are the different rise and fall times and the different arrival times of the pulse in the detector. 66
39 A compilation of different pulses with the same pulse length of 3 ms. You can see the influence of the different settings. 66
40 A compilation of different pulses with the same pulse length of 8 ms. 67
41 The DAC-Values of different resonator shaping. The reason for the low DAC-values of stage 9 and 11 are damaged shunt resistors. 67
42 Measurement of different resonator shapings. Due to the static mode of the resonator the convoluted chopper-opening function widens the pulse. 68
43 Measurements of different resonator shapings with subtracted background. A higher parameter for the Gaussian shape increases the pulse height. 68
44 We used different resonator lengths L to produce Gaussian-shaped TWM-pulses with different wavelength resolution. The strong variation in the background can be produced by the malfunctioning of VCN-coil controllers 69
45 Close up of the Gaussian-shaped TWM-pulses with different wavelength resolutions. 70
46 TOF-measurements of Gaussian-shaped TWM-pulses produced by resonators with different lengths. 70
47 The TOF-measurement with subtracted background. We can see the different wavelength resolution, even tough, this function is still a convolution between the pulse spectrum and the chopper-opening-function. 71
48 A close up of varying the adjusted wavelength of the resonator at a fixed guiding field strength. The pulse shape variation and the different arrival times are obvious. 72

49 Rising of the intensity during the measurements due to filling the box with helium. 73
50 Different offsets in air and 45 Å with a subtracted background. The pulse shape represents a convolution between the chopper-opening-function and the resonator-TWM-pulse shape. 74
51 Remeasuring the dependences of the offset in helium (45 Å, with subtracted background). The results are similar to the measurements in air except a high count rate. 74
52 The peak area of the neutron pulses already with subtracted background for the measurements in helium and air. These 75
53 Verification of the expected offset at 37 Å and 53 Å measured in helium. 75
54 Detailed view of the measurements of two overlapping 2 ms TWM-pulses, we can see a strong decrease of the neutron pulse intensity if both traveling waves matches. 76
55 Stage current measured with a current probe during the measurement of a bipartite resonator. 76
56 Measured peak area of two overlapping 2 ms TWM-pulses (total counts). A strong decrease occurs at the matching of the pulses due to double spin flips. 77
57 The VCN-spectra in air, before a power level rise of the reactor . 78
58 The VCN-spectra in helium 78
59 The rescaled VCN-spectra in helium. All spectra are divided per their total count rate. 79
60 The rescaled spectra of the monitor beams in air (low and high power level) and helium. All spectra are divided per their total count rate. In helium the neutron absorption is lower than in air, therefore the spectrum in helium has a higher fraction of neutron with longer wavelengths. 79
61 The gain in count rare due to supplanting air (78.08% $^{14}N_2$ + 20.95% $^{16}O_2$ + 0.93%^{40}Ar) with helium. 80
62 Spectrum of the VCN-beam in helium measured by the resonator with 2 ms TWM-pulses and the chopper. The background from the spin flippers and the super mirrors is well observable. 81
63 Detailed spectrum of the VCN-beam in helium with subtracted background measured by the resonator with 2 ms TWM-pulses and the chopper. A rescaled spectrum of the background in the test beam envelopes all pulses. 82
64 The peak area already with subtracted background measured by the resonator with 2 ms TWM-pulses and the chopper. The first strong deviation from the spectrum at 43 Å is due to the VCN-electronic. The second deviation is between 53 Å and 55 Å because the first nine measurements were done in a different night. 82
65 3 ms TWM-pulses for different wavelength settings (37 Å - 69 Å). 83
66 The peak area of 3 ms TWM-pulses which correspond to the spectrum of VCN-beam in helium. 83
67 Current through the stage coils during the Darwin-plot for different timing measured with a current probe 84
68 Measurement of the Darwin plot for different timing (number 2) 85
69 Measurement of the Darwin plot for different timing (number 4) 85

70 Current through the resonator coils during the Darwin plot for different shaping measured with a current probe 86
71 Measurement of a Darwin plot with different shaping of the sub-resonators (Darwin 4) 86
72 left panel of the MONOPOL-box 89
73 middle panel of the MONOPOL-box 90
74 Right panel of the MONOPOL-box 91

List of Tables

1 Neutron energies [3](p.3) 9
2 Important neutron properties 9
3 Guiding field parameters 32
4 Guiding field settings for prototype 3.1 32
5 x-compensation field solenoid parameters 35
6 y-compensation field coils parameters 35
7 Current sheets 38
8 chopper parameters 40
9 Coil controller parameters for one out of 48 stages 47
10 Polarization and spin-flip-efficiency measurement 61
11 VCN coil controller components 93